Geophys. J. Int. (1995) **120,** 599–645

Partitioning of crustal slip between linked, active faults in the eastern Qilian Shan, and evidence for a major seismic gap, the 'Tianzhu gap', on the western Haiyuan Fault, Gansu (China)

Y. Gaudemer,[1] P. Tapponnier,[1] B. Meyer,[1] G. Peltzer,[2] Guo Shunmin,[3] Chen Zhitai,[4] Dai Huagung[4] and I. Cifuentes[5]

[1]*Laboratoire de Tectonique, Institut de Physique du Globe de Paris, 4 Place Jussieu, 75252 Paris, Cedex 05, France*
[2]*Jet Propulsion Laboratory, 4800 Oak Grove Drive, Pasadena, CA 91109-8099, USA*
[3]*Institute of Geology, State Seismological Bureau, PO Box 634, Beijing, People's Republic of China*
[4]*Institute of Geology, Seismological Institute of Lanzhou, 20 Donggangxi Road, Lanzhou, People's Republic of China*
[5]*Department of Terrestrial Magnetism, Carnegie Institution, 5241 Broad Branch Road West, Washington, DC 20025, USA*

Accepted 1994 July 28. Received 1994 July 28; in original form 1994 March 30

SUMMARY

We have studied the Cenozoic and active tectonics of the north-eastern rim of Tibet west of the Yellow River (Gansu, China) where the western Haiyuan Fault enters the eastern Qilian Shan, a high mountainous region, which was the site of the 1927 May 23, $M = 8$–8.3, Gulang earthquake. Fieldwork, combined with analysis of aerial photographs and satellite images, reveals consistent cumulative left-lateral offsets of postglacial geomorphic features along the fault, but no recent rupture. West of the Tianzhu pull-apart basin, the levelling of offset-terrace risers implies Holocene horizontal and vertical slip rates on the steeply south-dipping, N110E-striking fault of 11 ± 4 and 1.3 ± 0.3 mm yr^{-1}, respectively. The presence of subordinate, mostly normal, throws due to local changes in fault strike, and kinematic compatibility at the SW corner of the Tianzhu basin, constrains the azimuth of the fault-slip vector to be N110–115E. On the less prominent, N85–100E-striking Gulang Fault, which splays eastwards from the Haiyuan Fault near 102.2°E, less detailed observations suggest that the average Holocene left-slip rate is 4.3 ± 2.1 mm yr^{-1} with a minor component of $\approx N$-directed thrusting, with no recent seismic break either. East of ≈103°E, coeval slip on both faults thus appears to account for as much as 15 ± 6 mm yr^{-1} of left-lateral movement between NE Tibet and the southern edge of the Ala Shan Platform, in a N105 ± 6E direction. West of ≈103°E, structural and geomorphic evidence implies that ≈NNE-directed shortening of that edge across the rising, north-eastern Qilian mountain ranges occurs at a rate of 4 ± 2 mm yr^{-1}, by movement on right-stepping thrusts that root on a 10–20° S-dipping décollement that probably branches off the Haiyuan Fault at a depth of ≈25 km. The existence of fresh surface breaks with metre-high free faces on a N-dipping, hanging-wall normal fault south of the easternmost, Dongqingding thrust segment, and of half-metre-high pressure ridges on that segment, indicates that the 1927 Gulang earthquake ruptured that complex thrust system. The ≈4 mm yr^{-1} shortening rate is consistent with the inference that the thrusts formed and move as a result of orthogonal slip partitioning in a large restraining bend of the Haiyuan Fault.

Based on a retrodeformable structural section, we estimate the cumulative shortening on the Qilian Shan thrusts, north of the Haiyuan Fault, to be at least 25 km. The finite displacements and current slip rates on either the thrusts or the left-lateral faults imply that Cenozoic deformation started in the Late Miocene, with slip partitioning during much of the Plio-Quaternary. Assuming coeval slip at the present rates on the Haiyuan and Gulang Faults in the last 8 Ma would bring the cumulative left-lateral displacement between NE Tibet and the Ala Shan Platform

to about 120 km, consistent with the 95 ± 15 km offset of the Yellow River across the Haiyuan Fault, but many times the offset (≈16 km) inferred on one recent strand of that fault east of the river. Relative to the SE Gobi Desert, NE Tibet thus appears to have moved by a fair amount in the Late Cenozoic and is still moving fast. While some of this motion probably contributes to displace (towards the ESE) and rotate (CCW) the south-west edge of the Ordos block, much of it appears to be transmitted to the South China block, which leads, with the additional contribution of other large left-slip faults to the south and despite thrusting in the Lungmen Shan, to the extrusion (towards the ESE–SE) of that block relative to the Gobi, hence to north-eastern Asia.

The ≈260 km long western Haiyuan Fault links two faults that ruptured about 70 years ago during two great earthquakes only seven years apart. Despite spectacular evidence of Holocene movement, it bears no trace of a large earthquake in the past eight centuries, either in the field or in the historical record. Given its relatively high slip rate, it should therefore be singled out as one of the most critical sites for impending great earthquakes (at least $M \geq 7.5$, probably $M \geq 8$) in the region. That such a seismic gap, called here the 'Tianzhu gap', lies only ≈100 km north of Lanzhou and Xining, largest population centres of west-central China, makes instrumental monitoring of that fault particularly urgent. That the $M \approx 8$, Gulang earthquake ruptured a complex thrust surface under high mountains in a restraining bend of the Haiyuan strike-slip fault suggests that the occurrence of comparable earthquakes in other areas with similar fault geometry, such as south of the big bend of the San Andreas Fault in California, should not be ruled out.

Key words: active faulting, seismic gap, slip partitioning, Tibet.

INTRODUCTION

The active, northern tectonic boundary of the Tibetan Plateau is composed of two parts. West of 94°E it is marked by the 1600 km long, ≈N70E-striking, left-lateral Altyn Tagh Fault, a narrow strike-slip zone that guides the north-eastward extrusion of the Plateau (Tapponnier & Molnar 1977; Armijo, Tapponnier & Han 1989). East of 94°E and north of the Qaidam Basin, that boundary is broader and more complex, with several splays of the Altyn Tagh Fault accommodating fractions of the movement of Tibet relative to the Gobi-Ala Shan Platform (Peltzer *et al.* 1988; Peltzer, Tapponnier & Armijo 1989) (Fig. 1). Those splay faults, which combine thrust with strike-slip movement, are responsible for the remarkable structure of the north-eastern border of the Tibet–Qinghai highlands, characterized by many parallel, NW–SE-trending ranges locally higher than 5500 m, including the Qilian Shan. Such oblique thrusts may merge at mid-lower crustal depth into a shallow south-dipping décollement, the north-eastern edge of Tibet thus forming a large crustal-stacking wedge (Mattauer 1986), with the detached underlying lithospheric mantle of the Gobi-Ala Shan Platform subducting ≈500 km farther south, beneath the Kunlun (Tapponnier *et al.* 1990; Meyer 1991).

West of 101°E, widespread oblique thrusting changes to more localized crustal strain along the Haiyuan strike-slip zone (Fig. 1, inset), a predominantly left-lateral fault that runs N110 ± 10E, roughly parallel to, and ≈70 km south of the frontal thrust ramps bounding the north-easternmost ranges of the Qilian Shan (Fig. 1). While the Tibetan highlands terminate around 103°E, the linear Haiyuan Fault zone continues east of the Huang He (≈104°E), then veers to a N140–160E strike along the active Liupan Shan thrusts (e.g. Tapponnier & Molnar 1977; Zhang *et al.* 1991), before merging with the Tianshui and Fengxian Faults near Baoji (≈107°E) and resuming a N100–110E strike along the northern boundary of the Qinling Shan, presently also a left-lateral fault, but with a normal component of slip (Tapponnier & Molnar 1977; Peltzer *et al.* 1985; Bellier *et al.* 1988).

In order to understand the present-day deformation and recent tectonic evolution of north-eastern Tibet and of adjacent regions, it is important to determine quantitatively how the oblique movements that take place within the

Figure 1. Seismotectonic map of eastern Qilan Shan (Gansu, China) and adjacent areas. Major fault traces are from satellite images, aerial photographs and fieldwork. Elevation contours, from 1/1,000,000 ONC maps G8 and G9 (Defense Mapping Agency 1972). Historical events locations, and isoseismals of 1927 May 23 earthquake, from Gongxu, Tinghuang & Zheniliang (1989) and State Seismological Bureau (1991). Locations and fault-plane solutions of 1986 August 26 and 1990 October 20 events, from Dziewonski *et al.* (1987, 1991) and Ekström (1987). The focal mechanism of the 1927 earthquake, and alternate locations of the 1927 and 1986 events are discussed in the text. Numbers in brackets indicate years during which intensities ≥ VI were felt at Xining and Wuwei (State Seismological Bureau 1991). Inset with box (bottom left) shows location of region of study within China. Other boxes show locations of Figs 2, 11 and 16.

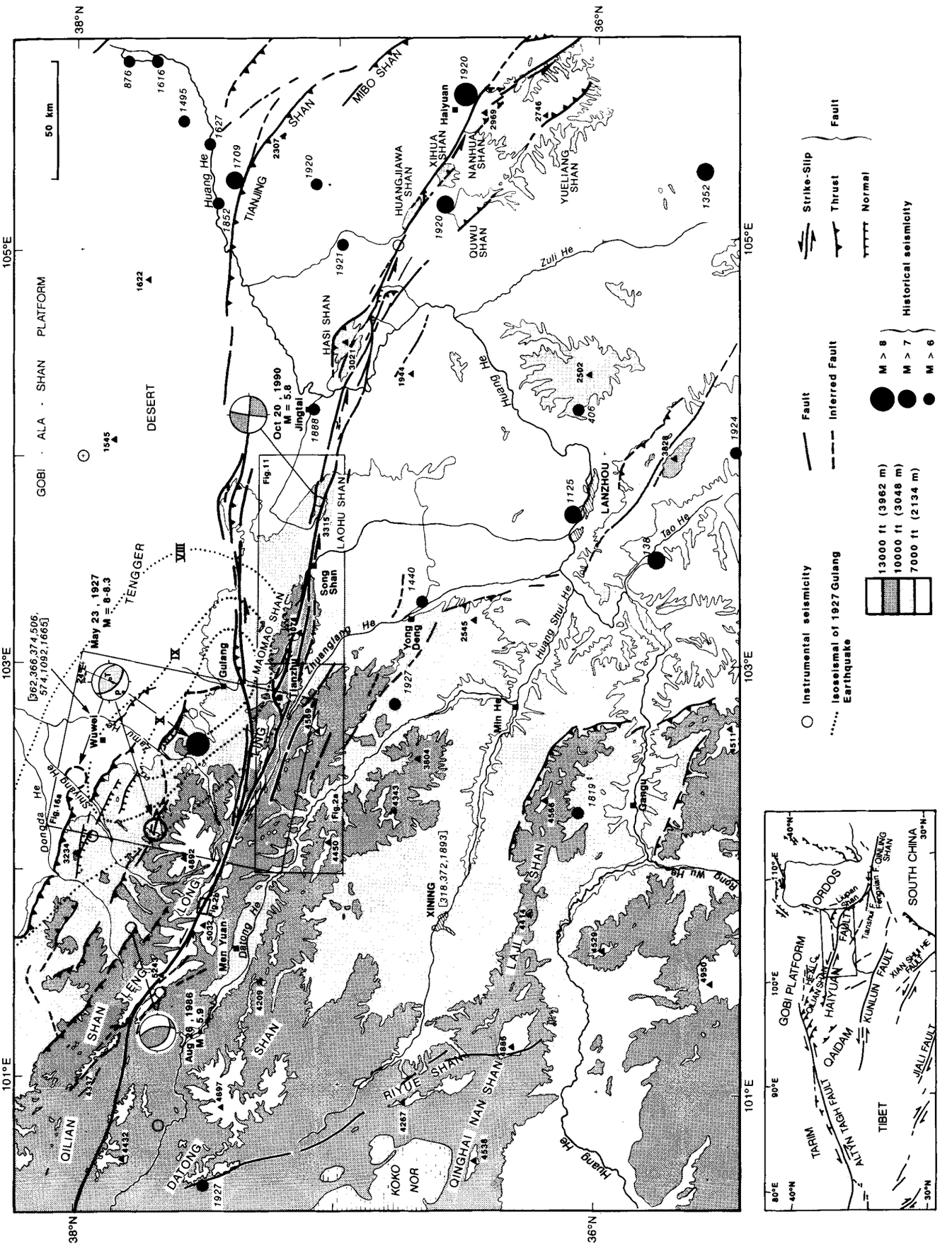

Qilian Shan relate to slip on the Haiyuan Fault zone and on faults farther east and north. This requires a precise analysis of the regional kinematics in terms of slip rates, slip-vector orientations, and cumulative displacements along the faults. As a step towards that goal, we studied the Haiyuan Fault zone between 102° and 104°E, west of the Yellow River (Huang He), as well as the region to the north, between Tianzhu and Wuwei, site of the great 1927 May 23, $M = 8.3$, Gulang earthquake (Fig. 1). In contrast to the well-studied segment of the Haiyuan Fault that ruptured during the greater, 1920 December 16, $M = 8.7$, Haiyuan earthquake, east of the Yellow River (e.g. Deng *et al.* 1984, 1986; Zhang *et al.* 1987, 1988a; Liu & Zhou 1986; State Seismological Bureau 1990), little is known about active faulting in regions located west of the river. The field observations we gathered during short traverses of those regions were supplemented by structural and morphological studies of satellite images (Landsat MSS and SPOT) and air photographs, and by analysis of the topography and geology on maps at scales of 1/100,000 and 1/1,000,000. Using a digital theodolite distancemeter, we mapped horizontal displacements and levelled vertical offsets of postglacial morphological features at two sites along the western Haiyuan Fault. Although restricted by military interdiction and snowy weather, our work brings first-order information on Holocene and Cenozoic movement along the principal regional faults, on the mechanism of the Gulang earthquake, on fault architecture within the crust, and on potential seismic hazard in the area located north of Lanzhou and west of the Yellow River.

THE WESTERN HAIYUAN STRIKE-SLIP FAULT

First-order segmentation of the fault

West of 104°E, the western Haiyuan Fault runs along ranges whose maximum elevations increase westwards from ≈3300 to ≈5200 m (Fig. 1). The main strand of the fault is composed of two fairly linear segments, separated near the small city of Tianzhu by a ≈ 7 km wide left step (Figs 1 and 2a). Owing to left-lateral motion on the fault, that step has resulted in the formation of a half-graben, bounded to the west by a prominent, mostly N30–80E-striking normal fault that connects the two linear segments. This half-graben, here named the Tianzhu pull-apart basin, interrupts the continuity of the ranges that follow the fault, thus providing fairly easy rail and road access to the Hexi corridor, into which it drains.

West of that pull-apart, the western segment, about 140 km long, first follows the north side of the Zhuanglang He Valley. Then, after merging with the Gulang Fault, it forms a narrow strike-slip rift across high, glaciated landforms along the Lenglong Ling (Dragon-of-Cold Range). East of the pull-apart, the eastern segment extends along the Maomao Shan and Lao Hu Shan (Old Tiger Mountain) to south of Jingtai, a distance of ≈120 km (Fig. 1). There, a ≈ 5 km-wide left-step and pull-apart jog marks the separation between the western and the eastern Haiyuan Fault, which lies mostly east of the Yellow River. The ≈230 km long break of the 1920 earthquake on the latter fault stopped at that jog, about 20 km west of the river, near Santang Shan (Deng *et al.* 1984, 1986; State Seismological Bureau 1990; Liu & Zhou 1986).

Zhuanglang He-Lenglong Ling (western) segment

Near 101.7°E, as it enters the highest part of the Lenglong Ling, the western segment of the fault cuts three extinct, north and east-draining glacial valleys (Fig. 2b). The valley floors are fairly flat, several hundred metres wide, often with lateral moraines, and in part occupied by hummocky glacial till. Much of the area near and south of the fault, whose trace is straight and sharp, stands above 4000 m a.s.l. The tips of three hanging glacier tongues lie only 1–1.5 km away from that trace. The bedrock topography peaks along thin crestlines (nunataks), implying thick ice-caps, during the last (Würm) glaciation, on much of the mountain relief visible on Fig. 2(b). The two most prominent mountain spurs between the glacial valleys are truncated by the fault, forming north-facing triangular facets. North of the fault, smooth, flat surfaces are preserved over a fairly large area between the glacial valleys. We interpret these surfaces, which have not been significantly incised by pluvial run off, to have been subject to efficient planation by periglacial erosion processes until a very recent epoch. The smooth texture of the surfaces also implies that they are mantled by loess. The edges of the glacial valleys and of the intervening ridges, which are in part outlined by lateral moraines, are clearly offset by the Haiyuan Fault, in a left-lateral sense (Fig. 2b). Such offsets range between 200 and 270 m. The fault also offsets, by smaller amounts (≈85 and ≈100 m), two stream channels that incise the floor of the westernmost valley (Fig. 2b).

The relationship between active faulting and glacial geomorphology derived from the interpretation of the SPOT image in the Lenglong Ling bears strong resemblance to that documented at several other Tibetan sites by Armijo *et al.* (1986, 1989). The freshness and size of the glacial landforms imply that they date mostly from the last glacial maximum (about 20 ka B.P.), a time at which glacier tongues fed by the ice capping the relief south of the fault may have extended several km northwards. The geomorphic offsets visible on the image thus probably postdate that maximum. More specifically, we interpret the 240 ± 40 m offsets of the glacial valleys edges to postdate ice retreat above the fault trace, some time between 20 and 14 ka B.P., and the smaller stream offsets on the valley floor to postdate the pluvial period that marked the Early Holocene climatic optimum. Such inferences would be consistent with a left-slip rate of 15 ± 5 mm yr^{-1} on the western Haiyuan Fault in the Lenglong Ling (Blusson, Tapponnier & Meyer 1989; Meyer 1991, p. 114, Fig. 10a).

Between 102°25′E and 102°45′E, west of the Tianzhu pull apart, the upper Zhuanglang river flows in an elongated basin with a flattish floor, at an elevation of ≈3100 m (Fig. 2a). Bounded by steep relief on either side, that basin is filled by Plio-Quaternary clastics. To the north, the Lenglong Ling mountains (locally Leigong Shan) rise to ≈4300 m, exposing mostly Silurian greenschists intruded by diorites (Gansu Geological Bureau 1975; Xu, He & Yan 1989). Well-preserved traces of the last glaciation are clear above 3700 m on the south flank of the mountains, in the

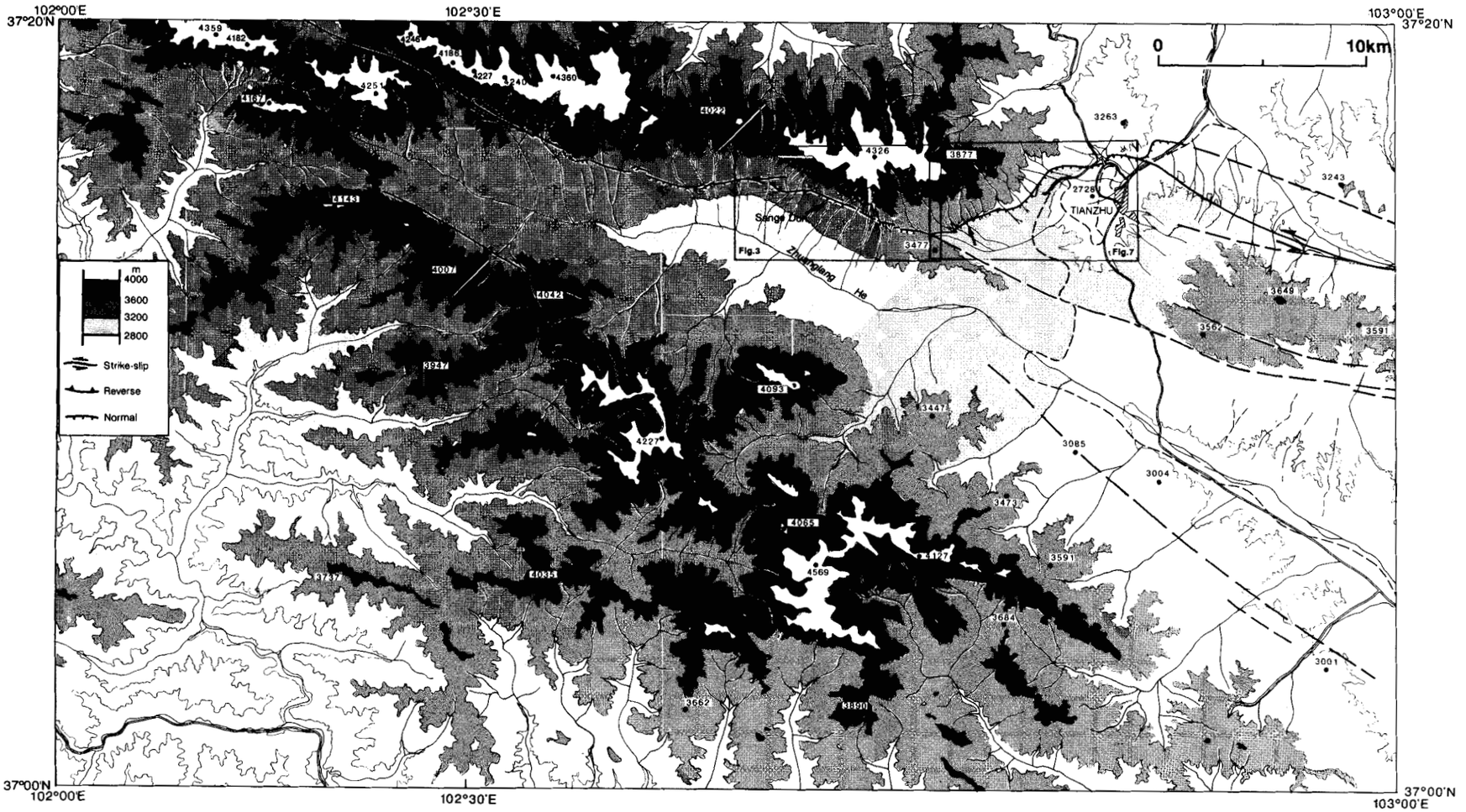

Figure 2. (a) Map of western Haiyuan Fault zone near Tianzhu pull-apart basin, at extremity of Lenglong Ling. Elevation contours and other information are from 1/100,000 Chinese topographic maps. Boxes are locations of Figs 3 and 7. Arrows show locations of Sange Dun and SW Tianzhu sites (Figs 4b–e and 8, respectively). (b) Glacial offsets in Lenglong Ling mountain near 101.7°E. Top: part of SPOT scene KJ 252-275. Note present glacier tongues separated by nunatak crestlines in bottom left corner of image, and Haiyuan strike-slip fault trace cutting prominent valleys draining to north and east. Bottom: geomorphic interpretation of central part of image. Offsets of moraines marking valley edges range between 200 and 270 m. Smaller offsets (85–100 m) are visible on western valley floor.

(b)

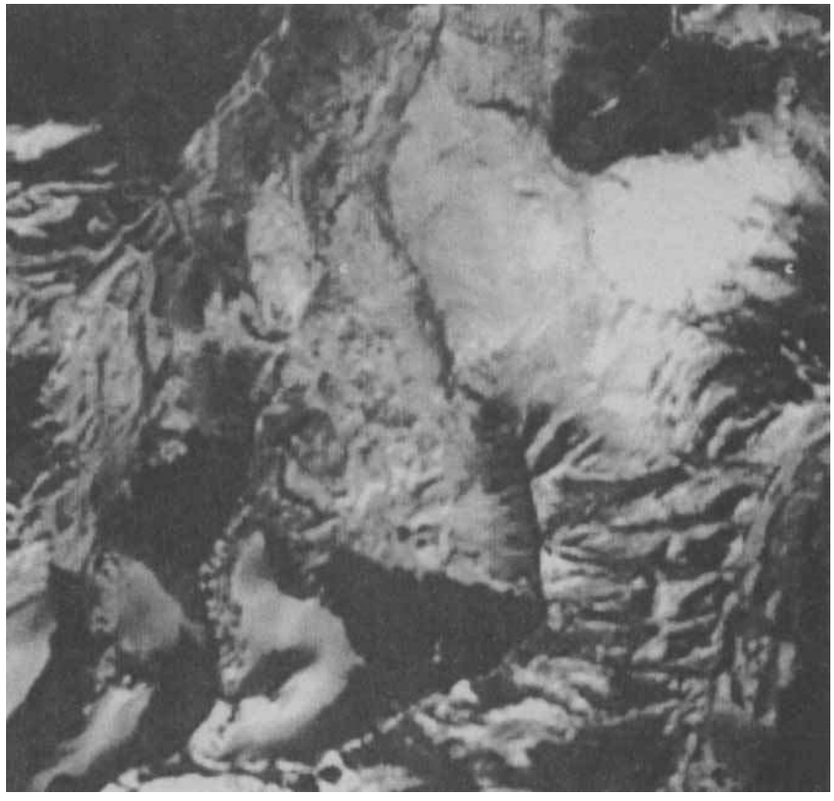

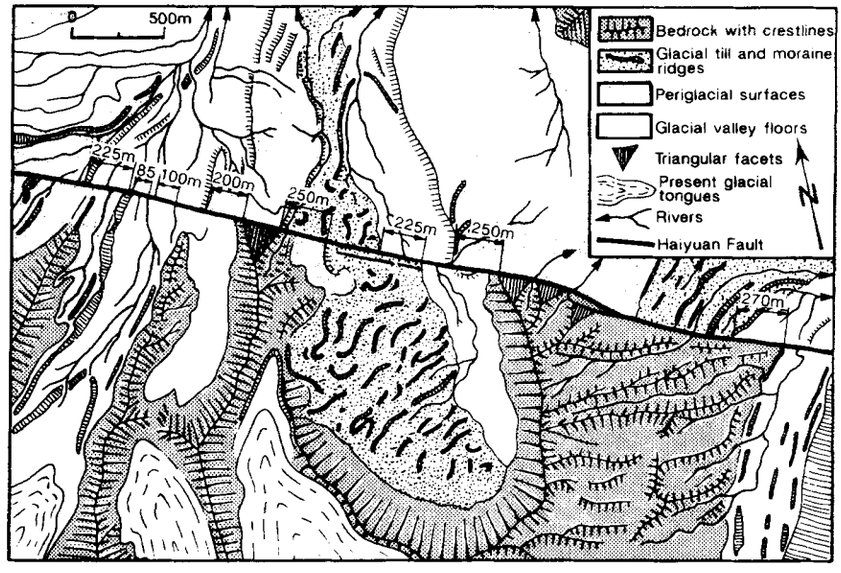

Figure 2. (*Continued.*)

form of fresh, hanging glacial cirques (Fig. 3a). The active Haiyuan Fault trace stands out along the north edge of the basin, near the 3500 m elevation contour (Figs 2a, 3 and 4). The fault runs mostly across the apex of fans (Fig. 4b) and boulder-bearing fluvio-glacial terraces (Fig. 4b) that have been fed by streams incising the steep southern flank of the Lenglong Ling. South of the fault, the fans coalesce to form a rather uniform, gently SW-sloping piedmont. Rare, isolated hills or ridges of hummocky ground that stand somewhat above the average piedmont surface may represent the smoothed remnants of large landslides. At one outcrop in the western part of the basin, where the fault

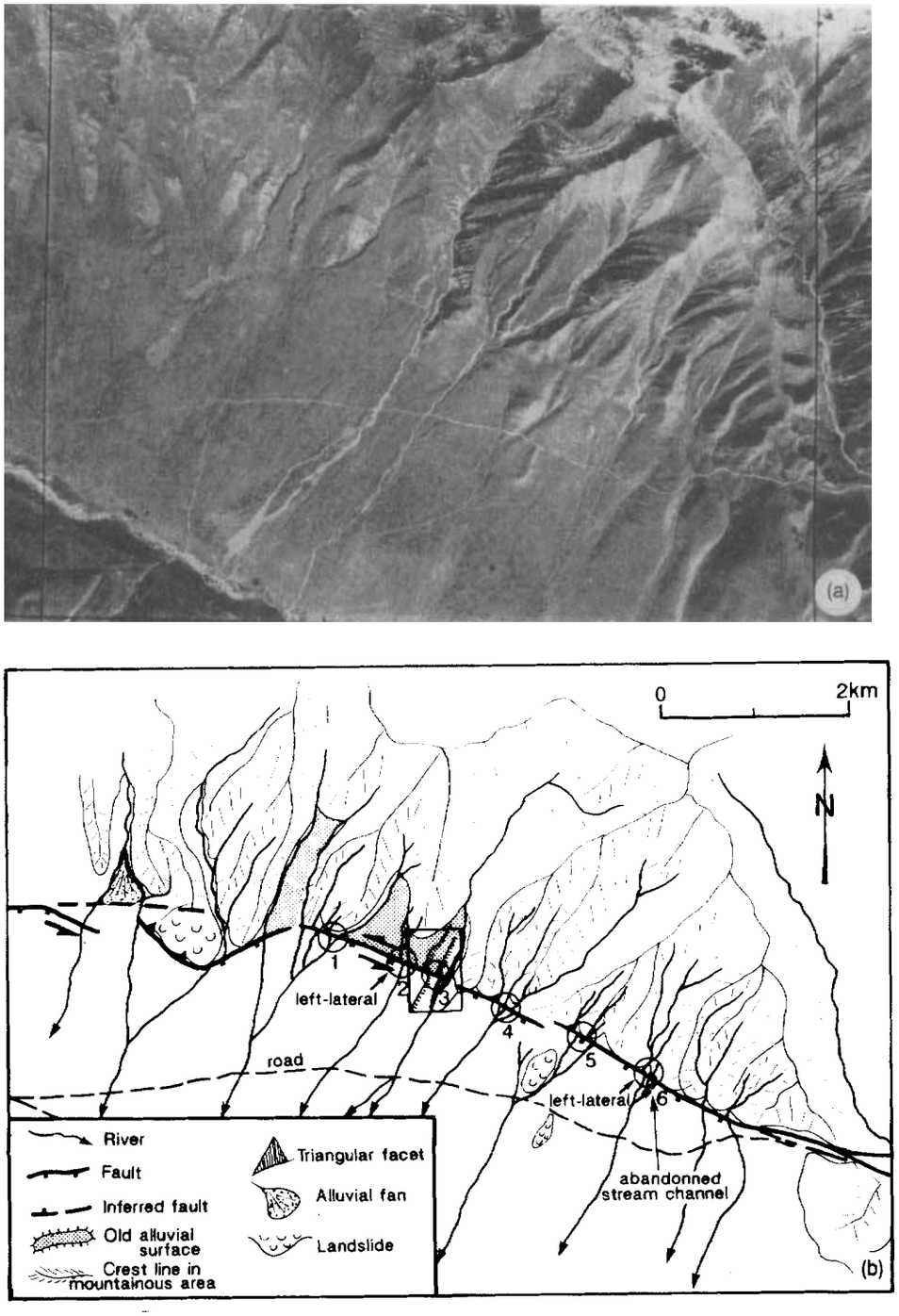

Figure 3. (a) Aerial view of Haiyuan Fault near Sange Dun site, Zhuanglang He Valley. (b) Morphotectonic map of area in Fig. 3(a). Scale bar is for centre of picture only. Azimuth of fault is distorted near edges of map. Note prominent left-lateral offsets of most streams in central part of map (circles). Box shows location of Fig. 4(e).

slices through bedrock, steeply south-dipping shear planes and cracks form a gouge zone several metres thick. The principal strand of the fault trace is outlined in most places by a south-facing, up to 30 metres high (Figs 4a and b), cumulative scarp with a rather steep slope (up to 35°), which makes it clear from afar in the landscape.

That scarp strikes mostly N110–120E but swings to a ≈N80E direction for ≈3 km near 102°40′E (Fig. 2a). Bends in the Zhuanglang He course and in the Lenglong Ling crest, which forms a saddle at this longitude, mimic that swing south of trig point 4022 (Fig. 2a). The strike component of slip on the fault is documented by left-lateral

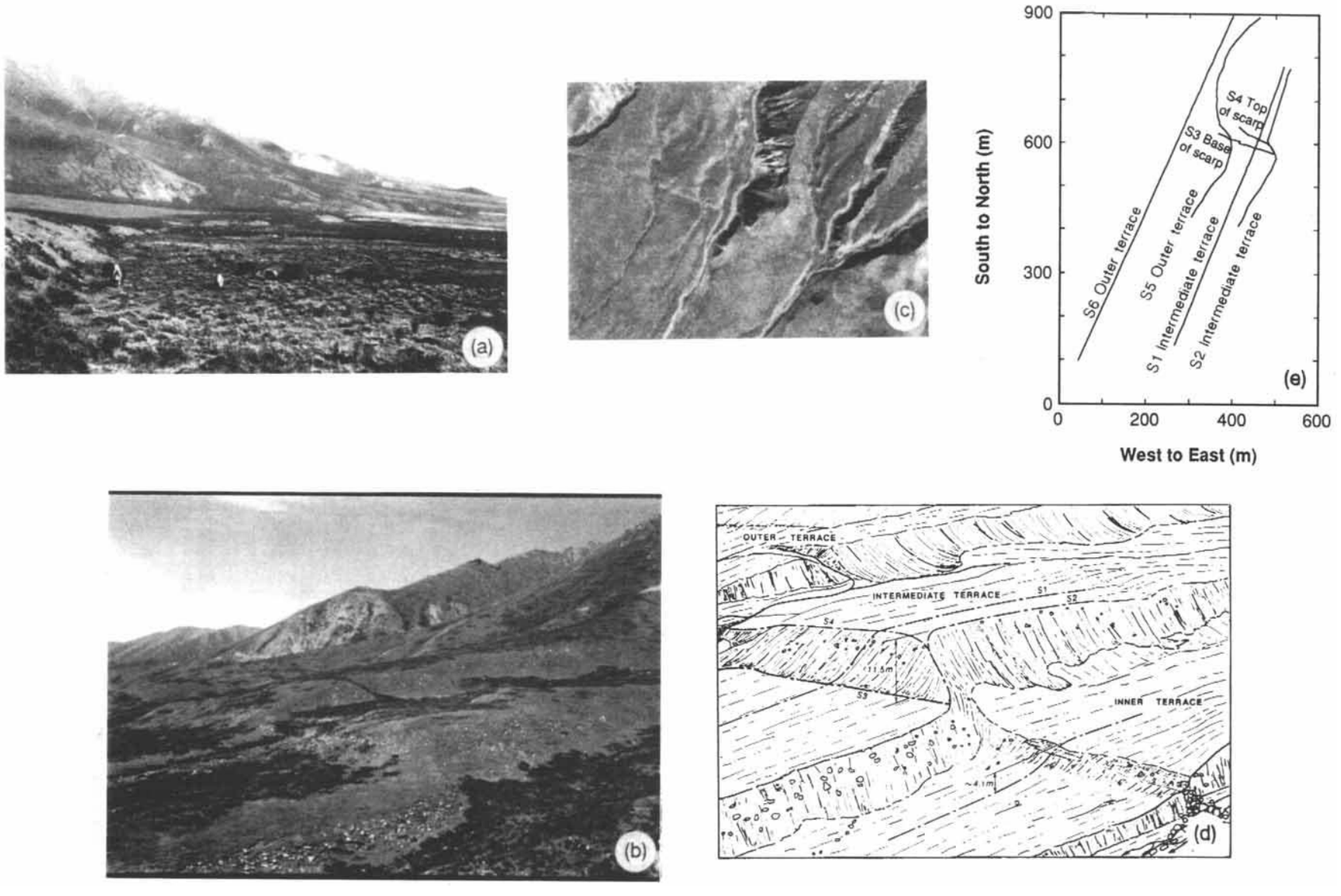

Figure 4. (a) Vegetated, smoothed out scarp, up to 6 m high, across young fan, west of Sange Dun. Pull-apart swamp where Yaks graze at foot of scarp is ≈100 m × 50 m wide (left edge of map in Fig. 3). (b) Obliquely offset flight of terrace risers at Sange Dun. (c) Enlarged aerial view of terraces. (d) Schematic drawing illustrating principal morphological elements visible in foreground of photograph of Fig. 3(d), with location of profiles S1–4. (e) Map view of profiles levelled at Sange Dun: S1 and S6, perpendicular to fault strike, S2 and S5 along intermediate and outer terrace-riser tops, and S3 and S4 along bottom and top of cumulative fault scarp, respectively.

offsets of stream channels and terrace risers (Figs 4b and c), and by the presence of small dilational jogs, marked by persistent sag ponds or swampy peat bogs (Fig. 4a). The dip component of slip appears to result from the difference between the azimuths of the fault trace and of the regional fault-slip vector, as commonly observed along great strike-slip faults, and quantitatively documented on the Changma fault in the western Qilian Shan (Peltzer *et al.* 1988). Here in the Zhuanglang basin, fault segments that strike more northerly than ≈N115E bear the clean-cut, steep morphology of normal fault scarps while rare segments striking more southerly than ≈N120E show the smoother relief and lobate geometry that typifies thrust-fault scarps (Figs 2a and 3).

At Sange Dun, ≈5 km west of the Tianzhu basin, the fault cuts a flight of three inset terraces of increasing height and age (Figs 4b and c). A good record of horizontal and vertical cumulative offsets is preserved here. The Sange Dun stream (Taqing He) has incised rather deeply into the terraces, and the offsets of the terrace surfaces and risers are clear on the right bank of the stream. Both the outer, uppermost terrace and the intermediate terrace are offset by tens of metres (Figs 4b and c). The inner, lowermost terrace, only 3.3 ± 0.5 m above the active streambed, is offset vertically by 4.1 ± 0.5 m (Fig. 4d). Big boulders within the streambed still outline a 1.7 ± 0.5 m high step across which the water cascades (Fig. 4d). Using a digital theodolite-distancemeter (Wild T2000–DI20), we levelled six profiles (S1 to S6) to document quantitatively the large-scale morphology of that site (Fig. 4e). S1 and S6 were levelled perpendicular to the fault in order to measure cumulative vertical offsets; S2 and S5, along the terrace-riser tops, to measure cumulative horizontal offsets. Two additional profiles (S3 and S4) were levelled along the bottom and top of the cumulative, N110E-striking fault scarp.

Several sources of uncertainty make measurement of offsets of morphological features such as terrace risers difficult. Given the maximum distance (typically of the order of a few km) between the station and measurement points, the high precision of the station instruments ($\approx 5 \times 10^{-6}$ rad for angles, and ≈ 3 mm + 1 mm km^{-1} for horizontal distance) makes instrumental errors (of the order of a few mm) negligible in view of the dimensions and offsets (typically of the order of several tens of metres) of the features studied (e.g. Peltzer *et al.* 1988). Another source of error arises from the fact that the top edge of a terrace riser may be locally difficult to identify because of degradation. At Sange Dun, however, the top edges of the risers are outlined by fairly sharp slope breaks, and we estimate in the field the error on the horizontal position of points measured along those edges to be of the order of ±0.5 m.

By far the most serious source of error comes from difficulties in defining the large-scale shapes of the risers and from changes of those shapes with increasing fault offset. Fig. 5(a) illustrates how such difficulties may lead to fairly large uncertainties on horizontal offsets. In map view, the cumulative horizontal offset of a terrace riser is the distance, measured along the fault, that separates the intersections (piercing points) of the fault scarp with straight lines approximating the terrace-riser tops upstream and downstream from the scarp. If entrenchment of the stream has been rapid and if the riser top edge is sharp, with similar, fairly straight strikes above and below the fault scarp, defining the piercing points (open circles, Fig. 5a, left) and measuring the offset is straightforward. Fairly long profiles, extending far enough upstream and downstream from the fault scarp, are nevertheless required. If the length of the profiles does not suffice to define straight- and long-enough riser segments with matching strikes, the offset will be fraught with uncertainty. Given the sigmoidal bend that morphological markers transverse to strike-slip faults usually exhibit, matching the upstream and downstream segments of risers defined by short profiles will in general lead to apparent offsets smaller that the real offset (open triangles, Fig. 5a, middle). Finally, if the formation of a terrace riser results from slow, progressive entrenchment of the stream into previously deposited fanglomerates, erosion by the stream may make the riser edge recede away. Differential erosion and deposition may also change the riser shape in map view. At Sange Dun for instance, riser edges above the fault and west of the stream might have receded westwards, with carving and depositional smoothing by the stream leading to a greater sigmoidal deviation of the risers across the fault and to estimation of an apparent offset greater than the real offset (open squares, Fig. 5a, right). Clearly, the uncertainties on horizontal offsets resulting from the ill-defined large-scale geometry of the risers dwarf all others. They may reach tens of metres, amounting to a significant fraction of the offset itself (Fig. 5a).

Similar problems are encountered when determining the vertical throw of offset surfaces. The throw is the elevation difference between the two points where the fault plane intersects the regional slopes above and below the scarp (Fig. 5b). Neglecting millimetric instrumental errors, three factors contribute to the uncertainty on the throw. The first one comes from fitting regional slopes to straight lines. We levelled profiles as long as possible (several hundred metres), smoothing out obvious, small-scale surface irregularities, such as minor gullies or large boulders. For profiles S1 and S6 at Sange Dun and for five of the six profiles levelled west of Tianzhu, straight lines provided excellent fits to measured profile points for ≈200 m above the scarps and for greater lengths below, thus constraining well the regional slopes. We estimate the uncertainty in those fits to be of the order of the scatter due to surface roughness, i.e. ±0.5 m. The second factor is the uncertainty in the position of the fault within the scarp slope (Fig. 5b). In general (e.g. Bucknam & Anderson 1979; Hanks *et al.* 1984), scarps that do not integrate the effect of multiple, close-spaced faults exhibit an inflection point near mid-width that separates a region of erosion (above) from a region of deposition (colluvial wedge, below) (e.g. Wallace 1977; Armijo *et al.* 1986). Here, we assume that the fault plane is unique and intersects the scarp slope near that point, and allow the scarp-fault intersection to vary between the levelling points that bound the inflection (filled circles, Fig. 5b, top). The third factor is the uncertainty on the dip of the fault plane, shallower dips leading to greater throws (Fig. 5b). Since the fault is normal and strike slip, we take its dip to be greater than 45°. Given such constraints, the combined uncertainty on the calculated values of vertical throws comes out to less than 20 per cent at Sange Dun and to generally less than 10 per cent at Tianzhu.

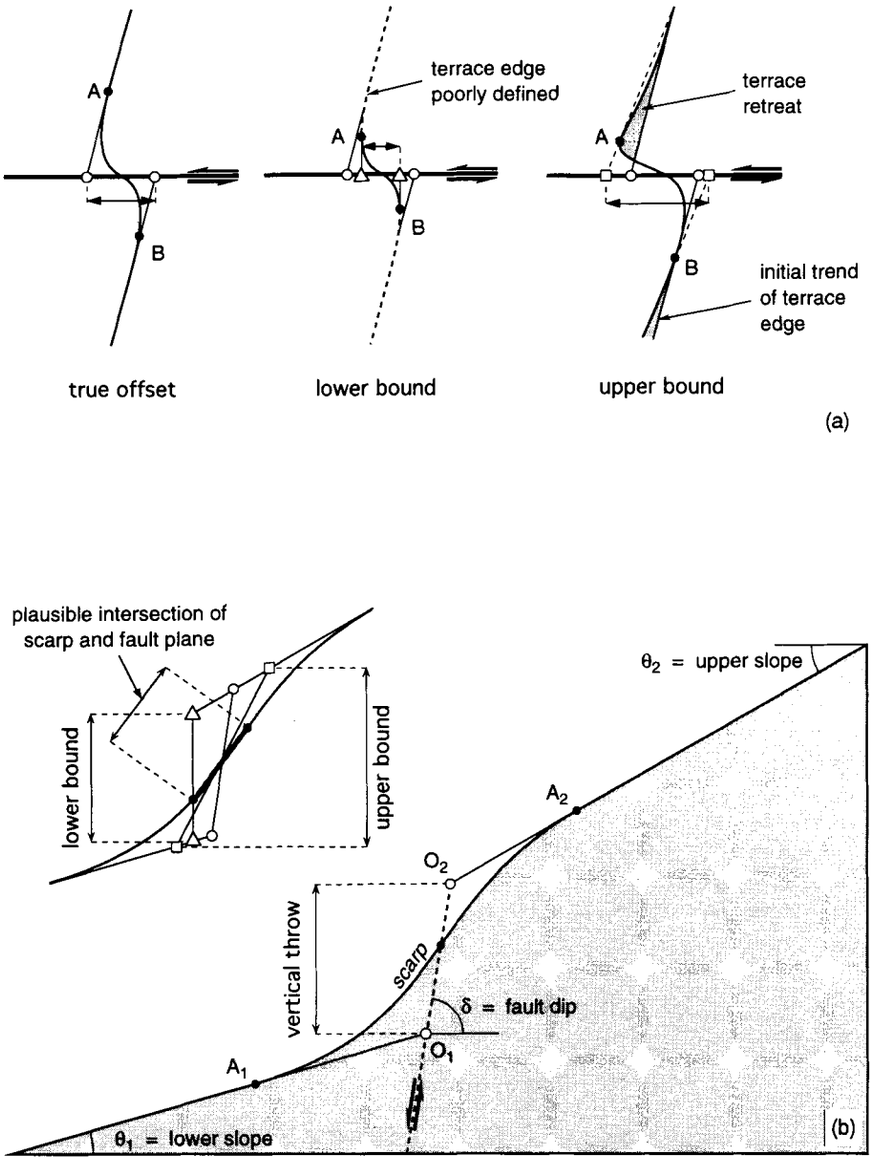

Figure 5. (a) Examples of problems besetting determination of cumulative horizontal offset of terrace risers. See discussion in text. (b) Problems besetting assessment of cumulative vertical throw from topographic profiles. Discussion in text.

At Sange Dun, the intermediate terrace riser has a dog-leg shape, with a linear upstream segment striking N18E for ≈200 m (AB, Fig. 6a) and a slightly curved, downstream segment that strikes N30E on average from C to D (Fig. 6a). These two segments are linked, across the fault scarp, by a transition segment, BC, striking ≈ N150E. Assuming the initial strike of the downstream riser segment to have been close to that now characterizing the upstream segment (N18E) would yield a cumulative left-lateral offset of 31.5 ± 1.0 m (open triangles, Fig. 6a, Table 1a). Taking the average strike (N30E) of the longest, best-defined downstream riser segment to be the original strike would lead to a larger offset: 37.5 ± 1.0 m (open squares, Fig. 6a, Table 1a). The distance, along the N100E fault strike, between the points that define the top and base of the fault scarp on profile S2 (B and C, Figs 6a and c) is 33.5 ± 1.0 m (Table 1a). Finally, projecting profiles S3 and S4 on a vertical plane striking N110E, parallel to the fault, yields a left-lateral offset of 37.4 ± 1.0 m between the riser tops at the base and top of the scarp (horizontal distance between *P* and *M*, Fig. 6b, Table 1a). We take the arithmetic mean of these four values (35.0 m), and the greatest difference between that mean and any such value (3.5 m), to be the most plausible value of, and uncertainty on, the horizontal offset of the intermediate terrace riser (Table 1a).

The more sinuous geometry of the outer terrace riser makes determination of its horizontal offset more difficult (Fig. 6a). Though curved and poorly defined, the segment of that riser that is farthest upstream, beyond E (Fig. 6a), strikes about N35E. Downwards, from E to F and below, the riser is more linear and takes a more northerly direction (N18E), before veering counter-clockwise across the fault

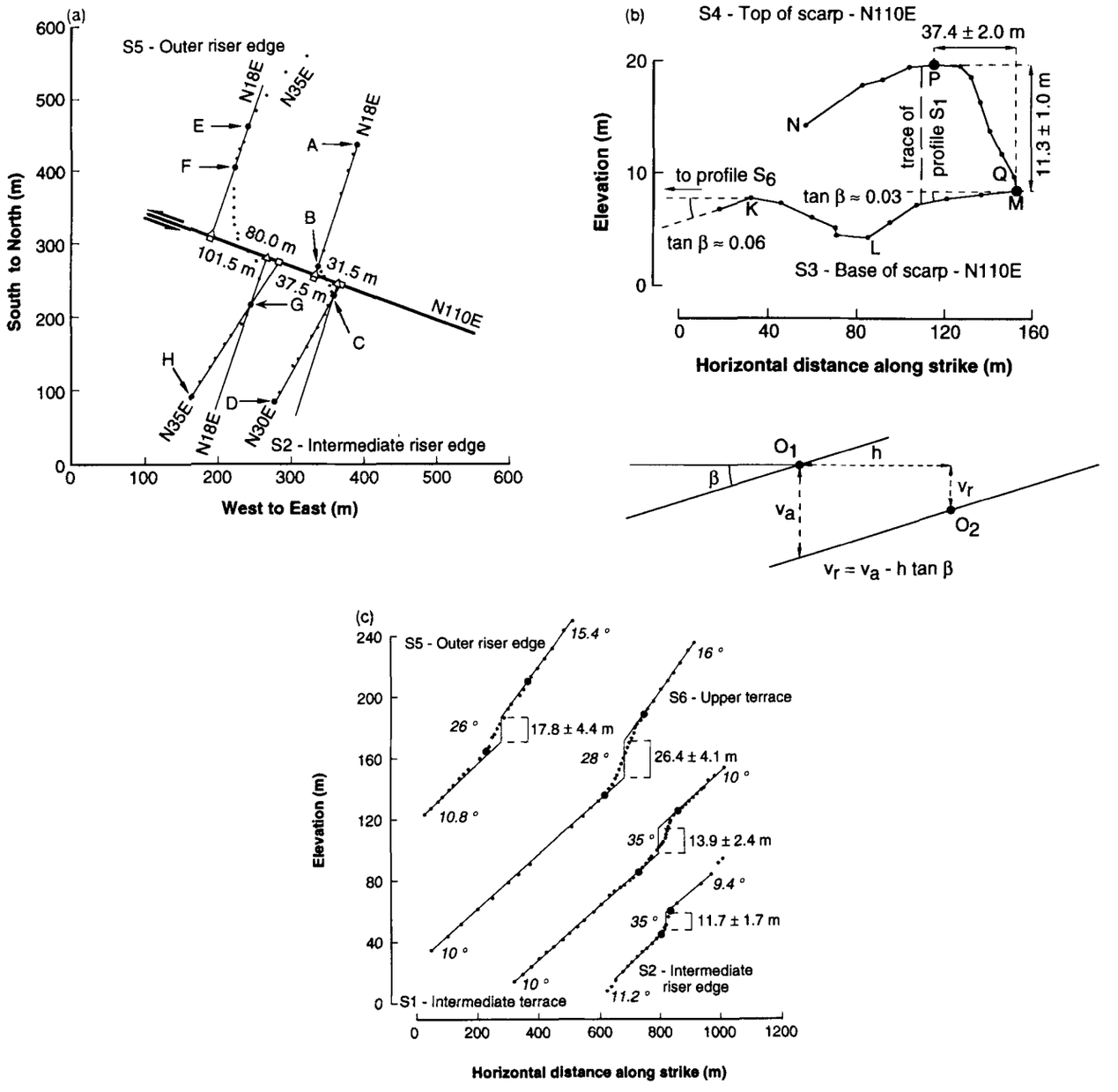

Figure 6. (a) Horizontal projection of terrace-risers profiles S2 and S5 at Sange Dun. Dots are levelling points. Thick solid line is fault trace. Thin lines are best fits to well-defined riser segments, discussed in text. Solid circles, open squares and triangles are points referred to in text. (b) Projection, on N110E-striking, vertical plane, of profiles S3 and S4 (top and bottom of scarp). Vertical exaggeration is 5. Symbols as in 6(a). Inset shows elements used in correcting apparent vertical offset due to surface slope parallel to fault, as discussed in text. (c) Projection, on a N20E striking, vertical plane, of profiles S1, S2, S5 and S6. Thin lines are best fits to slopes, discussed in text. Other symbols as in 6(a). (d) Relationship between various horizontal and vertical offsets at Sange Dun. Shaded sector shows range of vertical/horizontal-offset ratios consistent with constant slip vector for all three terraces. Solid circles within shaded boxes, and corresponding numbers, are preferred estimates of vertical and horizontal offsets, with attached uncertainties, discussed in text. (e) Comparison between offset distribution along Zhuanglang He Fault in Table 1(b) and offsets measured at Sange Dun. Light-gray filled curve is cumulative probability of offset values when ascribing a Gaussian probability function to each offset value of Table 1(b). Dark-grey filled curves are Gaussian probability functions for each offset measured or calculated at Sange Dun site.

scarp with a strike varying between NS and N150E. From the scarp base onwards (G, Figs 6a and c), the downstream segment of the riser veers back clockwise to N18E, then to N35E, a strike that it keeps for at least 150 m (to H, Fig. 6a). As for the intermediate terrace riser, inferences on the initial strikes of well-defined segments of this outer terrace riser upstream and downstream allow bounds to be placed on its offset by the fault. Taking both riser segments above and below the fault to have had initial strikes of N18E yields a cumulative left-lateral offset of 80.0 ± 1.0 m (open triangles, Fig. 6a, Table 1a). Taking the better-defined strike (N35E) of the longest downstream segment would increase

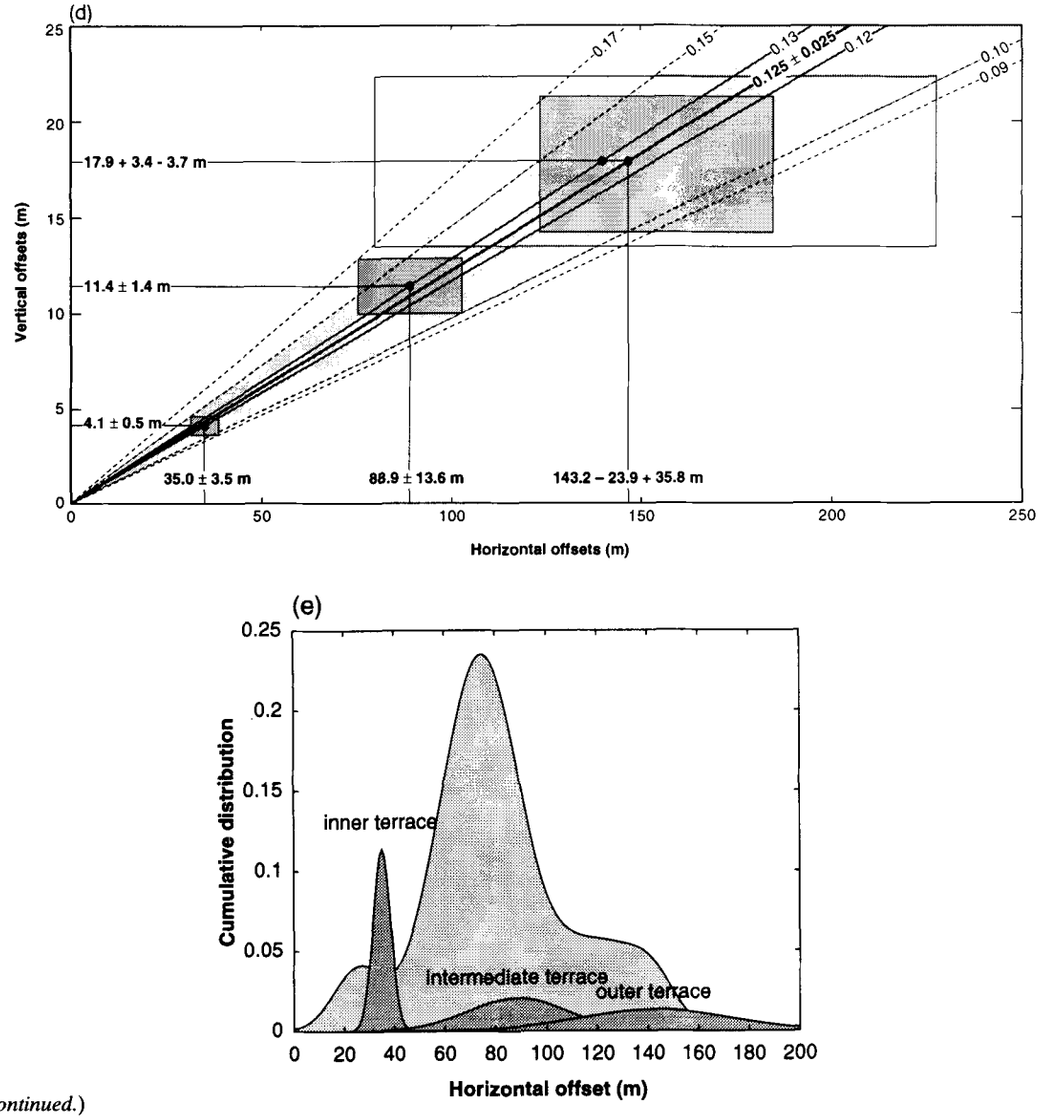

Figure 6. (*Continued.*)

that offset to 101.5 ± 1.0 m (open squares, Fig. 6a, Table 1a). Finally, the distance, along the N110°E fault strike, between the points that define the top and base of the fault scarp on profile S5 (F and G, Figs 6a and c) is 85.1 ± 1.0 m (Table 1a). As above, we assume the arithmetic mean of these three values (88.9 m), and the maximum difference between any of them and that mean (13.6 m), to correspond to the most plausible value of, and uncertainty on, the horizontal offset of the outer terrace riser (Table 1a).

Projecting S1 on a vertical plane striking N20E, perpendicular to the fault, shows that the intermediate terrace surface slopes ≈10°SW, both above and below the scarp (Fig. 6c). The scarp itself slopes 35°SW, a value close to the angle of repose of loosely consolidated alluvium (e.g. Hanks *et al.* 1984). The cumulative vertical throw on the fault is thus simply the vertical offset between the upper and lower segments of the profile (13.9 ± 2.4 m, Fig. 6c, Table 1a). Measured on the projection of the riser profile (S2) on a N20E-striking vertical plane, that throw comes out to be smaller (11.7 ± 1.7 m, Fig. 6c). This latter value is close to that deduced from projecting S3 and S4 on a vertical plane parallel to the fault (11.3 ± 1.0 m, elevation difference between *P* and *M*, Fig. 6b, Table 1a).

On profile S6, the outer terrace has different, but well-constrained, slopes above (16°SW) and below (10°SW) the scarp. The corresponding cumulative vertical throw is 26.4 ± 4.1 m (Fig. 6c, Table 1a). As for the intermediate terrace, that throw is smaller (17.8 ± 4.3 m, Table 1a) when measured on the projection of the outer riser profile (S5) on a N20E-striking vertical plane (Fig. 6c). This latter value is poorly defined, however, because that riser has suffered significant slope and elevation changes since formation. The tell-tale sign that such changes have occurred is the less distinct, much smoother shape of the cumulative fault scarp on S5 than on S6 (Fig. 6c). Close inspection shows that a small stream has incised across the riser near the scarp top and that another one, flowing near the riser base above the fault, has degraded its slope, thus lowering the elevation of

Table 1(a). Summary of vertical and horizontal offsets at Sange Dun site (u. = upstream, d. = downstream).

Sange Dun site	Outer Terrace		Intermediate Terrace riser		Inner Terrace riser	
Horizontal offsets	r = 0.13 ± 0.04	139.8 +90 - 60 m	S5 u. strike N18E d. strike N18E	80.0 ± 1.0 m	S2 u. strike N18E d. strike N18E	31.5 ± 1.0 m
	r = 0.125 ± 0.025	143 + 36 - 24 m	S5 u. strike N18E d. strike N35E	101.5 ± 1.0 m	S2 u. strike N18E d. strike N30E	37.5 ± 1.0 m
			S5 distance between projections of F and G on N110E vertical plane	85.1 ± 1.0 m	S2 distance between projections of B and C on N110E vertical plane	33.5 ± 1.0 m
					S3 and S4 horizontal distance between P and M	37.4 ± 1.0 m
	Preferred value	**143 + 36 - 24 m**	**Preferred value**	**88.9 ± 13.6 m**	**Preferred value**	**35.0 ± 3.5 m**
Vertical offsets (surfaces)	S6 u. slope 16° d. slope 10°	26.4 ± 4.1 m	S1 u. slope 10° d. slope 10°	13.9 ± 2.4 m		
	S6 corrected for N70W slope of 0.06 (see text)	18.0 ± 4.5 m	S1 corrected for N70W slope of 0.03 (see text)	11.2 ± 2.8 m		
	S5 u. slope 15.4° d. slope 10.8°	17.8 ± 4.3 m	S2 u. slope 11.2° d. slope 9.4°	11.7 ± 1.7 m		
			S3 and S4 elevation difference between P and M	11.3 ± 1.0 m		
	Preferred value	**17.9 ± 4.4 m**	**Preferred value**	**11.5 ± 1.4 m**		

Table 1(b). Horizontal stream and riser offsets along a 4.5 km long stretch of Zhuanglang He Fault, west and east of Sange Dun, visible on air photo of Fig. 4.

Catchment 1	122 ± 15 m	105 ± 15 m		
Catchment 2	79 ± 15 m			
Catchment 3 (Sange Dun)	*35 ± 3.5 m*	*88.9 ± 13.6 m*		
Catchment 4	26 ± 15 m	70 ± 15 m	79 ± 15 m	
Catchment 5	70 ± 15 m	87.5 ± 15 m	140 ± 15 m	87.5 ± 15 m
Catchment 6	53 ± 15 m	70 ± 15 m	61 ± 15 m	

its top to less than that of the outer-terrace surface on S6 (Figs 4b, d and 6c). Furthermore, below the fault, the latter stream has encroached upon the left-laterally displaced riser and, by depositing a small fan, raised the elevation and changed the slope of the outer terrace (Figs 4b, c and 6c). To account for these complexities, the 17.8 ± 4.3 m throw in Table 1(a) was calculated by forcing the slopes of the uppermost and lowermost segments of the outer riser on S5 to match as closely as possible those found for the outer terrace on S6 (15.4° versus 16°, and 10.8° versus 10°, Fig. 6c).

Because terrace surfaces on the right bank of the Sange Dun stream slope westwards, parallel to the fault (β, Fig. 6b), left-lateral offsets h by the fault increase the vertical offsets derived from profiles perpendicular to the fault (S1 and S6) by the quantity $h \tan \beta$ (Fig. 6c, insert on top). The real cumulative vertical throws v_r of the terrace surfaces by the fault are thus:

$$v_r = v - h \tan \beta. \quad (1)$$

Assuming the age of a terrace riser to be the age of the terrace at its base (e.g. Weldon & Sieh 1985; Bull 1991; Avouac *et al.* 1993), the cumulative horizontal offset of the

outer-terrace riser relates to the cumulative vertical throw of the intermediate terrace surface. For this terrace, $\tan\beta \approx 0.03$ (Fig. 6b). With a cumulative left-lateral offset of ≈88.9 m, the vertical-offset correction due to strike-slip motion thus amounts to ≈2.7 m, bringing the real vertical throw of that terrace on S1 to 11.2 ± 2.8 m (Table 1a), much closer to the offset of its riser top (11.3–11.7 m, Table 1a). We take the arithmetic mean of the three values (11.4 m), and the average error (1.4 m) on the two values that do not depend on slope correction to be the most plausible value of, and uncertainty on, the vertical offset of the intermediate terrace (Table 1a).

For the outer terrace, $\tan\beta \approx 0.06$ (Fig. 6c), but the cumulative horizontal offset is unknown. It seems reasonable, however, to assume that the attitude of the slip vector has not changed significantly between the emplacement of the outer and intermediate terraces. Therefore, the ratio between vertical throw v and horizontal displacement h by the fault ($r = v/h$) should be similar for both. Taking the ratio obtained for the intermediate terrace (0.13 ± 0.04) yields a real, corrected vertical throw of the outer-terrace surface

$$v_r = v/[1 + (\tan\beta/r)] \quad (2)$$

of 18.0 ± 4.5 m (Table 1a). This value is also much closer to the throw of the riser top on S5 (17.8 ± 4.3 m, Table 1a). The mean of these two values is 17.9 ± 4.4 m (Table 1a). With $r = 0.13 \pm 0.04$, such a vertical throw corresponds to a left-lateral offset of 139.8 m, between extreme values of 79.9 and 227.6 m (−60/+90 m, Table 1a).

The values of the left-lateral offsets and vertical throws of the three inset terraces, five of which derive from independent measurements, are summarized on the plot of Fig. 6(d). That the ratios between offset and throw for the inner and intermediate terraces are nearly identical (0.12 ± 0.03 versus 0.13 ± 0.04) supports the assumption that the attitude of the slip vector on the Zhuanglang He segment of the western Haiyuan Fault remained constant in recent times, as observed on other active, oblique-slip faults (e.g. Peltzer *et al.* 1988). This, in turn, permits us to place tighter, more plausible bounds on the throw and offset of the outer terrace. By assuming that they must be within the range of the throw/offset ratios common to the inner and intermediate terraces ($0.10 \leq r \leq 0.15$), such throw and left-lateral offset values become $17.9 \pm 3.4/-3.7$ m and $143 + 36/-24$ m, respectively (Fig. 6d, Table 1a).

The values, listed in Table 1(a), of the three horizontal offsets measured in the field at Sange Dun, are not unique to that site. Table 1(b) shows, for comparison, the left-lateral offsets of streams and risers in five catchments that cross the Zhuanglang He segment of the fault east and west of Sange Dun, over a distance of ≈4.5 km (Fig. 3). Such offsets, which are derived from inspection of an enlarged print of the aerial photo in Fig. 3(a), are only indicative, since they are not corrected for optical distortion. Nevertheless, most of them appear to cluster between 70 ± 15 and 105 ± 15 m, consistent with the 88.9 ± 13.6 m offset at Sange Dun. The overall range of offsets (from 26 ± 15 to 140 ± 15 m) is also consistent with that seen at Sange Dun (Table 1, Fig. 6e). Recall finally that the two clear postglacial-stream channel offsets visible in the Lenglong Ling (85 and 100 m, Fig. 2b) compare well with that of the intermediate terrace riser at Sange Dun (Table 1).

To our knowledge, none of the terraces at Sange Dun has been directly dated. Given the high elevation of the site (3400–3500 m) at 37°25′N, the fresh morphology of the high-level terraces, and the steep slopes of the prominent cumulative fault scarps that cut them, however, there can be little doubt that both the terraces and scarps postdate the last glacial maximum. Moreover, the rather large size of the terraces, and the fact that their material contains abundant reworked glacial boulders, suggests that the emplacement of that material, possibly in part by debris flows, was related to deglaciation, starting with melting of the ice that filled the now ice-free glacial cirques hanging right above the site, followed by increase in pluvial run off (e.g. Gasse *et al.* 1991). We infer that such deglaciation occurred roughly in tune with the rapid global warming that marked the onset of the present interglacial, causing the rapid rise of sea-level between 14 and 11.5 ka B.P. (Fairbanks 1989; Bard *et al.* 1991), and culminating in the Early Holocene climatic optimum. Melting of the ice on Lenglong Ling, followed by greater rainfall, would have temporarily increased the water discharge, inducing fast and powerful flush by the streams and deposition of coarse, boulder-rich debris near the foot of the range, at the edge of the Zhuanglang He basin. Lowering of the base level in the Zhuanglang He basin, in part due to normal throw on the Haiyuan Fault, would have led to stream entrenchment and abandonment of the high-level terraces, particularly upstream from the fault. The emplacement of several prominent postglacial terraces and fans along other high mountain piedmonts of western China appears to have followed similar patterns, orchestrated by climate change (e.g. Peltzer *et al.* 1989).

Assuming the oldest, outer terrace at Sange Dun to have been emplaced at 13.5 ± 2 ka B.P. would imply average horizontal and vertical slip rates of 11 ± 4 mm yr^{-1} and 1.3 ± 0.5 mm yr^{-1}, respectively (see Table 3 later), on the western Haiyuan Fault. If such rates had been constant, the age of the intermediate and inner terrace surfaces would be 8.4 ± 4 ka B.P. and 3.0 ± 1.5 ka B.P., respectively.

While the evidence we have at hand is insufficient to constrain with accuracy the parameters of individual seismic events on the Zhuanglang He segment of the western Haiyuan Fault, it is suggestive of rupture during infrequent, great earthquakes. That the 4 m high scarp across the inner terrace has been smoothed by erosion and cannot be traced within the high cumulative scarps of the intermediate and outer terraces (Figs 4c and d) suggests that the last rupture of that fault segment is at least several centuries old. This inference is corroborated by the lack of large ($M \geq 7$) recorded historical events in the region between the ancient cities of Lanzhou and Wuwei (Fig. 1) since 1125 A.D., 869 years ago. If the fault at Sange Dun were to break only during similar great earthquakes with return periods of the order of 800 years, the cumulative horizontal offset and throw of the inner terrace could result from four such earthquakes, each with a left-lateral slip of the order of 8.8 m. If the horizontal offset of the inner terrace were due to only three great earthquakes, then such earthquakes would be characterized by individual slip amounts of ≈11.7 m and would recur every ≈1060 years. In either case, the slip amount per event would imply a magnitude of at least 8. While such slip values are common, it seems

less likely that the inner-terrace offset could be the product of only two earthquakes, for such events would have caused ≈17.5 m of horizontal slip each, an amount ≈25 per cent greater than the largest known in any strike-slip earthquake worldwide. The magnitude, slip amounts and recurrence times we infer to be most plausible for large seismic events on the Zhuanglang He segment of the western Haiyuan Fault are thus roughly comparable to those of a Haiyuan-type event on the eastern Haiyuan Fault (Zhang *et al.* 1987, 1988a).

Tianzhu pull-apart basin

Five kilometres east of Sange Dun, the main strand of the western Haiyuan Fault takes a sharp bend to the north-east, forming an outstanding, ≈10 km long, cumulative scarp bounding the eastern side of the Tianzhu Basin (Figs 1, 2a and 7). That scarp, whose strike swings between N10E and N90E, truncates mountain spurs and marks the steep base of large triangular facets with hanging 'wine-glass' valleys, attesting to recent and fast normal uplift (Figs 7 and 8). The height of the triangular facets increases towards the north-east and the visible throw of the cumulative scarp commonly reaches tens of metres. In addition, a few subsegments of the Tianzhu Fault that strike N60 to 90E offset streams within active fan-heads in a left-lateral sense, on aerial photographs (Fig. 7). Near 102°50′E, the Haiyuan Fault bends back to a N125E, then N110E strike (Fig. 2a). In contrast with that west of Tianzhu, the recent vertical offset of the topography remains moderate for several kilometres east of that bend. Left-lateral offsets, on the other hand, are clear on SPOT images and aerial photographs. The southern side of the Tianzhu Basin appears to be bounded by a ≈N110E-striking fault, in rough continuity with the Zhuanglang He segment of the Haiyuan Fault, but with much more subdued morphological evidence of Late Quaternary movement. Similarly, there is little evidence of prominent Late Quaternary faulting along the eastern side of the Tianzhu basin.

The visible fill of the basin is composed of Quaternary fanglomerates that have been fed mostly from the south and west, and that form three main sets of imbricated surfaces. In the east-central part of the basin, the highest, most ancient, fan surface has been incised tens of metres by streams that drain the basin northwards (Figs 7a and b). In the western part of the basin, small active fans built by streams incising the faulted rangefront lap onto the surface that caps much of the subsiding hanging wall of the Tianzhu Fault (Fig. 7). Save for these fans, and despite the fairly high average elevation (2900 m), the entire basin is cultivated, due to the presence of a top-soil layer of loess. Although geologic maps available to us here provide insufficient detail (Gansu Geological Bureau 1975), it is possible that the oldest fanglomerates visible in the basin postdate the last glacial maximum.

For a first-order quantitative assessment of recent movement on the Tianzhu Fault, we selected one site in the south-west corner of the basin (Figs 7 and 8). At that site, the fault cuts and offsets the heads of two alluvial fan complexes bounded by higher, truncated spurs carved into the Lower Palaeozoic bedrock. Deposition and incision by rivers in the footwall has produced inset terraces within the fan heads, causing prominent changes in scarp height along the fault (Figs 8a and b). Unfortunately, although the fault strikes between N30E and N70E across the site (Figs 8b and c), we found no clear evidence of left-lateral movement along the more easterly striking parts of the scarp. In contrast with the differentially uplifted surfaces on the footwall of the fault, the hanging-wall surface is mantled by a rather uniform fanglomerate cover, implying that deposition prevailed, smoothing out most terrain irregularities, except for a few risers bounding flood channels of present-day streams. We infer such widespread deposition to have hidden evidence for cumulative horizontal offsets. Besides, sustained accumulation of fanglomerates upon the hanging wall makes all cumulative vertical offsets measured at that site lower bounds of the actual offsets.

Six profiles (T1 to T6) were levelled roughly perpendicular to the fault scarp (Figs 8c and 9). The uniformity of the hanging-wall surface, which slopes 6°–7° SW for hundreds of metres on all profiles (Fig. 9, Table 1a) is quite clear. But the footwall segments of the profiles, even on top of the highest bedrock spurs, also have fairly regular slopes, steeper by only 4–5° (up to 10–12°, Fig. 9, Table 1a). This implies, in particular, that the bedrock surface on top of the truncated spurs has been abraded and flattened by efficient surface-shaping processes, probably of glacial or periglacial nature. Besides having similar slopes, the hanging-wall segments of profiles T2, T3 and T5 have absolute elevations within ≈2 m of each other. On the other hand, the hanging-wall segment of T6 stands as much as ≈14.5 m above that of T1. Thus, between those profiles, that are farthest apart (≈500 m, Fig. 8c), the hanging-wall surface slopes gently, by about 2°NE, towards the northern outlet of the Tianzhu Basin (Fig. 7).

Though separated by a small, hanging-stream valley, the two highest spurs to the east stand at similar elevations (Fig. 8a). The maximum scarp slopes on the corresponding profiles (T1 and T2), 37° and 30°, are comparable to those at Sange Dun (Fig. 9, Table 2). Here, however, bedrock, which maintains steeper slopes for longer times than alluvium does (e.g. Wallace 1978), forms the top of the cumulative scarp. The scarp heights on T1 and T2, 45.5 ± 2.4 m and 41.2 ± 2.5 m respectively, yield the maximum throw visible at the site (43.4 ± 4.6 m, Table 2). The footwall segment of profile T4, on the spur separating the two fans (Figs 8b and 9), lies on top of the uppermost terrace visible at the site. Although that terrace is chiefly made of fanglomerates containing big boulders, such fanglomerates have filled a previously more irregular bedrock topography. Bedrock asperites, such as that forming the scarp top on T4, thus subsist within the terrace. This accounts for the particularly steep slope of that scarp (41°, Fig. 9, Table 2). The visible height of the cumulative scarp of the uppermost terrace on T4 is 28.2 ± 1.8 m (Fig. 9, Table 2). The footwall segments of profiles T3, T5 and T6 all hug the top surface of the most prominent, intermediate terrace on either side of the T4 spur (Fig. 8b). The cumulative scarp heights on those profiles range from 17.0 ± 2 m to 21.1 ± 1.5 m, with a mean value of 19.5 ± 3.0 m (Fig. 9, Table 2). None of the six profiles reveals the distinctive scar of a recent seismic dislocation within the high cumulative scarps, whether in the form of a steeper freeface or of smoothed out, but visible, slope breaks. Thus,

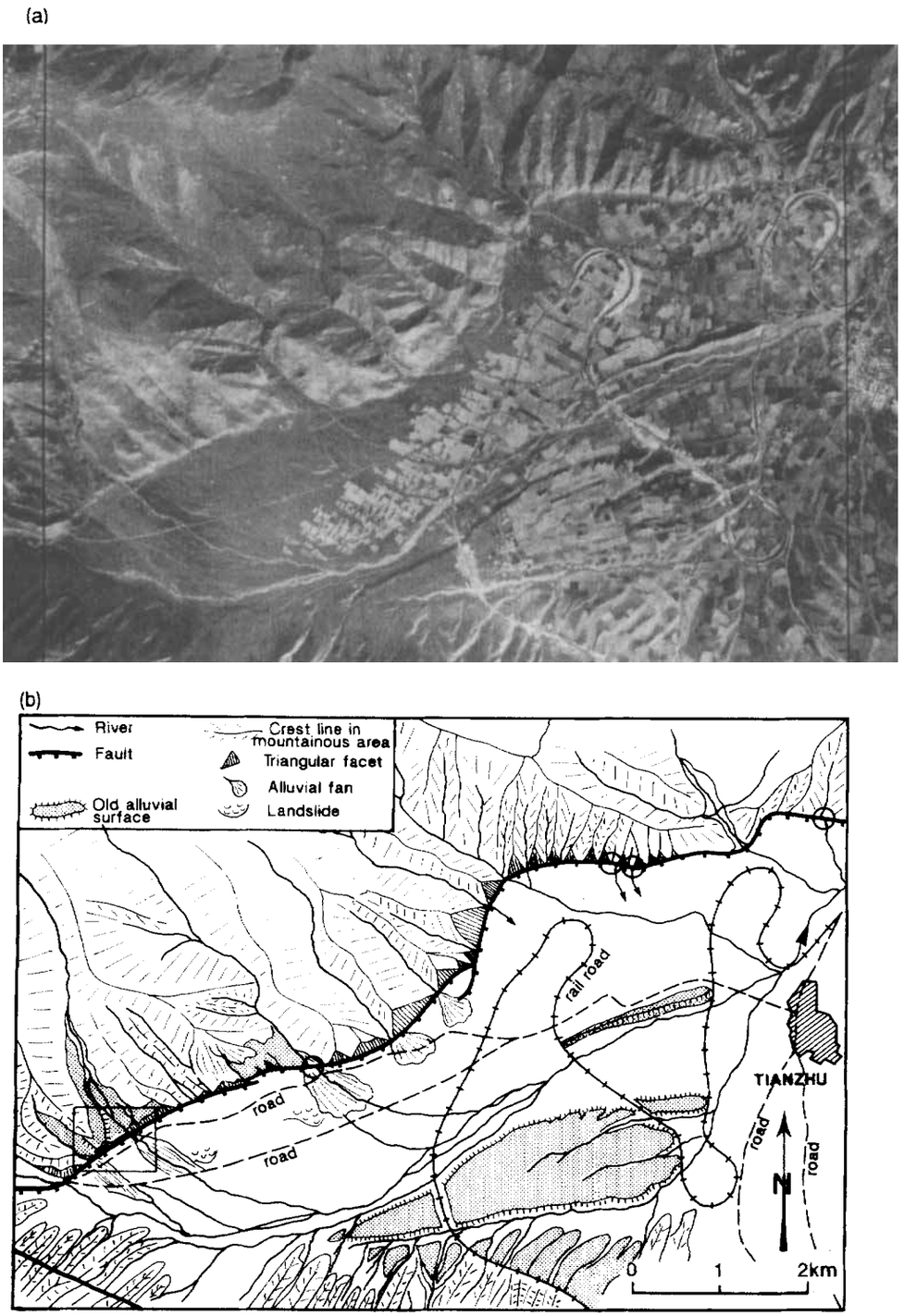

Figure 7. (a) Aerial view of Tianzhu normal fault and western part of Tianzhu pull-apart basin. Note prominent triangular facets along fault, and incised terrace cut by hairpin turns of Lanzhou–Urumchi railroad in centre of basin. (b) Morphotectonic map of area in Fig. 7(a). Circles single out left-lateral offsets of streams along more easterly trending segments of normal fault. Box is location of Fig. 8(c). Scale bar is for centre of picture only. Azimuth of fault is distorted near edges of map.

as at Sange Dun, the last earthquake to have ruptured the west Tianzhu normal fault must be at least several centuries old.

As at Sange Dun, none of the main surfaces that marks the footwall of the Tianzhu normal fault has been directly dated. As observed at that first site, however, only two main fluvioglacial terrace levels have been significantly uplifted by movement on the fault. It is therefore likely that the uppermost and intermediate terrace levels at the south-west corner of the Tianzhu Basin are coeval with the corresponding levels at Sange Dun, only ≈6 km to the west, and result from the same climatic forcing. In keeping with

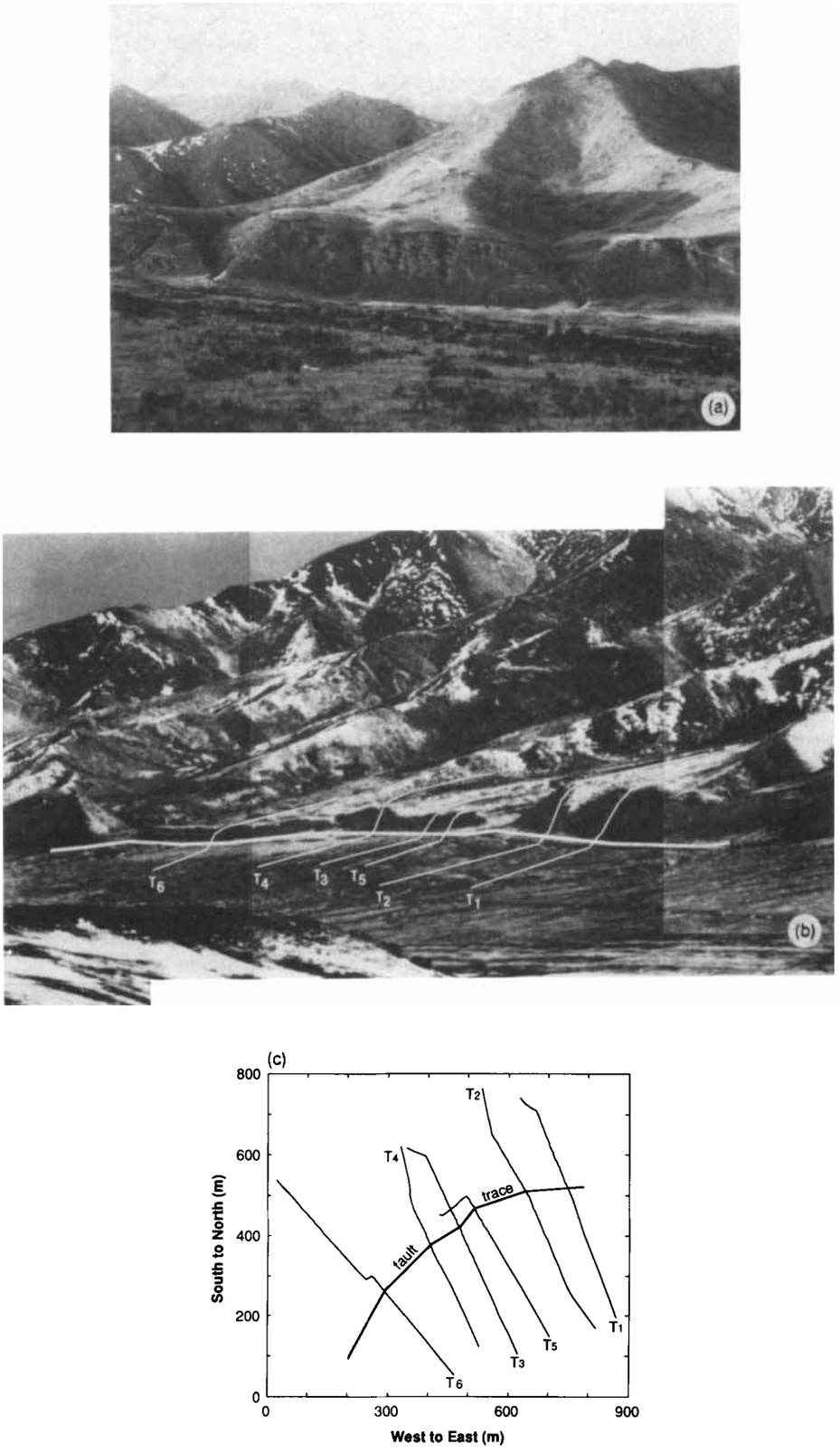

Figure 8. (a) West-looking view of southern part of Tianzhu normal fault. Cumulative scarp in middle ground is 40–45 m high, with prominent hanging valleys and no apparent recent seismic dislocation. Profiles T1 and T2 are on either side of valley to left of photograph. (b) West-looking view of varying offsets of terrace surfaces along whole length of SW Tianzhu site. Thick white line is base of scarp, thin white lines, profiles T1–6. (c) Horizontal projection of profiles levelled across cumulative scarp at SW Tianzhu site.

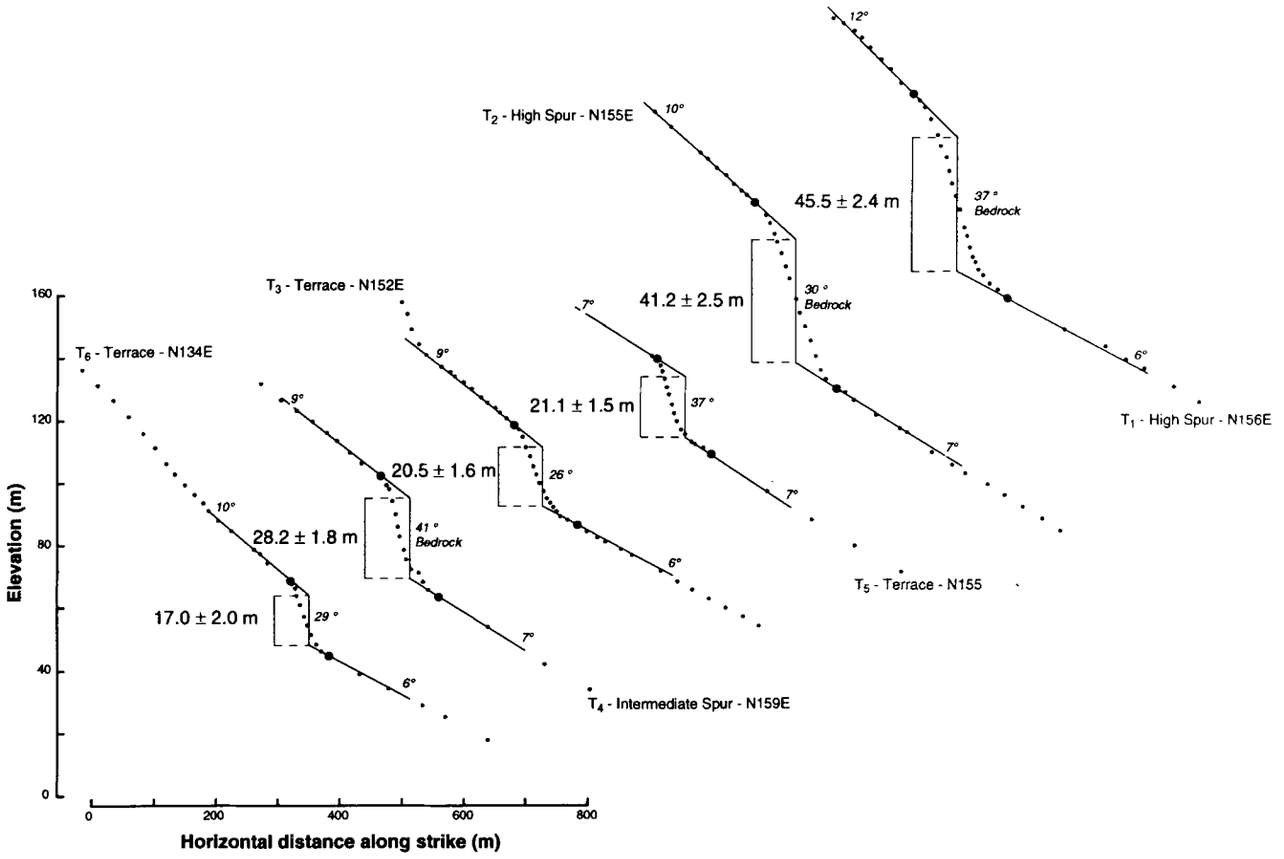

Figure 9. Vertical offsets of terraces and spurs across Tianzhu normal fault at SW Tianzhu site. Vertical exaggeration is five. Symbols as in Figs 6(a) and (c). See discussion in text.

Table 2. Summary of vertical offsets at Tianzhu site.

Tianzhu site	Profiles	Vertical offsets	Scarp slopes
High spur	T1 upstream slope 12° downstream slope 6°	45.5 ± 2.4 m	37°
	T2 upstream slope 10° downstream slope 7°	41.2 ± 2.5 m	30°
	Mean value	**43.4 ± 4.6 m**	
Intermediate spur, higher terrace	T4 upstream slope 9° downstream slope 7°	**28.2 ± 1.8 m**	41°
Intermediate terrace	T3 upstream slope 9° downstream slope 6°	20.5 ± 1.6 m	26°
	T5 upstream slope 7° downstream slope 6°	21.1 ± 1.5 m	37°
	T6 upstream slope 10° downstream slope 6°	17.0 ± 2.0 m	29°
	Mean value	**19.5 ± 3.0 m**	

Table 3. Summary of slip rates at Sange Dun and Tianzhu sites.

	Sange Dun		Tianzhu	
Horizontal slip rate	Outer terrace (13.5 ± 2.0 ka)	11.0 ± 4.0 mm/yr		
Vertical throw rate	Outer terrace (13.5 ± 2.0 ka)	1.3 ± 0.5 mm/yr	High spur surface (18 ± 2 ka)	2.4 ± 0.5 mm/yr
			Uppermost terrace (13.5 ± 2ka)	2.1 ± 0.5 mm/yr
			Intermediate terrace (8.4 ± 4 ka)	2.3 ± 1.5 mm/yr

this interpretation, we assume those two terraces to have ages of 13.5 ± 2 and 8.4 ± 4 ka B.P., respectively (Table 3). We also assume the well-planed surface of the highest spurs, which despite its flatness and uniform slope is not covered by alluvium, to have been smoothed by cryoplanation and gelifluction (e.g. Bloom 1978; Chorley, Schumm & Sugden 1984; Peltzer *et al.* 1988) till the end of the last glacial maximum. Thus, we infer the age of that surface to be 18 ± 2 ka B.P. (Table 3).

Using such ages, the minimum throw rates derived from the visible offsets of the three surfaces are 2.4 ± 0.5, 2.1 ± 0.5 (mean value: 2.3 ± 0.7 mm yr^{-1}) and 2.3 ± 1.5 mm yr^{-1}, respectively (Table 3). That such rates are within a few tenths of a millimetre per year of one another is consistent with the requirement that the slip rate on a segment of the Tianzhu normal fault only 0.5 km long be constant, and supports the inferences made on the ages of the surfaces. Though a lower bound, a throw rate of 2.3 ± 0.7 mm yr^{-1}, about 80 per cent faster than that at Sange Dun (Table 3), is expected from the more abrupt mountain front and more northerly direction of the fault west of Tianzhu.

Lacking information on the postglacial sediment thickness in the Tianzhu Basin, we can only hypothesize what the actual, total throw rate on the Tianzhu Fault might be. Plausible inferences can be made, however, by assuming the rate of deposition to have been roughly the same anywhere along the base of the scarp at any one time since the last glacial maximum (≈18 ka B.P.). Taking the total vertical throw-rate v_t on the Tianzhu Fault to have been constant, and v_{s1}, v_{s2}, v_{s3} to be constant deposition rates between 18 and 13.5 ka B.P. (from the glacial maximum to the onset of deglaciation), 13.5 and 6 ka B.P. (from the onset of deglaciation to the end of early Holocene climatic optimum, Gasse *et al.* 1991), and between 6 ka B.P. and the present, respectively, the throws and ages of the surfaces require such rates to be related by the following linear system:

$$\begin{aligned} 4.5(v_t - v_{s1}) + 7.5(v_t - v_{s2}) + 6(v_t - v_{s3}) &= 43.4 \\ 7.5(v_t - v_{s2}) + 6(v_t - v_{s3}) &= 28.2 \\ 2.4(v_t - v_{s2}) + 6(v_t - v_{s3}) &= 19.5. \end{aligned} \quad (3)$$

Fixing the value of v_{s1} determines uniquely the three other rates. If the sedimentation rate before the onset of deglaciation had been negligible ($v_{s1} \approx 0$), then the total throw rate on the fault would be ≈3.4 mm yr^{-1}, with $v_{s3} \approx 0.8$ mm yr^{-1} and $v_{s2} \approx 1.7$ mm yr^{-1}. Assuming $v_{s1} \approx 1$ mm yr^{-1}, v_c would become ≈4.4 mm yr^{-1}, and subsequent deposition rates $v_{s2} \approx 2.7$ and $v_{s3} \approx 1.8$ mm yr^{-1}, respectively. In the latter case, the corresponding total cumulative throw and sediment thickness deposited since ≈13.5 ka B.P. would be ≈59.4 and 31.2 m. Hence, a little over half the total throw would be hidden by sediment.

Although such calculations, which are non-unique, are given as mere examples, they provide reasonable values. The second one, in particular, balances the visible relief of the scarp with the sediment thickness at its base and implies plausible ratios between deposition rates since the last glacial maximum while yielding a throw rate fast enough to be consistent with the spectacular morphology of the mountain front. That the throw rate on the Tianzhu normal fault should be faster than is typical of isolated normal faults (1–2 mm yr^{-1}) is to be expected because that fault connects two relatively fast-slipping strike-slip fault segments. In southern Tibet for instance, Armijo *et al.* (1986) documented particularly fast throw rates (≥6 mm yr^{-1}) on normal faults linked with the Beng Co right-lateral strike-slip fault, whose horizontal slip rate is of the order of ≈15 mm yr^{-1} (Armijo *et al.* 1989).

Kinematic compatibility between the Zhuanglang He and Tianzhu Faults

The prominent Holocene throw along the Tianzhu normal fault suggests that it takes up most of the movement on the Zhuanglang He Fault (Figs 7 and 10a). It is therefore worth exploring to what extent motion on those faults is compatible if one assumes rigid-block kinematics around the ≈45° bend between them, and what constraints our measurements at Sange Dun and near the SW corner of the Tianzhu Basin then place on fault dips and on the slip vector.

On average, the two faults strike N110E and N65E, respectively, at the sites studied. Near the surface, the dip of the Tianzhu Fault must be greater than the maximum slope of its steepest cumulative scarp (41°). We allow it to vary between 45° and 90° (bold great circles, Fig. 10b). In addition, the existence of left-lateral offsets on N60–90E-striking segments of the Tianzhu Fault east of our levelling site (Fig. 7) implies a left-lateral component of slip at that site too, even though we could not quantify it.

If strain within crustal blocks north and south of the faults were negligible, the slip vector on both fault planes would lie along their intersection (e.g. Armijo *et al.* 1986). Left-slip and a dip ≥ 45° on the Tianzhu fault would thus constrain the azimuth of the slip vector common to both faults to range between N110E and N155E, and the dip of the Zhuanglang He Fault to be at least 55° (light-shaded sector and bold great circle, respectively, on Fig. 10b). Given such a minimum dip, the ratio between postglacial throw and left-lateral offset at Sange Dun ($r = v/h = 0.125 \pm 0.025$, Fig. 6d) would impose tighter bounds on the slip-vector azimuth.

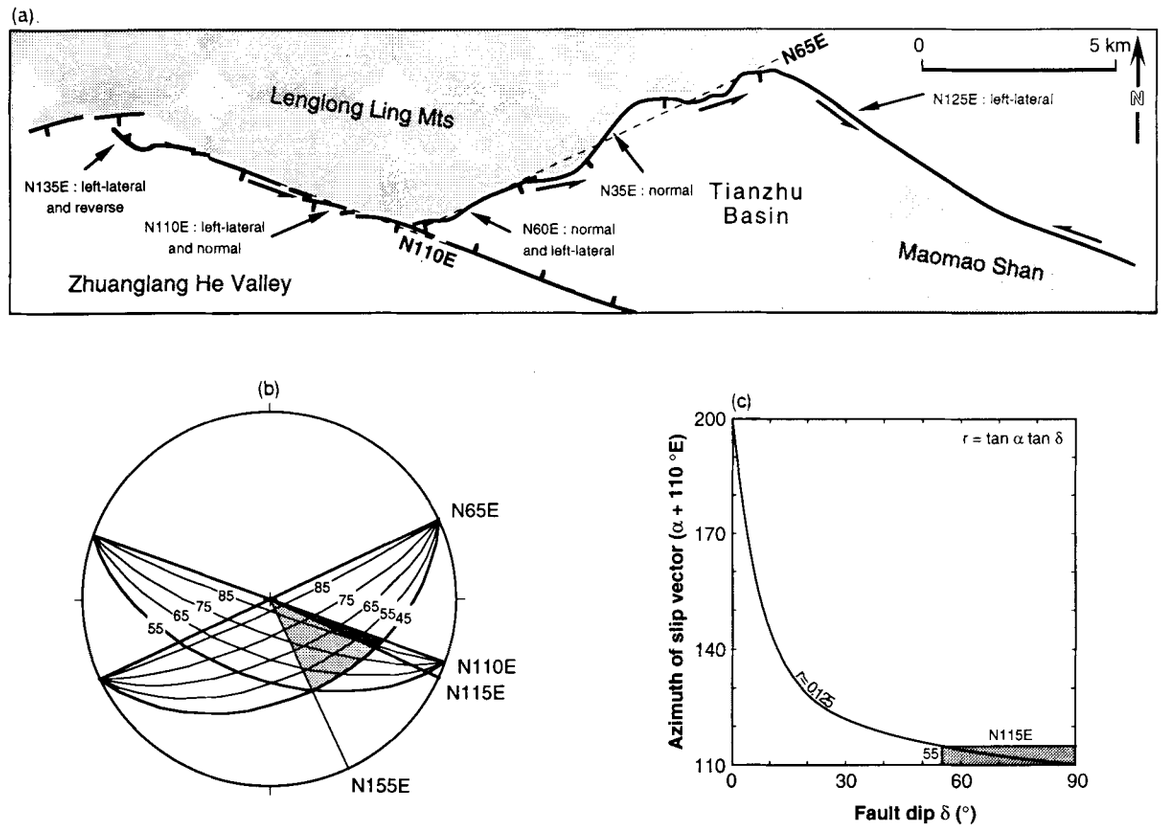

Figure 10. (a) Map summarizing local strikes and slip styles along Haiyuan Fault and Tianzhu normal fault. Shaded area is mountain relief. Arrows nearer to west tip of Tianzhu pull-apart basin point to Sange Dun and SW Tianzhu sites. (b) Lower-hemisphere stereographic projection showing relationship between fault dips and slip-vector azimuths at both sites, assuming rigid-block kinematics around W Tianzhu bend. Shaded sectors indicate ranges of compatible dips and azimuths discussed in text. (c) Plot of slip-vector azimuth as a function of fault dip assuming $r = v/h = 0.125$. Shaded box corresponds to narrowest shaded sector on Fig. 10(b). See discussion in text.

Since this ratio relates the fault-dip δ to the angle α between slip-vector azimuth and fault strike through

$$r = \tan\delta \tan\alpha \qquad (4)$$

that azimuth could only range between N110E and N115E (Fig. 10c, and dark-shaded sector on Fig. 10b). This in turn would force the dip of the Zhuanglang He Fault to be quite steep ($\delta \geq 83°$), and the throw to left-lateral offset ratio on the Tianzhu Fault to be $v/h = (1.1 \pm 0.1)\tan\delta$.

Although both results are in qualitative agreement with the observation that the Zhuanglang He and Tianzhu Faults appear to be predominantly strike slip and prominently normal, respectively, they draw attention to a significant shortcoming of the rigid-kinematics assumption. From the diagram of Fig. 10(b), the plunge of the intersection between the fault planes would have to be steeper than ≈34°, which cannot be reconciled with the steepest slip-vector plunge (≈7°) permitted by the v/h ratio of 0.125 at Sange Dun. That a common slip vector cannot be found along the intersection of the two planes is also clear from comparing the throw estimated from the height of the Tianzhu cumulative scarp to that predicted by rigid-block kinematics from the offsets measured at Sange Dun. Taking the movement on the Zhuanglang He Fault in the last 13.5 ka (≈143 m) to have been transferred rigidly to the Tianzhu fault (with $\delta \geq 45°$) would imply at least ≈106 m of vertical throw on that fault, as much as ≈75 per cent more than inferred with $v_{s1} = 1\ \text{mm yr}^{-1}$.

A sizeable fraction of the horizontal slip on the Zhuanglang He Fault must therefore be taken up, past the bend, by the fault whose more subdued trace follows the southern limit of the Tianzhu pull-apart basin. In keeping with the hypotheses made above, 47 m of left-lateral slip on that fault since 13.5 ka B.P. would be required to bring the coeval offset and maximum throw at Sange Dun and Tianzhu to fit. The corresponding slip rate would be $\approx 3.5\ \text{mm yr}^{-1}$. While that rate could be smaller if the sedimentation rate along the Tianzhu fault had been faster, the evidence we have at hand is insufficient to resolve the trade-off between these two parameters.

Although rigid-block kinematics does not hold at the south Tianzhu bend, the compatibility analysis points to three fairly reasonable inferences. First, the dip of the Zhuanglang He Fault is probably very steep (80–85°), while that of the Tianzhu Fault could not be much steeper than 45°. Second, the slip-vector azimuth along the western Haiyuan Fault near Tianzhu probably lies in a narrow range, between N110E and N115E. Third, the fault along the southern limit of the Tianzhu Basin must be active. At a more detailed level, we take the subdued morphological signature of this latter fault to imply that its postglacial left-slip rate is unlikely to have exceeded $3.5\ \text{mm yr}^{-1}$ (≈30

per cent of that at Sange Dun). Therefore, we find it plausible that sedimentation rates in the western part of the Tianzhu Basin could have exceeded 2.7 mm yr^{-1}, which suggests that this intramontane basin might have remained isolated from outside catchments until recently.

That the last earthquake on either of the two main faults that meet at the south Tianzhu bend is at least several hundred years old suggests that they may slip together during the same event. Given the slip partitioning we infer at that bend, events with ≈8.8 or ≈11.7 m of left-lateral offset at Sange Dun might then produce at least ≈3.5 or ≈4.7 m of normal throw on the west Tianzhu Fault north of the bend. During such events, the south Tianzhu Fault might slip left laterally by as much as ≈2.8 or ≈3.7 m, respectively. Whether this scenario, rather than slip of the three faults in a sequence of distinct earthquakes, possibly clustered in time, is more likely cannot be decided without trenching. But the fact that free faces are known to last at least ≈250 yr on normal fault scarps higher than ≈2 m in west-central China (Zhang *et al.* 1986) supports the inference that if the west Tianzhu Fault does rupture during great earthquakes, it last did long ago.

Maomao Shan-Lao Hu Shan (eastern) segment

From 103°E to 104°E, over a distance of ≈100 km, most of the present movement along the Haiyuan Fault zone is taken up by a principal, continuous strand striking N100–105E on average (Fig. 11). On either side of that strand and less than 10 km north or south of it, subordinate splays or disconnected, active-fault segments strike mostly between N90E and N100E. Between 103°E and 103°20′E, the main fault strand hugs the northern flank of Maomao Shan, a bulky, 40 km long, 8 km wide, mountain ridge that culminates at 4074 m. The core of the mountain exposes Silurian greenschists in the north and Ordovician volcanics in the south, separated by a pinched fault slice of Triassic sandstones parallel to the main active fault strand (Gansu Geological Bureau 1975; Xu *et al.* 1989). We could not reach that strand north of the mountain, but the satellite images and a few aerial photographs reveal high north-facing triangular facets in addition to prominent left-lateral offsets. As expected from the N110–115E slip vector found at Tianzhu, normal throw thus occurs on the fault, though in a sense opposite to that along the Lenglong Ling range, west of the Tianzhu jog (Figs 1 and 2). Such throw must have contributed to uplift the Maomao Shan.

East of Maomao Shan, the main fault strand crosses an area with more subdued relief (Fig. 11), mantled by loess. Whether on SPOT images, aerial photographs or in the field, its strike-slip trace is nonetheless outstanding. It becomes particularly spectacular east of its junction with a west-directed splay that may be linked, through faults along the south side of Maomao Shan, with the south Tianzhu fault (Figs 2, 11 and 12a). In the steppe north-east of Song Shan, a small fortified city whose wall, erected during the Ming Dynasty, stood intact until the $M \approx 5.8$ shock of 1990 October 10 (Figs 1 and 11), a 2 km long pull-apart basin signals a minor left step in the fault trace (Fig. 12b). Towards the west, left-stepping pressure ridges, several metres long and well smoothed by erosion, or a small north-facing scarp limit the floor of that basin (Fig. 13a). Farther westwards, terrace tongues incised several metres deep by the streams that feed the prominent fan north of Song Shan (Fig. 12) have recorded clear cumulative left-lateral displacements. The risers that bound the entrenched stream channels are offset 20–40 m (Fig. 13b). While such evidence is too limited to warrant quantitative analysis, the observation that low-level terraces are offset a few tens of metres and that the last large seismic event to have ruptured the fault is at least several centuries old (the Ming dynasty lasted from 1368 till 1644 A.D.) is in keeping with the conclusions reached at Sange Dun.

East of Song Shan, the western Haiyuan Fault slices the lower-Palaeozoic core of the Lao Hu Shan into two massifs of unequal width but similar elevations (3222 and 3316 m, respectively, Figs 11 and 14). From 103°45′E onwards, a 14 km long, 2400–2800 m high stretch of the fault cuts across the north slope of the southern massif, a fairly rugged area incised by streams with comparable spacing (a few hundred metres) and upstream lengths (1 to 2 km from massif crest to fault trace, Fig. 14b). That stretch displays outstanding cumulative offsets, whether of the stream channels or of the intervening crests, some of which are capped by high-level terraces (Figs 14a). By restoring the linearity, across the fault trace, of left-laterally displaced channels and crestlines clear on the SPOT image, the aerial photographs and the topographic map, we obtained 12 measurements of well-defined offsets (Fig. 14b). The offsets range between extremes of 75 ± 20 and 200 ± 20 m, with 60 per cent of them clustering between 100 ± 20 and 150 ± 20 m, and an arithmetic mean of 120 m. Short of detailed field sampling, which has not been done, one may only hypothesize what the ages of such offsets are. But it is at once apparent that the range of offset values is similar to that of the high-level terrace offsets near Sange Dun and in Lenglong Ling (Figs 6d and e, Table 1a). We interpret this to imply that, although the elevation of the fault trace and of the mountains south of it is 500 to 1000 m lower here than west of Tianzhu, the evolution of landforms was similarly influenced by the warmer, more humid climate that accompanied deglaciation. Hence we infer, as we have at Tianzhu and Sange Dun, that much of the entrenchment of small streams on the north slope of Lao Hu Shan occurred between the last glacial maximum and the end of the early Holocene climatic optimum (18–6 ka B.P.), and that increasing offset values result from increasing ages of entrenchment. Such a range of morphological ages would make postglacial horizontal slip rates on the Maomao-Laohu Shan and Zhuanglang He segments of the western Haiyuan Fault compatible (8.7–13.9 mm yr^{-1} versus 11 ± 4 mm yr^{-1}, Fig. 15a). If for instance, as near Tianzhu, the largest offsets (≈200 m) were 18 ± 2 ka old, the slip rate would be 11.1 ± 2.3 mm yr^{-1}. Similarly, taking the ages of the 120–150 m and 75–100 m offsets to be 13.5 ± 2 ka B.P. and 8.4 ± 4 ka B.P., respectively, as at Sange Dun, would imply rates of 10 ± 3 mm yr^{-1} and 10.4 ± 7 mm yr^{-1}. Recall that the greatest merit of such reasoning, which is no substitute for direct dating of the offsets, is to test whether results that rest on the assumption that landforms over fairly vast regions are principally and coevally shaped by global changes of the climate are self-consistent, as argued in particular by Armijo *et al.* (1986, 1989), Peltzer *et al.* (1988, 1989) and Avouac *et al.* (1993). We think that such

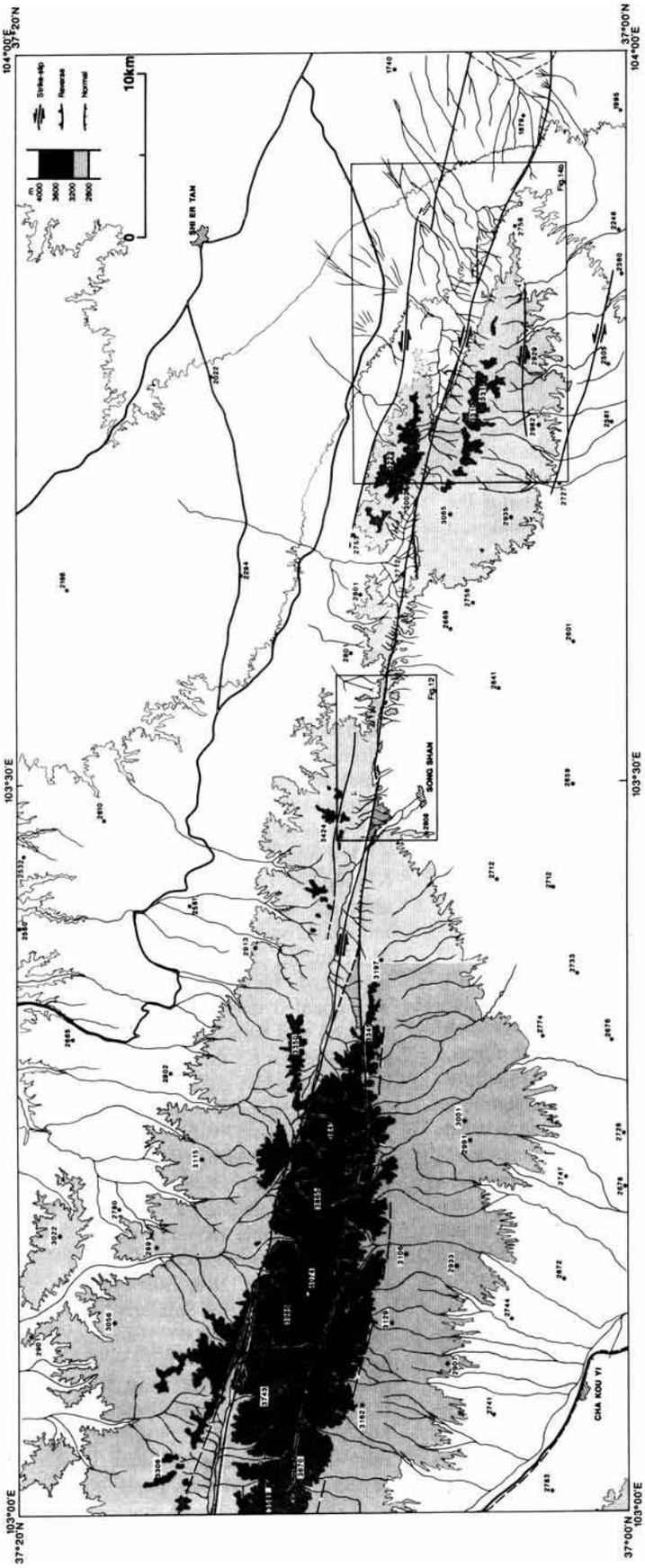

Figure 11. Map of western Haiyuan Fault zone along Maomao and Lao Hu Shan, east of Tianzhu pull-apart basin. Symbols as in Fig. 2. Boxes are locations of Figs 12 and 14.

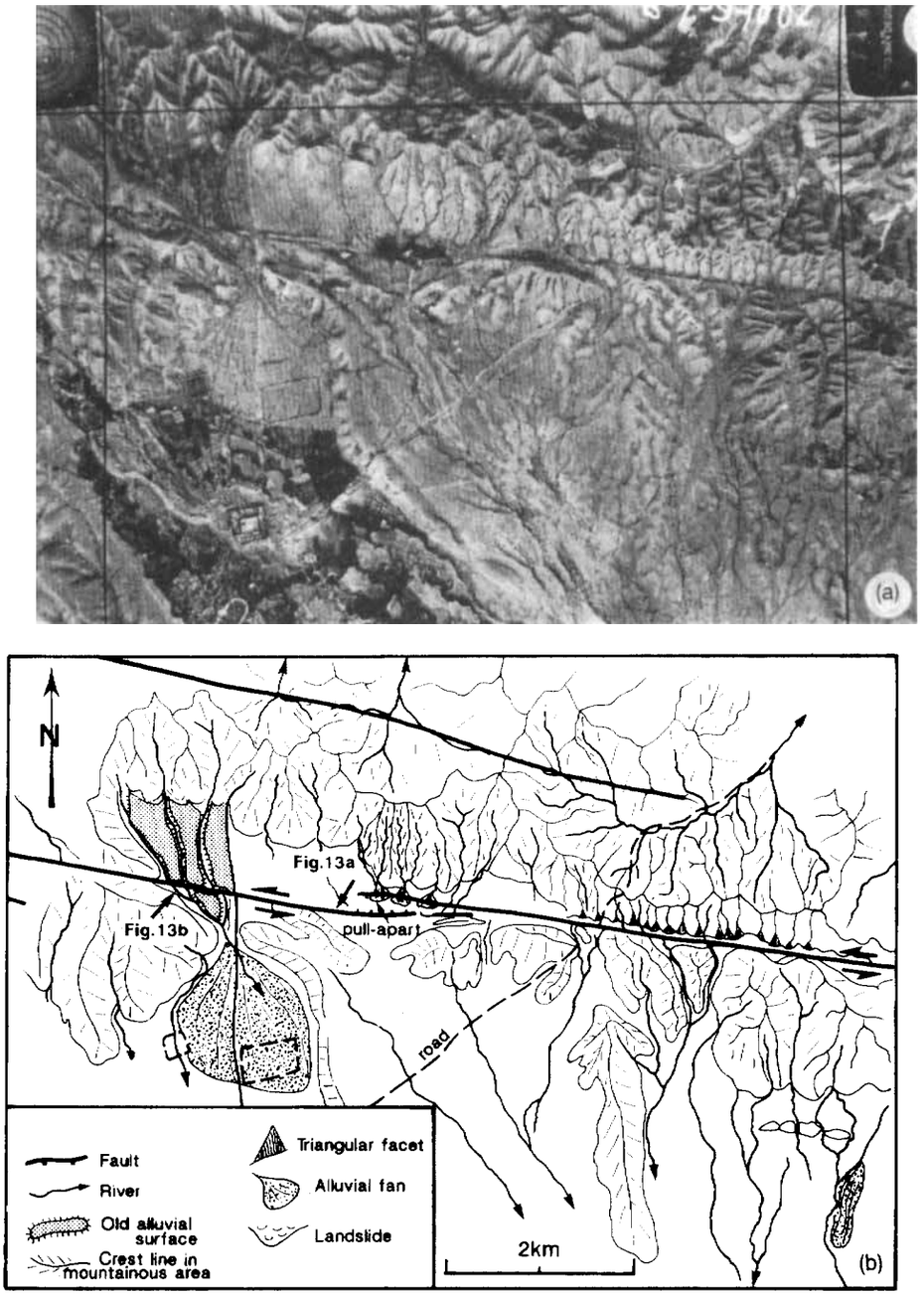

Figure 12. (a) Aerial view of Haiyuan Fault north of walled Ming city of Song Shan (doubly ringed, roughly square house cluster amidst cultivated fields south of large fan on bottom left of photograph). Note spectacular drainage disruption, shutter ridges, and dark, vegetated area along fault trace marking floor of small, left-lateral, Song Shan pull-apart. (b) Morphotectonic map of area shown in Fig. 12(a). Limitation concerning scale-bar and feature azimuth, due to optical distortion, as in Figs 3 and 7. Black arrows show locations of Figs 13(a) and (b), from east to west, respectively.

consistency, for a length of about 200 km, between ≈102° and ≈104°E, along the Haiyuan Fault, may be taken to justify our use of that assumption as a first-order tool.

Whether on satellite images or maps, two left-lateral offsets of much greater size than those discussed above stand out in the topography east of Song Shan. The first one is between the southern and northern massifs of the Lao Hu Shan, which have comparable elevations. In the direction parallel to the fault (N108E), the separation of the massifs eastern tips, as defined by the 2800, 3000, and 3200 m elevation contours on the 1:100,000 topographic map (Fig. 14b), is 7.8 to 11 km. Assuming a constant rate of 11 ± 3 mm yr^{-1}, such a cumulative offset would result from slip on the western Haiyuan Fault since 1 ± 0.4 Ma B.P. (Fig.

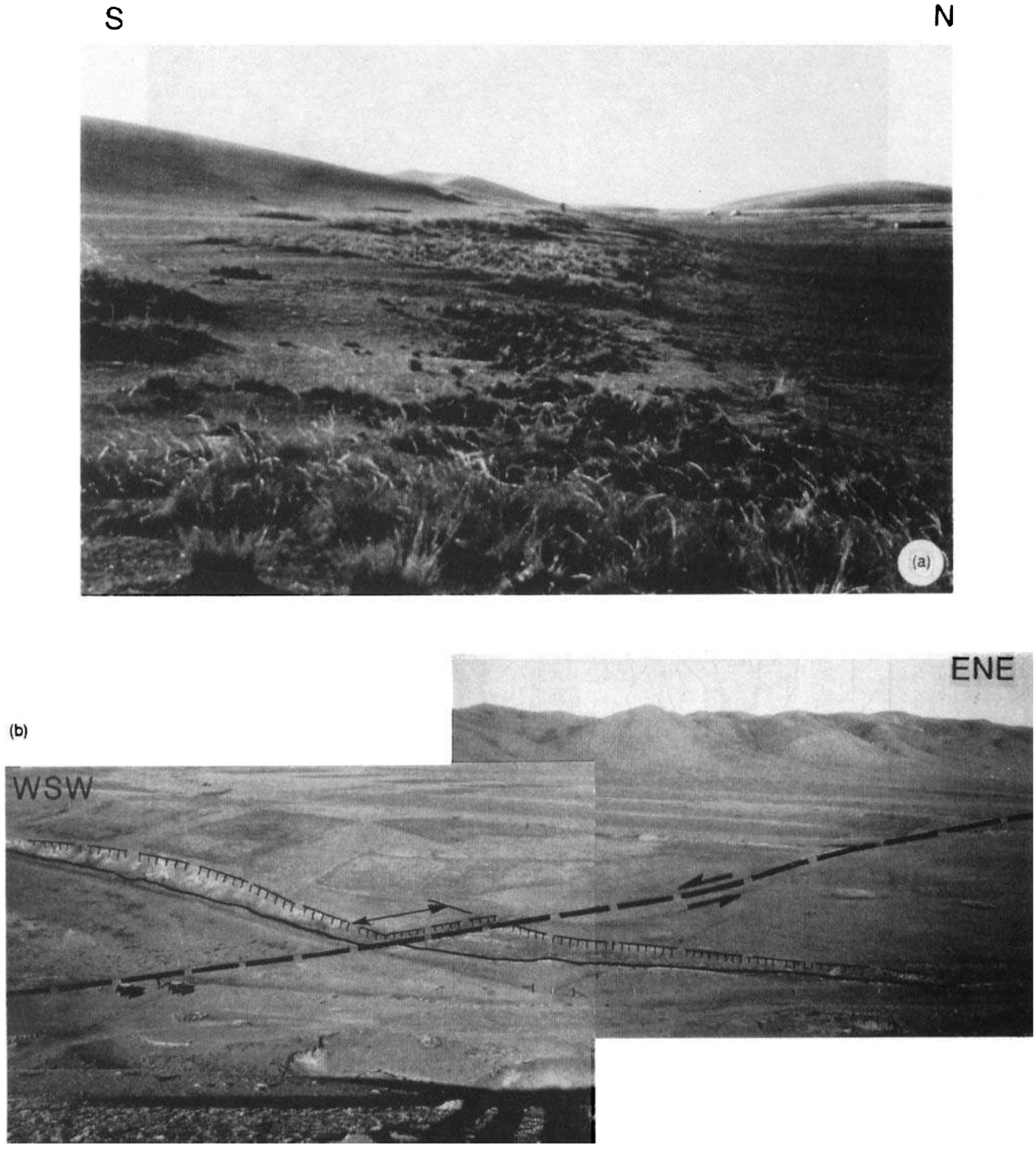

Figure 13. (a) West-looking view of north-facing, Haiyuan Fault scarp and associated pressure-ridges near western extremity of Song Shan pull-apart. Pressure-ridge relief and ground disruption due to last seismic event, now overgrown with short, thick grass tufts, are well smoothed out. Silhouette and two jeeps in background give scale. (b) NE-looking view of left-laterally offset (double-headed arrow) of terrace riser (line with ticks) north of Song Shan. Jeeps give scale. Thick dashed line marks fault trace.

15b). The second one, in our view the most remarkable long-term offset of a large morphological object along the Haiyuan Fault zone, is that of the Huang He valley 100 km north-east of Lanzhou (Gaudemer, Tapponnier & Turcotte 1989). Despite kilometre-wide meanders, the clear, broad-scale swing of the river course across the fault has a nearly symmetrical, sigmoidal shape (Fig. 1). Striking first ≈N–S for ≈15 km past the confluence with the Zuli He, that swing veers to N135–115E over the next ≈40 km, then back to ≈N–S for ≈25 km (Fig. 1). The inflexion in the S-shape does not coincide with the intersection of the river with the present trace of the fault, but lies less than ≈8 km south of

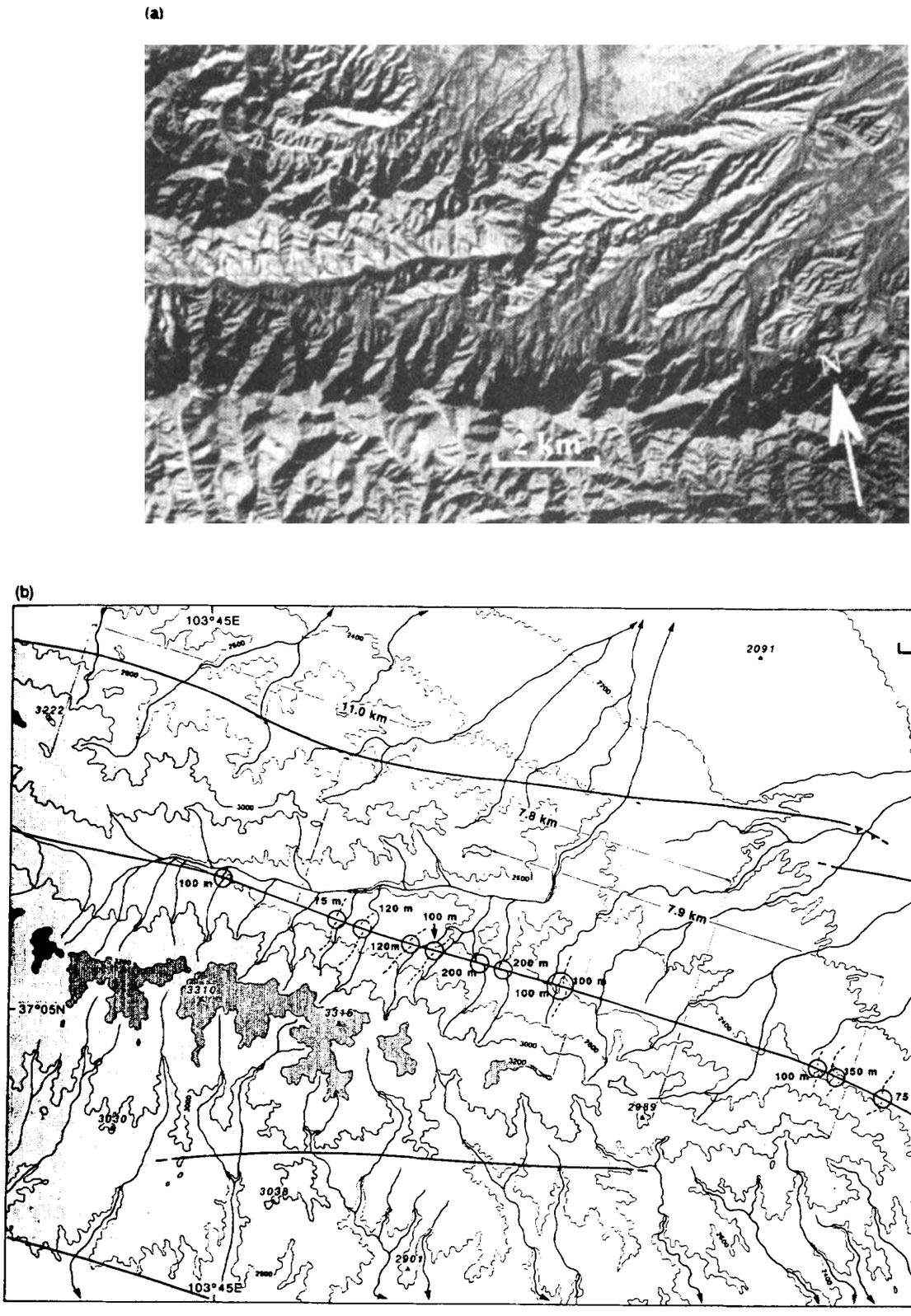

Figure 14. (a) Detail of SPOT scene 257-276 1986 November 12 showing Lao Hu Shan segment of Haiyuan fault, with clear left-lateral offsets of stream channels, risers and intervening hill crests. (b) Enlarged part of Fig. 11 including area shown in Fig. 14(a). Circles and associated numbers point to well-defined short-term cumulative offsets, ranging between 75 and 200 m. Double-headed arrows and associated numbers indicate long-term, 8–11 km cumulative offset of mountain relief, as defined by increasing elevation contours.

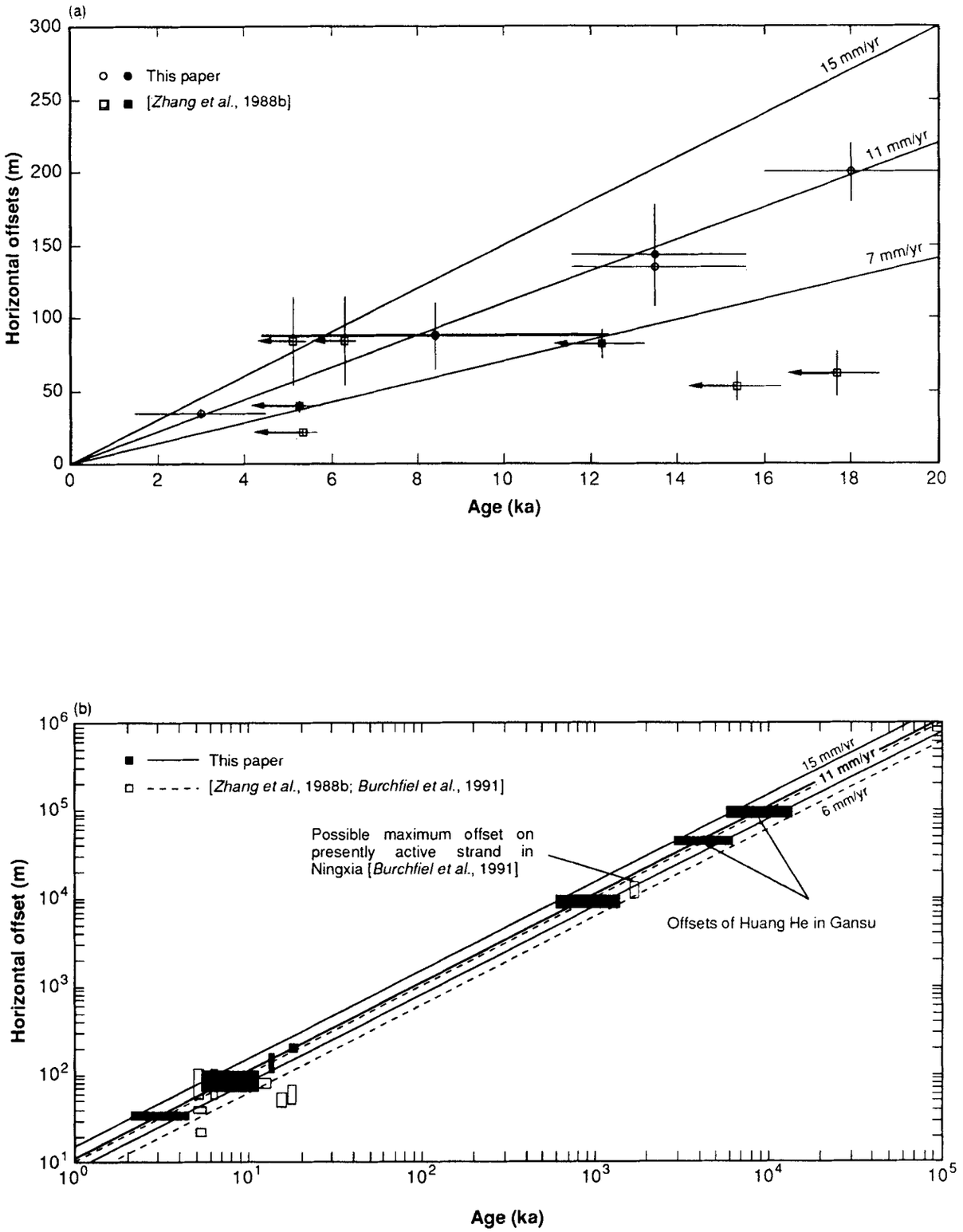

Figure 15. (a) Summary plot of short-term cumulative offsets of morphological features on western and eastern Haiyuan Fault, as function of maximum or inferred ages. Squares are values from Zhang *et al.* (1988b), circles are values discussed in this study. Solid symbols indicate best-constrained, preferred numbers. Vertical and horizontal bars represent estimated uncertainties on offsets and ages, respectively. Left-pointing horizontal arrows recall that Zhang *et al.*'s values are lower bounds. 11 ± 4 mm yr^{-1} is value preferred in this study (see discussion in text). (b) Inferred ages of long-term geological or geomorphic offsets across Haiyuan fault, assuming constant slip rates consistent with short-term, postglacial offsets. Scale is log–log. Boxes are offsets discussed by Zhang *et al.* (1988b), Burchfiel *et al.* (1991) (open symbols), and in text (solid symbols).

that trace, near another Late Cenozoic fault visible both on extant maps (Gansu Geological Bureau 1975; State Seismological Bureau 1990) and satellite images (Fig. 1). Since the swing links two fairly straight, ≈80 km long valley segments with similar average strikes north and south of the fault (N63 ± 3E and N55 ± 3E, respectively, Fig. 1), the offset between the two is well defined. Measuring that offset as we did for the terrace risers at Sange Dun, and allowing the fault strike in the area to range between N100E and N120E, yields a value of 95 ± 15 km. Closer to the fault, the offset of the two NS-striking valley segments within the swing is 45 ± 5 km. Fairly deep entrenchment (≈500 m) of the Yellow River downstream from the fault probably reflects regional uplift of the upper crust above the active, south-dipping Tianjing thrust (Fig. 1). Even upstream, the river meanders in a flood channel (at most 6–7 km wide) that stands well below the summits of the mountainous landscape. The river course has therefore long been captive to the surrounding relief, unable to wander tens of kilometres away as great rivers can do on occasion of millenal floods where flowing across flat plains. Besides, there is little evidence of capture, or of large abandoned river channels, on satellite images or on topographic and geologic maps. Therefore, we infer the 95 ± 15 km left-lateral offset of the Huang He Valley across the Haiyuan Fault zone to represent a lower bound of the total displacement on that zone (Gaudemer *et al.* 1989). At a constant rate of 11 ± 4 mm yr^{-1}, 8.6 ± 4.5 Ma would have been required to produce such an offset, implying slip along the fault zone since the upper Miocene, and at least since the onset of the Pliocene (Fig. 15b). The smaller offset within the Yellow River swing would be mostly of Plio-Quaternary age (4.1 ± 1.9 Ma).

ACTIVE FAULTING AND CRUSTAL SHORTENING NORTH OF THE HAIYUAN FAULT

Recent crustal deformation north of the Haiyuan Fault involves fairly complex faulting, principally along the Gulang left-lateral ramp and the en échelon, Shiyang–Dongqingding thrusts (Figs 1 and 16). There is convincing, though mostly indirect, evidence that the 1927 May 23, $M \approx 8.3$, Gulang earthquake ruptured the latter thrusts rather than the Gulang ramp. Our observations of surface breaks related to that earthquake, however, bear little resemblance to those previously reported (e.g. Jia 1982; Molnar & Deng 1984).

3-D geometry of faulting and regional structure

Gulang Fault

A clear, linear feature on the Landsat image (Tapponnier & Molnar 1977), the Gulang Fault zone splays eastwards from the Haiyuan Fault about 60 km west of Tianzhu (Figs 1 and 16). For ≈150 km, its closely spaced strands strike between N80E and N100E, oblique both to the Qilian Shan front and the Haiyuan Fault. Near 103°45′E, ≈60 km east of Gulang, one strand veers to N110E at the base of the north-dipping limb of a ≈30 km long ridge of folded Palaeozoic rocks. East of that ridge, the ≈EW fault trace becomes less conspicuous as it steps to the north and traverses desert sandy flats. It then resumes its sharpness, crosses the Huang He river along the base of a ≈N100E-striking, ≈500 m high, north-facing topographic step, and merges with the curved trace of the south-dipping, Tianjing Shan thrust ramp (Tapponnier & Molnar 1977; Deng *et al.* 1984; Zhang *et al.* 1990) (Fig. 1).

Left slip on the Gulang Fault is attested by morphological offsets of decametric and kilometric scale. The most outstanding kilometric offset is that of the Gulang River, ≈8 km south of Gulang, which is deflected ≈5 km by a prominent shutter ridge that places uplifted Lower Palaeozoic rocks north of the fault against Cretaceous red beds south of it (Figs 1 and 16b). Clear decametric offsets exist at Tianxiao Kou in the upper valley of the Xiamenzu River (Figs 16 and 17), a ≈4 km wide trough between ≈4400 m high ranges bearing strong, recent glacial imprint. On the north side of the valley, three strands of the fault cut the gently SSE-sloping surface of a terrace that caps abraded Triassic beds (Fig. 17a and b) and is incised 50–90 m by tributaries of the river. Two of the strands, which strike N90–100E, meet with a third, middle strand that bends to ≈N80E (Figs 16 and 17). While the first two strands show only minor dip slip, normal throw is prominent on the middle strand, possibly because of its more northerly azimuth. The northern and middle strands show inconclusive evidence for consistent horizontal offsets on the SPOT image. By contrast, a succession of four entrenched tributary channels are offset left laterally 60 to 70 ± 20 m by the southern strand, which we therefore infer to accommodate most of the strike component of slip along the Gulang Fault zone at this site (Figs 17a and b). Vertical throw on the middle strand has created a north-facing, cumulative scarp up to ≈40 m high on the terrace top (Fig. 17c) and led to deeper entrenchment, hence greater width, of triburary channels south of that scarp (Fig. 17a).

As at Sange Dun, the freshness of glacial landforms around the mountain-locked, ≈3300 m high Tianxiao Kou site implies that incision of the terrace by the tributary streams postdates the last glacial maximum. The terrace forms the highest flat surface north of the Xiamenzu river and covers a broad part of the Tianxiao Kou trough. Moreover, it blends gently with the mountain slope. Hence, we infer much of the planation of the terrace surface to be due to periglacial smoothing, as inferred by Peltzer *et al.* (1988) in a comparable area of western Gansu. While such smoothing probably reached a climax during the last glacial maximum, it could have continued till the onset of rapid deglaciation on the mountains. Assuming entrenchment of the tributary streams to have started at most 18 ka and at least 14 ka B.P., their channel offsets (65 ± 25 m) would be consistent with a constant left-slip rate ranging between 2.2 and 6.4 mm yr^{-1} (4.3 ± 2.1 mm yr^{-1}), in a direction ranging between N85E and N100E (N92 ± 7E), on the Gulang Fault. The 5 km offset of the Gulang River would thus result from slip during 1.5 ± 0.7 Ma. Although the evidence from which such bounds derive is too limited to draw firmer conclusions, the values obtained are in keeping with the qualitative observation that the morphological signature of the Gulang Fault is less impressive, on satellite images and in the field, than that of the Haiyuan Fault, and imply coeval slip on those faults during much of the Quaternary.

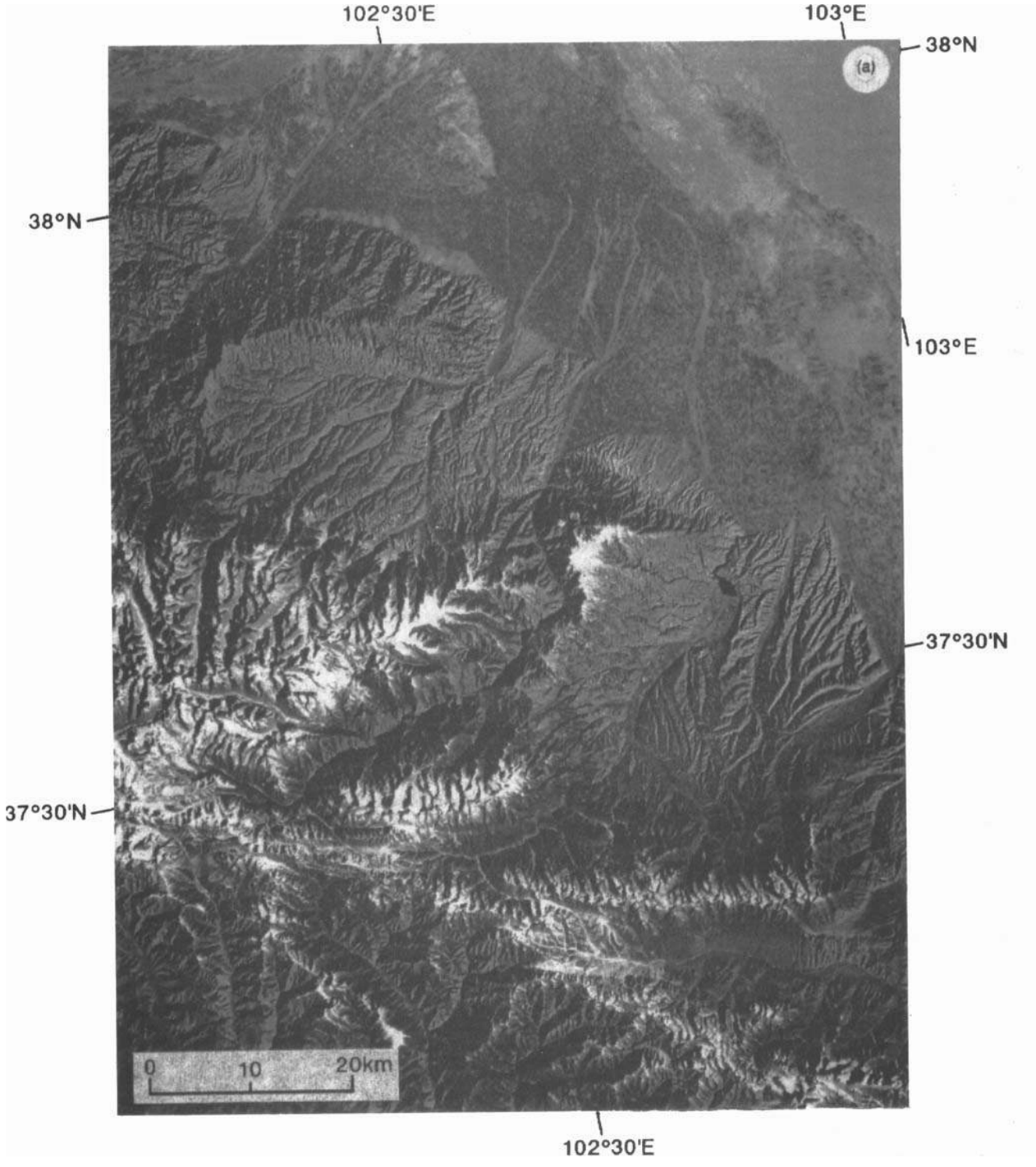

Figure 16. (a) MSS Landsat image (142-34, 1976 November 23) of eastern Qilian Shan south of Wuwei and west of Gulang. Note clear traces of Haiyuan and Gulang Faults, merging within Lenglong Ling range at bottom of image, particularly steep range fronts along east Shiyang and Dongqingding thrusts, and flat, uplifted planation surfaces south of them. (b) Schematic structural and tectonic map of area shown in Fig. 16(a). Geological contours and major faults are from 1/1 000 000, Geologic Map of Gansu province (1975), satellite image analysis, and fieldwork. Continuous line with open triangles at base of Carboniferous is inferred regional décollement. A–A′ is line of section in Fig. 16(c). Epicentre of great 1927 earthquake (solid circle) is from Repetti (1928). Box is location of Fig. 17. (c) Top: interpretative cross-section of eastern Qilian ranges along line A–A′ in Fig. 16(b). Topographic profile, with vertical exaggeration of ≈7, above geological section is from 1/500 000 TPC map G-9A (Defense Mapping Agency 1983). Carboniferous to Quaternary sediment thicknesses are from Gansu Geological Bureau (1975) and Xu *et al.* (1989). Solid circle is inferred hypocentre of great 1927 thrust event, dashed open circle figures plausible hypocentre of strike-slip event similar to great 1920 Haiyuan earthquake (see discussion in text). Note flat mountain tops and simply folded basal surface of post-Caledonian sedimentary cover. Bottom: retrodeformed section, assuming surface conservation and restoration of Carboniferous base to flat surface. (d) Waveform modelling of *P* and *SH* waves of 1927 May 27 earthquake recorded at UCCLE. Inversion method from Nabelek (1984). *SH* waveform rules out strike-slip faulting on N115E-striking Haiyuan Fault.

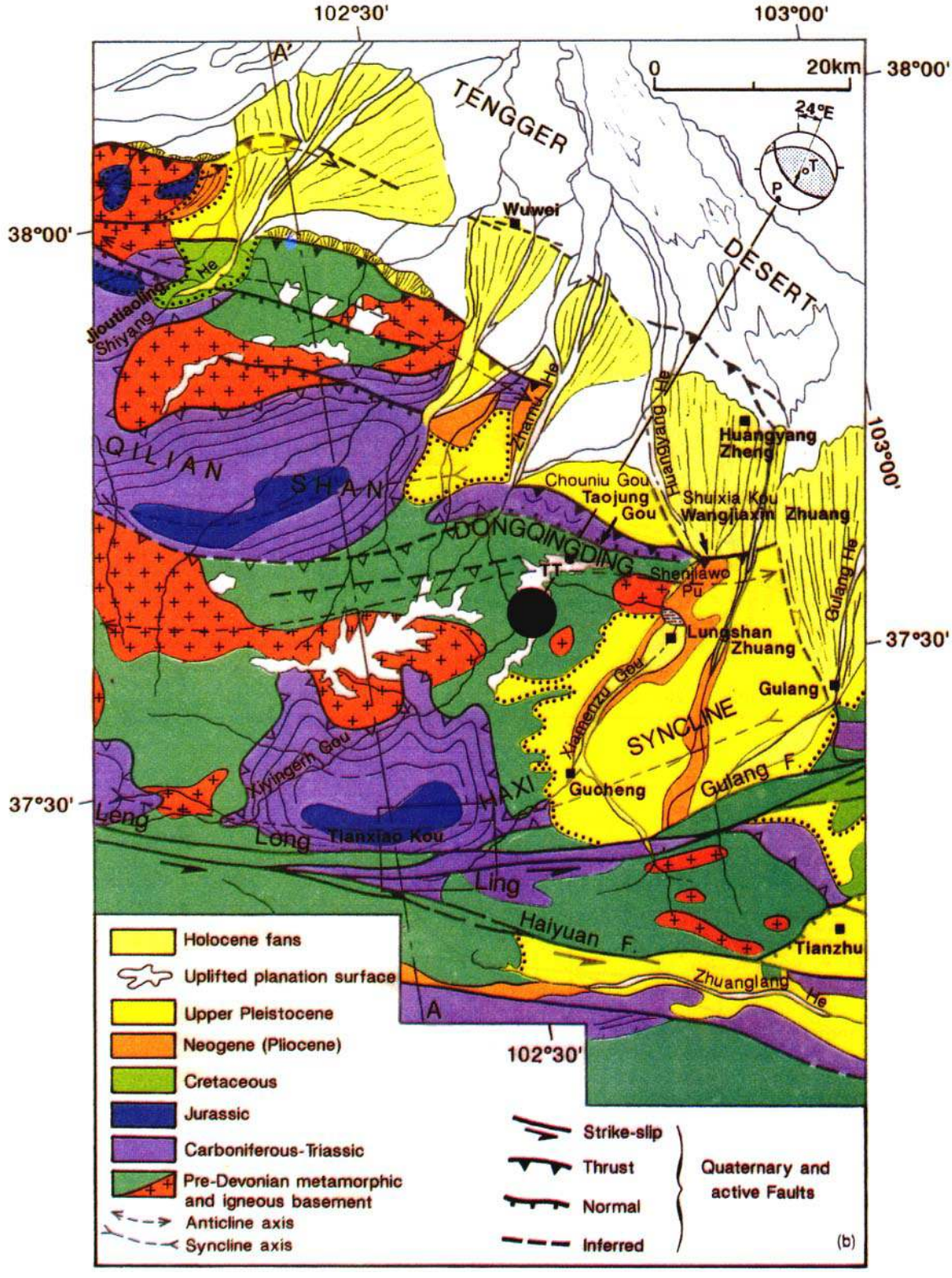

Figure 16. (*Continued.*)

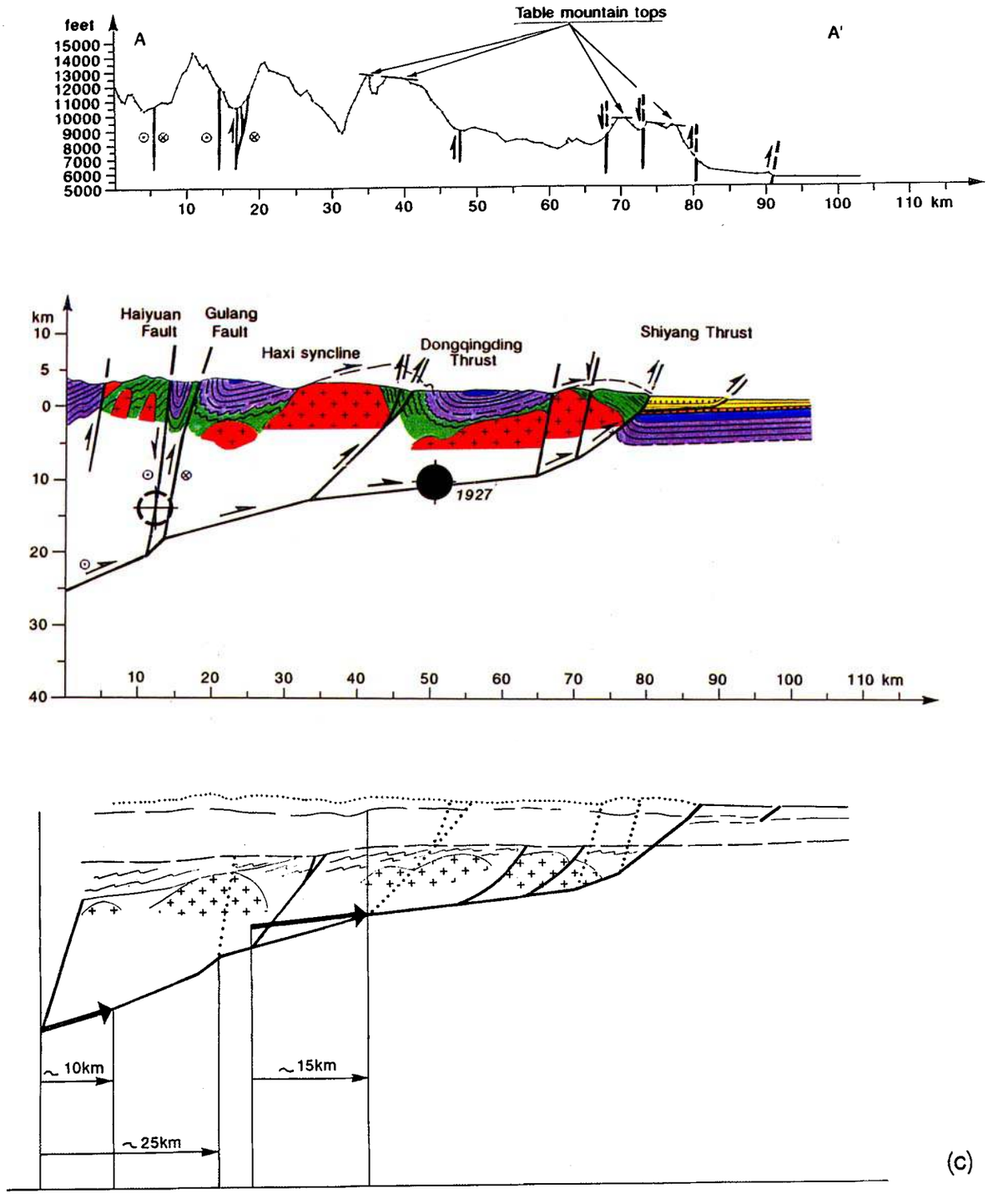

Figure 16. (*Continued.*)

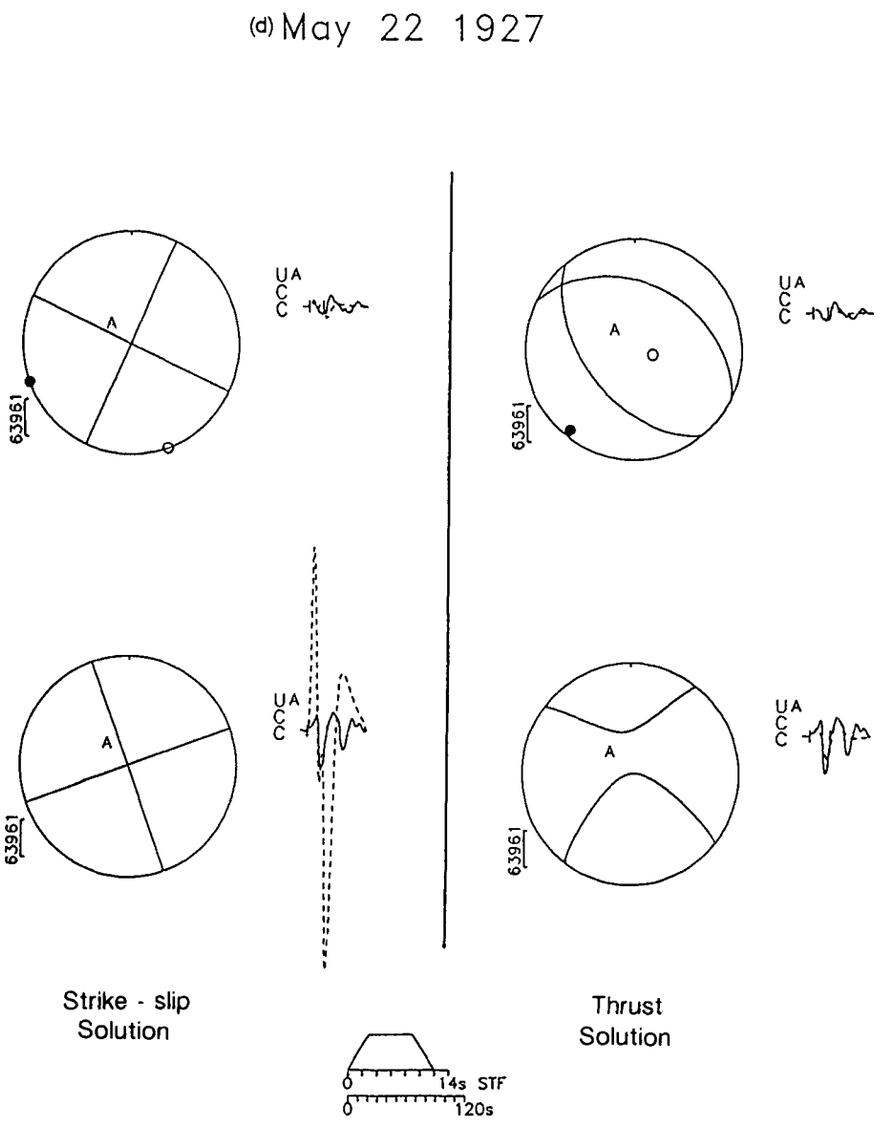

Figure 16. (*Continued.*)

Besides left-lateral slip, the Gulang Fault shows subordinate vertical throw over most of its length. In contrast with the Haiyuan Fault, along which normal slip components or pull-apart jogs are common, and save for the Tianxiao Kou scarp near that fault, however, such throw appears to result mainly from shortening. The Gulang River shutter ridge, for instance, and the larger ridge near 103°45′E (Fig. 1), which reach elevations of 2800–2900 m, are best interpreted to represent growing ramp anticlines in compressional jogs along the fault. In addition to such features, the Gulang Fault follows the edge of an area of gently rising relief, made of uplifted pre-Cenozoic rocks, south of the Tengger Desert (Fig. 1). Most highs north of the fault are capped by north-sloping, thickly loess-mantled, Pleistocene alluvial aprons fed by the erosion of such relief. Moderate uplift south of the fault, the existence of push-up jogs along it, and the fact that it merges eastwards with the Tianjing thrust, are all consistent with a minor component of north-directed thrusting. Hence, we interpret the Gulang Fault to represent the surface trace of a south-dipping lateral ramp, whose main function is to transfer some crustal shortening from the Qilian Shan to the Tianjing, Mibo and Yantong Shan thrusts. Given the strike difference of $38 \pm 5°$ between the Gulang Fault and the thrusts, a left-slip rate of $4.3 \pm 2.1\ \mathrm{mm\ yr^{-1}}$ on that fault would be compatible with $2.8 \pm 1.6\ \mathrm{mm\ yr^{-1}}$ of shortening across these thrusts. Such a value allows for the $1.5–2.7\ \mathrm{mm\ yr^{-1}}$ shortening rate estimated by Burchfiel *et al.* (1989) and Zhang *et al.* (1990).

Where we could gain access to the Gulang Fault in the field, south of Gulang and at Tianxiao Kou, we found no clear evidence of recent seismic breaks on it. These two localities bracket the westernmost segment of the fault, which lies closest to the epicentre of the 1927 May 23 earthquake (e.g. Tapponnier & Molnar 1977; Figs 1 and 16), implying that the fault was not activated by that $M \approx 8.3$ event.

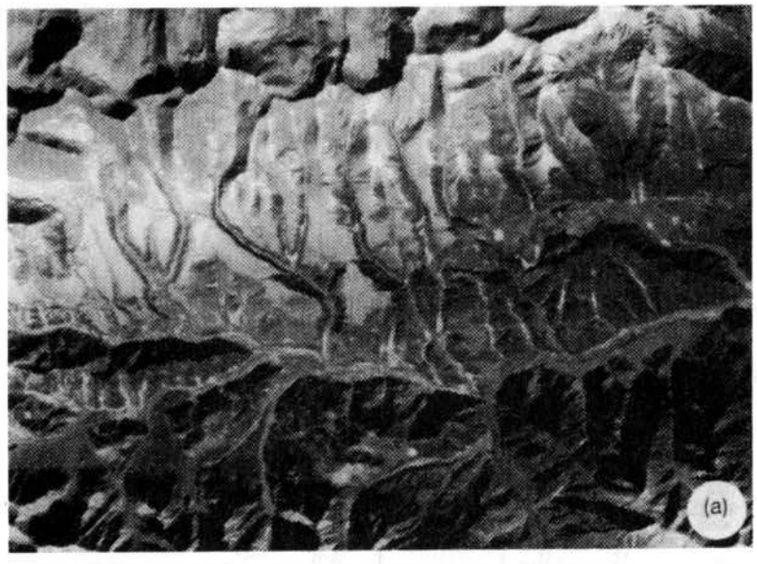

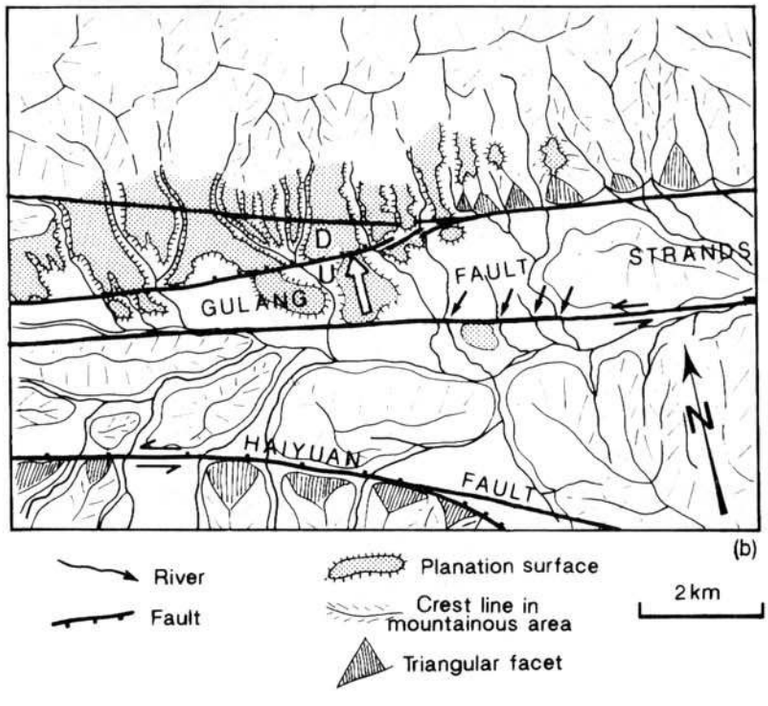

NE SW

Figure 17. (a) Detail of SPOT scene 253-275 (1986 December 12) showing Tianxiao Kou site, east of jucntion between Haiyuan and Gulang Faults. Note prominent stream incision into planation surface blending smoothly with mountain slope north of main river, prominent north-facing (shaded) scarp along middle strand, and consistent left-lateral channel offsets along southern, main strand of Gulang Fault. (b) Morphotectonic map of area shown in Fig. 17(a). Single solid arrows point to 60–70 m left-lateral offsets, open arrow, to scarp in Fig. 17(c). (c) SW-looking view of ≈40 m high, cumulative scarp offsetting planation surface along middle Gulang Fault strand at Tianxiao Kou.

Shiyang–Dongqingding thrusts

From ≈101°45′E to ≈103°E, south-dipping, ≈N115E-striking thrusts follow the topographic front of the eastern Qilian Shan, bringing Paleozoic and Mesozoic rocks over Neogene and Quaternary deposits (Gansu Geological Bureau 1975; Xu *et al.* 1989) (Fig. 16). The sharpness of the thrust traces, marked by outstanding slope breaks on satellite images and in the field, implies contemporaneous shortening and uplift along them (Fig. 16). West of Wuwei (Figs 16a and b), such uplift has in fact led to the formation of fresh, prominent colluvial-alluvial aprons north of the thrust trace, a feature characteristic of most active mountain fronts in Gansu and Qinghai (Tapponnier *et al.* 1990; Meyer 1991). In map view, the thrusts are arranged in a right-stepping array, with three principal segments (west Shiyang, east Shiyang and Dongqingding) offset from one another, along the base of three en échelon mountain ridges that rise to more than 3200 m, ≈1700 m above the Tengger Desert (Figs 1 and 16). The thrust traces thus step closer to the Haiyuan Fault towards the east (from ≈70 to ≈40 km, Figs 1 and 16).

There is additional evidence for active shortening 10–30 km north of the topographic front. Such shortening is clearest west of the Shiyang River, where it is marked by local uplift of the river-fan surface along a narrow, ≈N110E-trending ridge incised by divergent fan channels (barren, light-grey stripe on the Landsat image, Figs 16a and b). That ridge, which is comparable to those that cross Holocene piedmont fans in the western Qilian Shan and Tien Shan (Meyer 1991; Avouac *et al.* 1993), appears to form the top of a growing anticline, which we interpret to signal the emergence, along a south-dipping ramp, of a shallow foreland décollement branching off the thrust beneath the mountain to the south (Fig. 16c). Slightly entrenched piedmont-bajada channels (Figs 16a and b) suggest that a similar foreland thrust ramp may exist near and east of Wuwei, but agriculture and construction in the populated city oasis obscure other surface evidence.

Constraints on the overall geometry and development of the active thrust system may be derived from the main structural traits of the eastern Qilian Shan. To a first order, the rocks belong to two principal units. The older unit is a basement of Early Palaeozoic rocks (mostly Cambro–Ordovician greenschists and slates, with some volcanics, quartzites and marbles) deformed, metamorphosed and intruded by large bodies of syn- to post-tectonic granodiorites and granites at the time of the Caledonian orogeny (Fig. 16c) (Gansu Geological Bureau 1975; Xu *et al.* 1989). The younger unit is a cover of platform sediments of Devonian to Quaternary age, ≈6000 m thick on average, resting unconformably on top of the basement. Locally thin Devonian red beds are overlain by Carboniferous black shales with interbeds of richly fossiliferous marine limestone, then by a massive sequence of Permo–Triassic and Jurassic continental sandstones with some conglomerates (Fig. 16c). There is little disconformity within this sequence, which reaches a thickness of ≈4500 m and forms impressive ≈20°S-dipping monoclines north of Tianxiao Kou and on the Shiyang He-Jioutiaoling section west of Wuwei (Figs 16b and c). The most significant angular unconformity is at the base of the Jurassic sandstones, which contain coal horizons and whose thickness is variable (up to 1500 m at places). Lower Cretaceous red beds (at most 500 m thick) fill disconnected basins whose depocentres do not coincide with Permo–Triassic or Jurassic depocentres (Xu *et al.* 1989). Ochre-pink Neogene (particularly Pliocene) sandstones and siltstones, locally with metre-scale cross-bedding and at least 500 m thick, are exposed in the two steps between the thrusts and in the Haxi syncline (Fig. 16b). At places, Neogene strata are capped by hundreds of metres of Quaternary conglomerates. The Plio-Quaternary beds, as well as other exhumed rocks, are commonly mantled by layers of loess up to several tens of metres thick

The regional geology thus implies that a rather peaceful regime of shallow marine to terrestrial sedimentation presided over the Late Palaeozoic and Early Mesozoic epochs, with the Triassic–Jurassic boundary marking the onset of resumed tectonic warping and faulting, as in the Tien Shan (e.g. Bally *et al.* 1986; Peng & Zhang 1989; Carroll *et al.* 1990; Graham *et al.* 1990; Hendrix *et al.* 1992; Enkin *et al.* 1992; Avouac *et al.* 1993). That the Lower Cretaceous red beds fill isolated basins implies that further faulting controlled their deposition, whether in pull-apart or synclinal troughs (Gansu Geological Bureau 1975; Xu *et al.* 1989). The absence of Late Cretaceous and Early Tertiary deposits, except in the Xining basin (Gansu Geological Bureau 1975; Bureau of Geology and Mineral Resources of Qinghai Province, 1991), is suggestive of moderate elevation and relief at that time. Following this sedimentation lapse, the renewed, growing flux of Neogene–Quaternary clastics probably reflects the increasing proximity of rising relief, particularly since the Late Miocene.

In the Shiyang Valley, the cover is separated from the basement by a décollement (Fig. 16b). Intense strain, including tight disharmonic folding, flatish shear zones and boudinage, remains mostly localized within the Carboniferous shales, with the bulk of the more competent strata above showing only gentle warping and high-angle brittle faulting. The granite below the décollement displays retrograde shear and cataclasite zones. Various shear indicators imply NNW-directed transport in the present geographic coordinates. Disharmonic folding is also prominent under the massive sandstone monocline on the Xiamenzu–Tianxiao Kou section. On the way up to Dongqingding mountain (Fig. 16b), a granite below Carboniferous rocks has been converted to gneiss, with a strong stretching lineation. From these three distant outcrops, we hypothesize decoupling between cover and basement to be of regional extent. The décollement, which dips towards the north at Dongqingding or in the northern part of the Shiyang He section and towards the south north of Tianxiao Kou, has been folded in harmony with the Carboniferous–Jurassic sedimentary cover, whose main patches on the map of Fig. 16(b) correspond to two large, asymmetric synclines with steep north-dipping south limbs. On the section of Fig. 16(c), both limbs are truncated by the south-dipping Gulang and Dongqingding thrust ramps, which bring the Ordovician metamorphic rocks onto the Permo–Triassic sandstones. A pinched syncline of steeply dipping Triassic beds separates the Gulang from the Haiyuan Fault at Tianxiao Kou.

The structure and morphology of the two mountain ridges south of the Dongqingding and Shiyang thrust traces (Fig. 16) imply that they form basement-ramp anticlines (e.g. Tapponnier *et al.* 1990; Meyer 1991). That such anticlines

are recent and still growing is clear from the canyons ('cluses') incised across them by rivers such as the Dongda He and Huangyang He, from the ponded floodplains upstream from such cluses, and from the flat tabular surfaces that top the ridges (Figs 1 and 16). Though hanging 1200–2400 m above the foreland and 500–1200 m above adjacent, entrenched valleys, those flats, which display complexly indented contours and slope gently (2–6°) towards the Tengger Desert west of the Zamu He, still withstand vigorous erosion. We interpret them to represent vestigial patches of planation surfaces, heaved by relatively rapid movement on the underlying basement ramps, and dismembered by the resulting incision and headward retreat of streams. The age of planation is uncertain and may not be uniform, but the surfaces clearly postdate exhumation of the décollement and apparently, at one locality, the Upper Pleistocene (Q_{2-3}) basal unconformity (Gansu Geological Bureau 1975; Xu *et al.* 1989) (Fig. 16). Thus, planation of the surfaces appears to have taken place well after the onset of folding, possibly at most 700 ka B.P., and may be thought to result chiefly from glacial abrasion and/or periglacial smoothing.

Though large-scale shortening characterizes the Late Cenozoic tectonics of the eastern Qilian Shan, several recent, ≈N115E-striking faults that cut the hanging-wall wedge of upper crust north of the Haiyuan–Gulang strike-slip zone appear to be normal. Those subordinate faults, which have particularly sharp and linear traces on satellite images (Fig. 16a), lie near and roughly parallel to the frontal thrusts (Fig. 16b). Three of them dip steeply, apparently towards the south, along the backs of the Shiyang ranges. Both the west Shiyang and east Shiyang rangeback faults are located north of the westward projections of the east Shiyang and east Dongqingding active thrusts, respectively (Figs 1 and 16). Given their orientation, the three faults may accommodate a component of left slip, in addition to down-to-the-south throw. Another normal fault dips north, only 2–4 km south of the east Dongqingding thrust (Fig. 16). We surmise that the chief function of all four faults is to accommodate the hanging-wall strain that results from dip changes between flats and ramps on sole thrusts with weak frictional resistance (Meyer *et al.* 1990; Tapponnier 1993; Avouac, Meyer & Tapponnier 1992). More specifically, we interpret the Dongqingding normal fault as a simple compatibility fault (e.g. Avouac *et al.* 1992), possibly guided by the basement-cover décollement, and the Shiyang range back faults, as former thrust ramps, steepened and inverted while displaced past a flat-to-ramp kink on the basal, active Shiyang thrust (Fig. 16).

The interpretative, retrodeformable section of Fig. 16(c) (A–A′, bottom) summarizes the overall, deep geometry of faulting that we infer from the regional structure (Figs 16a and b) and the topography (Fig. 16c, top). That three distinct, overlapping thrusts are active while more or less vigorous uplift affects the whole wedge of crust north of the Haiyuan Fault suggests that they merge downsection into a single, active, gently south-dipping sole thrust or décollement and terminate to the east along lateral tip-lines or ramps (e.g. Boyer & Elliott 1982). We assume the dips of the Dongqingding and Shiyang thrust ramps to vary between 30° and 60° (45° ± 15°), a range of values common in other thrust belts of west-central China (e.g. Meyer 1991; Zhang *et al.* 1991; Avouac *et al.* 1993). With 45° dips, the width of the table-topped anticline ridges would imply that the ramps reach depths of ≈12 and ≈18 km, respectively. The sole thrust, which probably steepens southwards under the high hinterland relief, thus ought to lie 12 to 25 km deep and to dip only 10° to 20°S, consistent with the attitudes of the Tianxiao Kou and Jioutiaoling monoclines (Fig. 16c). Similar reasoning implies that the shallow foreland décollement north of the east Shiyang range lies 1 to 2.5 km deep, probably near the base of the Pliocene (Fig. 16c).

Beneath the Lenglong Ling range, we infer the Haiyuan Fault to extend steeply ≈25 km down to a branchline with the sole thrust (Fig. 16c). That inference is in keeping with the presumed depth of the $M \approx 8.7$, Haiyuan earthquake rupture (20 km, Molnar & Deng 1984) and hypocentre (17 km, Gongxu, Tinghuang & Zhenliang 1989, Fig. 16c), which broke through thinner crust in a less mountainous region to the east. The observation that the right-stepping thrust ramps emerge farther from the Haiyuan Fault westwards, as hinterland relief becomes higher and broader, implies that the branch line between that fault and the sole thrust plunges even deeper west of the section of Fig. 16(c). Conversely, as this branch line shallows eastwards, the innermost parts of that section also shallow, resembling its outermost parts. That the inner thrust traces become less sharp and that hinterland-dipping normal faults come into being west of the lateral tip lines of the outer thrusts, suggests that a significant fraction of the present-day shortening is transferred to the latter along section, as ought to occur within a leading, northwards growing, imbricate thrust fan (Boyer & Elliott 1982). Hence, though non-unique, the schematic section of Fig. 16(c) suffices to account fairly simply and completely for the large-scale structure and recent evolution of the eastern Qilian Shan, which is but a variant of a style similar to that in other active, central Asian thrust belts (Tapponnier *et al.* 1990; Meyer 1991; Avouac *et al.* 1993).

Conservation of surfaces on the cross-section of Fig. 16(c), and restoration of the folded and faulted cover/basement décollement to a flat, slightly south-dipping unconformity, yields ≈25 km of horizontal shortening between the Gulang Fault and the foreland (≈25 per cent of an initial length of ≈100 km). The greatest source of uncertainty on that number comes from the dips inferred for the thrust ramps and flats. The existence of the tight syncline south of the Gulang ramp and thrust slip on that ramp probably add a few kilometres to the cumulative shortening across the mountains north of the western Haiyuan Fault. Although the basement/cover décollement apparently postdates the Jurassic, our observations are insufficient to determine whether movement on it took place during, or prior to, the Cenozoic (Yenshan orogeny), and how large its contribution was to upper-crustal shortening. We simply conclude that 25 km is a lower bound on the amount of Late Cenozoic shortening between the Haiyuan Fault and the Tengger foreland.

Rough estimates of uplift and shortening rates may also be derived from Section A–A′ (Fig. 16c). If most of the elevation difference (≈1200 m) between the foreland and the planation surfaces topping the east Shiyang and east Dongqingding anticlines were due to tectonic uplift in the

last 700 ka, the vertical throw rate on the underlying ramps would be of the order of 1.7 mm yr^{-1}. This number would represent a lower bound if the assessment of the Quaternary stratigraphy (Q_{2-3}) on the geologic map were taken at face value. For the east Dongqingding ramp, the same rate (1.7 mm yr^{-1}) would be obtained assuming that the Q_{3-4} fanglomerates that stand ≈200 m above the piedmont and cap the gently ESE-dipping upper-Neogene beds of the north limb of the Haxi syncline (Gansu Geological Bureau 1975) were deposited by the Xiamenzu and adjacent river mostly during the Riss–Würm interglacial (≈120 ka B.P.). That number would represent an upper bound if abundant fanglomerate deposition were restricted to warm and humid interglacials. Both estimates are in keeping with those derived farther west along the thrust belt from evidence of postglacial faulting and folding (0.9 to 1.9 mm yr^{-1}: Yumu Shan, Meyer 1991; Tapponnier *et al.* 1990, 1.5 ± 0.3 mm yr^{-1}: Taxueh Shan, Meyer 1991). The highest planation surface, on top of the west Dongqingding range north of Xiyingerh Kou (Figs 1 and 16), might testify to more vigorous upheaval above the west Dongqingding ramp. If that surface, now up to 3900 m high, had risen ≈2400 m relative to the piedmont in 700 kyr, the vertical throw rate on the ramp might have reached 3.4 mm yr^{-1}. Alternatively, and probably more likely in view of the distance between that range and the piedmont, planation might have taken place at a higher initial elevation and/or earlier than 700 ka B.P. We conclude that plausible shortening rates along the eastern Qilian Shan thrust system probably lie between 2 and 6 mm yr^{-1} (4 ± 2 mm yr^{-1}), a range of values not unlike that inferred in the northern Tien Shan (3 ± 1.5 mm yr^{-1}), (Avouac *et al.* 1993). At 4 mm yr^{-1}, roughly 6 Myr would have been necessary to absorb 25 km of shortening.

Mechanism of the 1927 May 23 earthquake

As located by Gongxu *et al.* (1989), the hypocentre of the Wuwei–Gulang earthquake of 1927 May 23 lies at 37.7°N–102.2°E, under the west Dongqingding range front (Figs 1 and 16). Alternative locations place the epicentre at 37.6°N–102.6°E (Repetti 1928; Lee, Wu & Jacobson 1976), about 10 km south of the east Dongqingding thrust or at 38.05°N–102.37°E (Molnar & Deng 1984), near the eastern extremity of the west Shiyang thrust trace in the foreland. Although the macroseismic depth of the earthquake hypocentre is reported to be ≈12 km (Gongxu *et al.* 1989, Fig. 16c), that value is probably a 'default depth'. While the magnitudes reported by various authors vary between 8 (Gongxu *et al.* 1989) and 8.3 (Molnar & Deng 1984), there is little doubt that the main shock, which had a $M \approx 5.5$ foreshock 49 minutes earlier, many large aftershocks (of which 2 with $M \approx 6$, and 6 with $M \geq 5.25$) in the following 10 months, and a moment $M_0 \approx 4.3 \times 10^{20}$ N m (Chen & Molnar 1977), ranks as a great earthquake. As defined by the isoseismal of intensity VIII (Gongxu *et al.* 1989, see also State Seismological Bureau 1993, and Ding 1985, p. 176), its meizoseismal area is ≈200 km long and ≈90 km wide, with a long axis oriented ≈N130E (Figs 1 and 16). Though the macroseismic evidence used in deriving the isoseismals is probably biased by the existence of rugged, high and uninhabited terrain towards the south-west, that area, which extends between 101.6–103.5°E and 3.1–38.4°N, encompasses most of the Shiyang and Dongqingding ranges, as well as the southern part of the Tengger foreland, and includes the three inferred epicentral locations. Its long axis lies roughly along the right-stepping thrust traces that stretch north-west from Gulang past Wuwei (Fig. 1). The isoseismal of intensity IX (≈110 km × 45 km) still surrounds completely the Dongqingding and east Shiyang thrust traces. Hence, although neither the epicentral locations nor the isoseismal contours should be considered accurate, the areal coincidence of all the above elements, together with the absence of surface ruptures along the Haiyuan and Gulang Faults near Tianzhu and Gulang, suggests that the 1927 earthquake resulted from slip on the Shiyang–Dongqingding thrust system. The body-waveform least-squares inversion method of Nabelek (1984) was used to examine the plausibility of that inference. The waveforms of the radial component *P* wave and the *SH* wave recorded on the horizontal component Galitzine instrument at the station UCCLE (Brussels, Belgium) rule out pure strike-slip faulting and are consistent with N24E-directed thrusting on a N136E-Striking, 50°S-dipping fault plane, with a minor component of right slip (Figs 1, 16b and d).

The most common, if imprecise, description of surface breaks attributed to that earthquake (e.g. Jia 1982; Deng *et al.* 1984; Molnar & Deng 1984) invokes two 'conjugate' fault segments intersecting at high angle in map view. Reportedly, 2 to 6 m of reverse throw with a component of right slip took place on a 33 km long segment oriented N160E, while 2 to 7.5 m of reverse throw with some left slip occurred on a 28 km long, south-dipping segment oriented N110E, with slip maxima on either segment near their intersection. Deng *et al.* (1984, Landsat image of Fig. 2a in their paper) identify the first and second segments with the escarpments truncating the Haxi syncline north of Gulang, and marking the Dongqingding range front, respectively (Figs 1 and 16). Although we had only limited access to those escarpments, our field observations and conclusions are generally not consistent with the above numbers, and hence with earthquake parameters and other speculations derived from them (Molnar & Deng 1984).

The first N160E-striking escarpment, for instance, is only ≈17 km long on the Landsat image, about half the length alleged above, with an average strike of ≈N170E (Fig. 16). For most of its length, it forms the western riser of the Gulang river fan, resembling the other riser facing it east of the river. At a more detailed level, its slope is steeper and its height greater than are those of the eastern riser, and one hill remains isolated east of it (Fig. 16). From a distance of 1 to 2 km, however, and with binoculars (the utmost we could achieve in that strategic valley!), we saw little evidence for fresh, east-facing scarps several metres high along the base of that escarpment. Hence, though we cannot, for lack of access, rule out faulting along the north Gulang escarpment during the 1927 earthquake, nor question, for regional strain-compatibility reasons, the style of faulting, both the length of faulting and the amount of throw reported seem exaggerated, each probably by at least a factor of two.

The second escarpment is indeed ≈28 km long, with an average strike of N115E. But in the field, at two different sites about 10 km apart (Fig. 16), again we found no evidence of large, recent, seismic throws. Near Chouniu

Gou, north of the Dongqingding summit, we could see no clear, fresh scarp along the loess-smeared range-front thrust. At Wangjiaxin Zhuang, near Shuixia Kou, above the east bank of the Huangyang river, we examined a ≈N110E-striking, 6–7 m high scarp limiting a high-level, cultivated terrace behind adobe houses and reported to have formed in 1927 (State Seismological Bureau 1993). But neither the rather smoothed-out shape and slope of that scarp, nor ground disruption along it—all possibly altered by human action—testified unambiguously to a single rupture less than 70 years old. Having not been able to see a 1927 photograph, we thus infer this fairly high step, which stretches only ≈1 km eastwards, to represent the cumulative record of several earthquakes on the high-level terrace. That inference is corroborated by the occurrence, about 1 km farther east along strike, of small (30–50 cm high), well-preserved pressure ridges and thrust scarplets that fold and cut the turf (Fig. 18a). In aspect, these relatively fresh features are indistinguishable from those seen along the breaks of either the 1932, Changma (e.g. Peltzer *et al.* 1988; Meyer 1991) or 1920, Haiyuan earthquakes (e.g. Deng *et al.* 1984) and thus may be attributed to an earthquake in 1927. They lie along the base of the 20–30 m high cumulative scarp that marks quite sharply here the eastern end of the Dongqingding range-front thrust by lifting into hanging position, relative to the Holocene piedmont bajada, loess-mantled troughs dug into gently south-dipping Neogene sandstones (Figs 16a, b and 18a). Our observations near Wangjiaxin Zhuang may thus be taken as consistent with sustained seismic thrusting on the Dongqingding range front, but the 1927 surface throw appears to have been modest, probably only about one tenth of the value used by Molnar & Deng (1984) to derive the seismic moment.

More impressive ground ruptures scar the landscape south of the range front. Their size and freshness testify to formation during the great 1927 earthquake, the only large regional event in the last few centuries. Many of these ruptures simply correspond to the free-faced head scarps of local, thin-skinned loess slides down steep valley slopes. Such slide-related scarps are widespread throughout the Haxi syncline and surrounding mountains, implying particularly strong ground shaking there, in keeping with the fact that the area lies within isoseismal X (Figs 1 and 16). But kilometres-long, free-faced scarps that slice uplifted Palaeozoic basement rocks and seem unrelated to superficial landsliding also exist within the Dongqingding range, mostly north of its crest. Several such scarps, oriented roughly parallel to the range crest and facing north or south, are clear when looking down from the television tower on top of the range (TT, Fig. 16b). They appear to belong to a discontinuous system, extending for at least 14 km between the Huangyang He in the east and the Zamu He in the west (State Seismological Bureau 1993, Fig. 5, p. 129). Upstream from Chouniu Gou, we could follow and crudely map one particularly prominent scarp zone across rugged mountainous terrain on either side of an E–W pass between two north-draining valleys (Figs 16, 18b, c, d, 19a and b). Certain features along that zone resemble those depicted on photographs taken farther east, at Shenjiawo Pou (State Seismological Bureau 1993, photographs 34 and 35, p. 129).

Severe ground disruption starts transverse to the first, eastern valley (Taojung Gou), in the form of a narrow, N100–110E trending stretch of chaotically contorted turf, with exhumed boulders separated by water-seeping lenses of black and grey-green gouge, which climbs up the west side of the valley. Movement appears to have raised the rocks and ground surface up valley, south of that zone (Fig. 19a). Farther up slope, antithetic scarps with well-preserved free faces up to ≈1 m high enclose a N120–130E-trending pull-apart depression, about 10 m wide and several tens of metres long, with 1 to 2 m wide and deep collapse pits at either end (Fig. 19a). The zone then narrows into a narrower crack-like furrow oriented ≈N90E, and continues as a single north-facing, N100–110E-trending, free-faced scarp (Fig. 18b) all the way to the pass, whose distance from the valley floor we estimate to be of the order of 600 m (Fig. 19a). Consistently higher north-facing scarps all along the scarp zone east of the pass, as well as cumulative slope offsets of up to 3.4–3.9 m opposite to the generally south-directed slope gradient (Figs 18b and 19a, inset AB), indicate down-to-the-north throw, which rules out a superficial landslide origin. At a more detailed level, the orientation, in map view, of the pull-apart depression relative to that of adjacent segments of the scarp zone suggests some component of right slip across that zone (Fig. 19a).

At the pass, the north-facing scarp is particularly outstanding, about 50 m long and 1 to 1.7 m high, with a fresh free face and a modest debris wedge at its base (Fig. 18c). Sudden slippage has uprooted willow trees or cut and exposed their roots along that free face. The grass-covered morphological saddle of the pass is affected by open fissures roughly parallel to the free face, as well as by smaller, north-facing scarps, implying probably as much as 2 m of down-to-the-north seismic throw and significant extension in a ≈NNE azimuth, roughly parallel to the local divide (Fig. 19a, inset CD). West of the pass, the zone splays into two main, N- to NE-facing, free-faced scarps (Fig. 19a). The first one, which we did not follow, continues due west across willow thickets. The second one veers to N155E, then back to N130E, running obliquely down slope above the narrow gorge of a small stream, all the way to the confluence of that stream with the river west of the pass (Fig. 19a), a total distance of ≈800 m. That second scarp, which is 0.5 to 2 m high with down-to-the-north-east throw, opposite to the local slope gradient, limits a fairly linear and continuous furrow that cuts across basement rock and surface debris (Fig. 18d). One stretch of en échelon, paired scarps bounding metres-wide, right-stepping, N120E-trending grabens, indicates a component of left-lateral slip (Fig. 19a). Fresh landslides up slope from the scarp furrow funnel into it, implying that surface debris collapsed into ground fissures at the scarp base (Fig. 19a, inset EF). Short fir trees, with straight vertical trunks, at most several decades old, have grown in the furrow and associated slides.

In summary, the overall attitude of the ≈1.5 km long scarp zone relative to the topographic relief, the freshness, amount and consistency of the deformation observed across the ≈300 m high mountain spur between the two valleys—with south-side up and opposite components of lateral slip east and west of the pass—all concur to indicate formation, in 1927, by as much as 2 m of surface-slip on a ≈60°NNE-dipping normal fault, and testify to local, N25 ± 15E-directed extension (Fig. 19a). More credit should

Gou, north of the Dongqingding summit, we could see no clear, fresh scarp along the loess-smeared range-front thrust. At Wangjiaxin Zhuang, near Shuixia Kou, above the east bank of the Huangyang river, we examined a ≈N110E-striking, 6–7 m high scarp limiting a high-level, cultivated terrace behind adobe houses and reported to have formed in 1927 (State Seismological Bureau 1993). But neither the rather smoothed-out shape and slope of that scarp, nor ground disruption along it—all possibly altered by human action—testified unambiguously to a single rupture less than 70 years old. Having not been able to see a 1927 photograph, we thus infer this fairly high step, which stretches only ≈1 km eastwards, to represent the cumulative record of several earthquakes on the high-level terrace. That inference is corroborated by the occurrence, about 1 km farther east along strike, of small (30–50 cm high), well-preserved pressure ridges and thrust scarplets that fold and cut the turf (Fig. 18a). In aspect, these relatively fresh features are indistinguishable from those seen along the breaks of either the 1932, Changma (e.g. Peltzer *et al.* 1988; Meyer 1991) or 1920, Haiyuan earthquakes (e.g. Deng *et al.* 1984) and thus may be attributed to an earthquake in 1927. They lie along the base of the 20–30 m high cumulative scarp that marks quite sharply here the eastern end of the Dongqingding range-front thrust by lifting into hanging position, relative to the Holocene piedmont bajada, loess-mantled troughs dug into gently south-dipping Neogene sandstones (Figs 16a, b and 18a). Our observations near Wangjiaxin Zhuang may thus be taken as consistent with sustained seismic thrusting on the Dongqingding range front, but the 1927 surface throw appears to have been modest, probably only about one tenth of the value used by Molnar & Deng (1984) to derive the seismic moment.

More impressive ground ruptures scar the landscape south of the range front. Their size and freshness testify to formation during the great 1927 earthquake, the only large regional event in the last few centuries. Many of these ruptures simply correspond to the free-faced head scarps of local, thin-skinned loess slides down steep valley slopes. Such slide-related scarps are widespread throughout the Haxi syncline and surrounding mountains, implying particularly strong ground shaking there, in keeping with the fact that the area lies within isoseismal X (Figs 1 and 16). But kilometres-long, free-faced scarps that slice uplifted Palaeozoic basement rocks and seem unrelated to superficial landsliding also exist within the Dongqingding range, mostly north of its crest. Several such scarps, oriented roughly parallel to the range crest and facing north or south, are clear when looking down from the television tower on top of the range (TT, Fig. 16b). They appear to belong to a discontinuous system, extending for at least 14 km between the Huangyang He in the east and the Zamu He in the west (State Seismological Bureau 1993, Fig. 5, p. 129). Upstream from Chouniu Gou, we could follow and crudely map one particularly prominent scarp zone across rugged mountainous terrain on either side of an E–W pass between two north-draining valleys (Figs 16, 18b, c, d, 19a and b). Certain features along that zone resemble those depicted on photographs taken farther east, at Shenjiawo Pou (State Seismological Bureau 1993, photographs 34 and 35, p. 129).

Severe ground disruption starts transverse to the first, eastern valley (Taojung Gou), in the form of a narrow, N100–110E trending stretch of chaotically contorted turf, with exhumed boulders separated by water-seeping lenses of black and grey-green gouge, which climbs up the west side of the valley. Movement appears to have raised the rocks and ground surface up valley, south of that zone (Fig. 19a). Farther up slope, antithetic scarps with well-preserved free faces up to ≈1 m high enclose a N120–130E-trending pull-apart depression, about 10 m wide and several tens of metres long, with 1 to 2 m wide and deep collapse pits at either end (Fig. 19a). The zone then narrows into a narrower crack-like furrow oriented ≈N90E, and continues as a single north-facing, N100–110E-trending, free-faced scarp (Fig. 18b) all the way to the pass, whose distance from the valley floor we estimate to be of the order of 600 m (Fig. 19a). Consistently higher north-facing scarps all along the scarp zone east of the pass, as well as cumulative slope offsets of up to 3.4–3.9 m opposite to the generally south-directed slope gradient (Figs 18b and 19a, inset AB), indicate down-to-the-north throw, which rules out a superficial landslide origin. At a more detailed level, the orientation, in map view, of the pull-apart depression relative to that of adjacent segments of the scarp zone suggests some component of right slip across that zone (Fig. 19a).

At the pass, the north-facing scarp is particularly outstanding, about 50 m long and 1 to 1.7 m high, with a fresh free face and a modest debris wedge at its base (Fig. 18c). Sudden slippage has uprooted willow trees or cut and exposed their roots along that free face. The grass-covered morphological saddle of the pass is affected by open fissures roughly parallel to the free face, as well as by smaller, north-facing scarps, implying probably as much as 2 m of down-to-the-north seismic throw and significant extension in a ≈NNE azimuth, roughly parallel to the local divide (Fig. 19a, inset CD). West of the pass, the zone splays into two main, N- to NE-facing, free-faced scarps (Fig. 19a). The first one, which we did not follow, continues due west across willow thickets. The second one veers to N155E, then back to N130E, running obliquely down slope above the narrow gorge of a small stream, all the way to the confluence of that stream with the river west of the pass (Fig. 19a), a total distance of ≈800 m. That second scarp, which is 0.5 to 2 m high with down-to-the-north-east throw, opposite to the local slope gradient, limits a fairly linear and continuous furrow that cuts across basement rock and surface debris (Fig. 18d). One stretch of en échelon, paired scarps bounding metres-wide, right-stepping, N120E-trending grabens, indicates a component of left-lateral slip (Fig. 19a). Fresh landslides up slope from the scarp furrow funnel into it, implying that surface debris collapsed into ground fissures at the scarp base (Fig. 19a, inset EF). Short fir trees, with straight vertical trunks, at most several decades old, have grown in the furrow and associated slides.

In summary, the overall attitude of the ≈1.5 km long scarp zone relative to the topographic relief, the freshness, amount and consistency of the deformation observed across the ≈300 m high mountain spur between the two valleys—with south-side up and opposite components of lateral slip east and west of the pass—all concur to indicate formation, in 1927, by as much as 2 m of surface-slip on a ≈60°NNE-dipping normal fault, and testify to local, N25 ± 15E-directed extension (Fig. 19a). More credit should

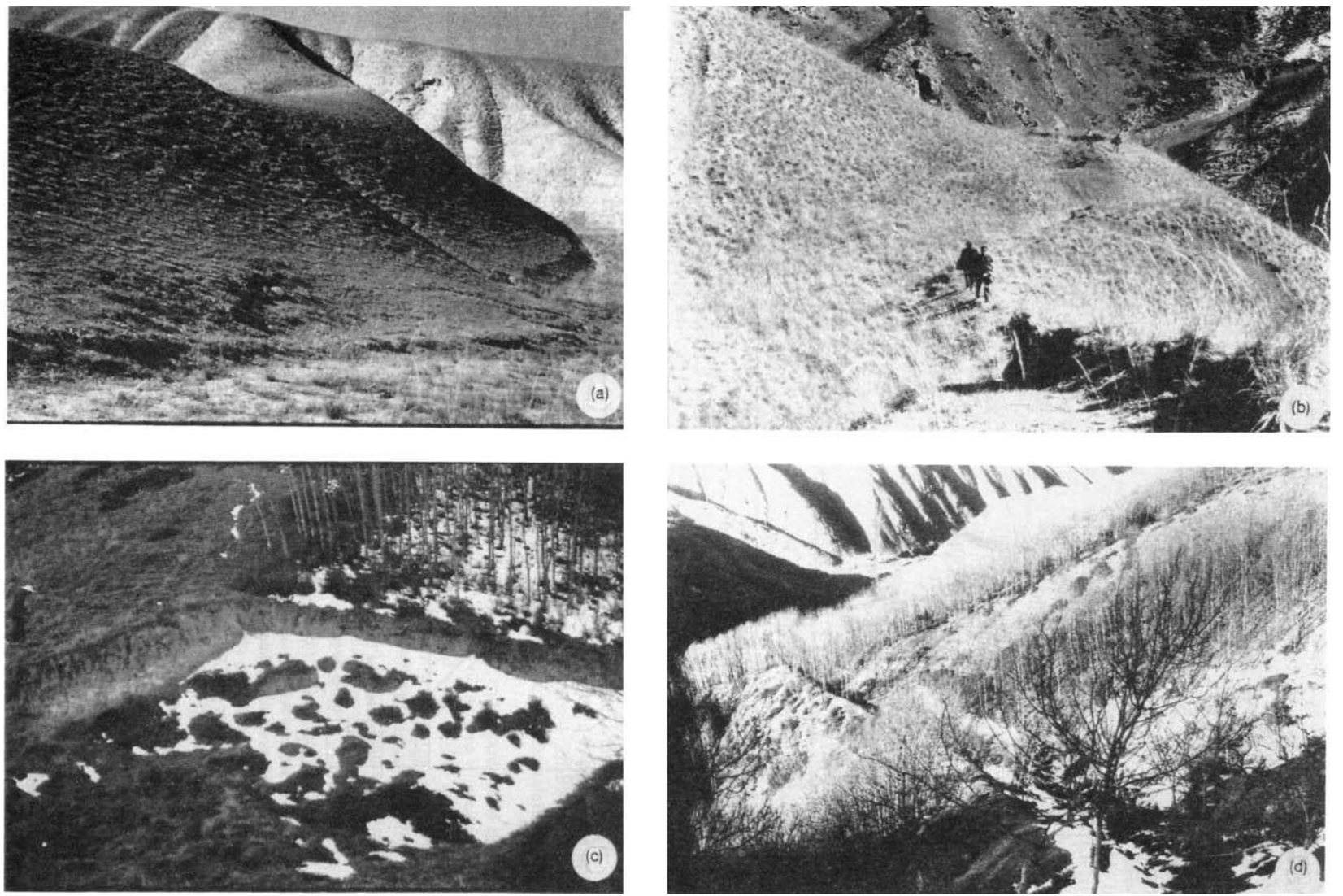

Figure 18. (a) SW-looking view of 1927 thrust scarplets and pressure ridges, 1.5–2 km east of Shiuxia Kou. Scarplets follow base of cumulative scarp marking eastern end of Dongqingding thrust. Note trough hanging at midheight of cumulative scarp. (b) East-looking view of 1927, free-faced normal fault scarp west of Taojung Gou, within Dongqingding mountains. South side moved up, opposite to slope gradient. Note 3.5–4 m cumulative throw. (c) South-looking view of same scarp at pass west of Taojung Gou. Free face is 1–1.7 m high. (d) NE-looking view of scarp and associated furrow west of pass. Note landslide above scarp in foreground right. See discussion in text.

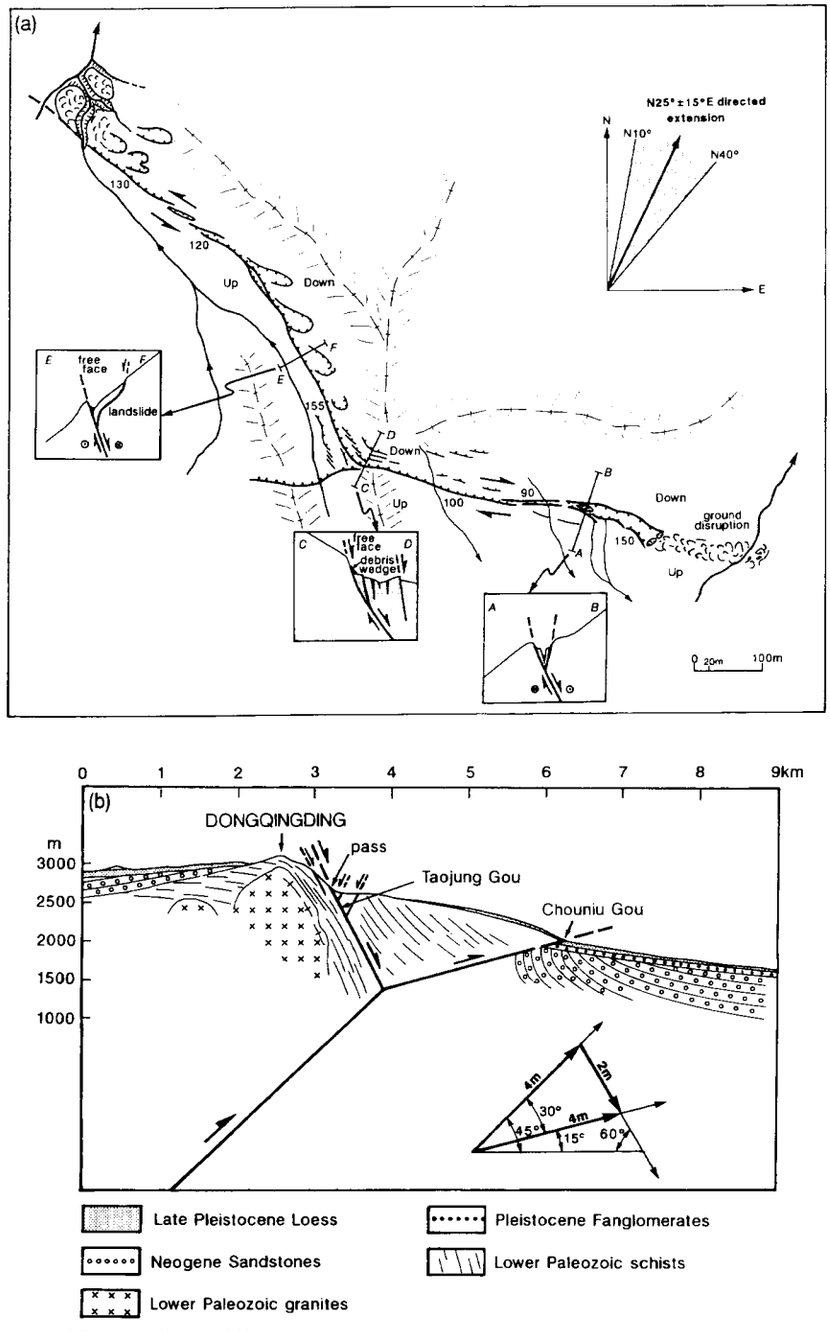

Figure 19. (a) Schematic map of Taojung Gou, 1927 scarp zone north of Dongqingding range crest. Scale is approximate. Numbers indicate local strike of main scarp. Inset sections AB, CD and EF summarize features visible on photographs of Figs 18(b), (c) and (d), respectively, with zones of severe ground disruption or landslides stippled, and colluvial wedges, shaded. Top-right inset shows slip-vector azimuth range compatible with observations along entire scarp zone. (b) Section showing possible link between Dongqingding normal fault and underlying thrust, consistent with geological evidence and observed 1927 seismic slip. Dongqingding fault is interpreted to absorb strain resulting from ramp-to-flat bend on thrust. Inset vector diagram shows inferred relationship between 1927 slip amounts on three faults, assuming conservative thrust slip at bend.

thus be given to the map compiled by the State Seismological Bureau (Fig. 5, p. 129, 1993) than to other reports (e.g. Jia 1982; Deng *et al.* 1984; Molnar & Deng 1984). Not only are the scarps that cut the rugged relief just north of the Dongqingding range crest of clear tectonic origin, but, in the area we could visit, they are the largest surface ruptures due to the 1927 event. They do not seem, however, to accommodate shortening and left-lateral strike slip (State Seismological Bureau 1993, Fig. 5, p. 129). Rather, we interpret most of them to reflect, as that at Taojung Gou, extensional strain and normal slip on the north-dipping Dongqingding fault and related splays (Fig. 19b).

The picture that emerges is therefore one in which thrust

slip on the Dongqingding ramp at depth caused incremental growth of the Dongqingding anticline and extension at its apex, with the Dongqingding normal fault accommodating down-to-the-north throw, probably due to flattening of the shallower part of the thrust past the anticlinal crest (Fig. 19b). While the scale here is greater, this interpretation is in line with well-documented occurrences of coseismic normal faulting in thrust earthquakes elsewhere, particularly in Algeria. The only clear surface break produced by the 1954 September 9, $M \approx 6.7$, El Asnam event, for instance, was along the south-dipping Beni Rached normal fault, several kilometres north of the surface trace of the thrust (Rothé 1955). The $M \approx 7.3$ event of 1980 October 10 at the same locality caused extensive, discontinuous normal faulting along the crest of the anticline above the thrust ramp (e.g. Yielding *et al.* 1981; Philip & Meghraoui 1983; Meyer *et al.* 1990; Avouac *et al.* 1992). That we could see only modest surface evidence of thrust faulting due to the Gulang earthquake should perhaps come as no surprise in view of the example of the 1906 Manas earthquake which, despite a comparable size ($M \approx 8$), produced only small thrust scarps (≈0.8 m high) in only a few places (Avouac *et al.* 1993). If thrust offsets in 1927 had been no greater than those we saw near Wangjiaxin Zhuang, they could easily have gone undetected and/or have disappeared in most places in only a few decades, particularly if they formed at the edges of, or within, cultivated fields. It is possible that such was the fate of most segments of the elusive N160°E-striking break reported by Jia (1982), whether it extended along the base of the north Gulang escarpment and farther north or, as shown in a more recent map (State Seismological Bureau 1993, Fig. 7-1, p. 176), 9–10 km west of it, in part across the irrigated foreland and along the western edge of the Huangyang river fan, all the way to the tip of the east Shiyang thrust (Fig. 16).

While the actual lengths and throws of either the Dongqingding normal fault zone or the two 'conjugate' segments north of Dongqingding and Gulang (Molnar & Deng 1984) seem too small to have generated an earthquake of magnitude 8 to 8.3, the deformation mechanism in Fig. 19(b) and the fault geometry in Figs 1 and 16 suggest alternative ways to account for the moment and magnitude of the great 1927 event. Taking the shallower part of the Dongqingding thrust on Fig. 19b to dip ≈ 15°S, the ≈60° dip of the Dongqingding normal fault and the distance between its trace and the range front (≈3 km) would imply a ramp to flat bend about 1–1.5 km deep under the range. With ≈2 m of slip on the Dongqingding normal fault, kinematic compatibility at that 30° bend (e.g. King & Vita-Finzi 1981) would require ≈4 m of thrust slip at depth (Fig. 19b, inset). Assuming an average slip $\Delta u \approx 4$ m on the entire surface of the Wuwei–Dongqingding thrust, from ≈101.3 to ≈102.9°E and between the topographic front and the branch line with the Haiyuan–Gulang Fault ($Lw = 8.5 \times 10^3$ km^2, Figs 1 and 16), with a shear modulus $\mu = 3.3 \times 10^{10}$ N m^{-2}, would yield a seismic moment $M_0 = \mu Lw\Delta u \approx 11.2 \times 10^{20}$ N m, consistent with a magnitude $M_w \approx 8.0$ (e.g. Kanamori 1977). If less than the north-eastern half of that thrust surface ($Lw \approx 3.3 \times 10^3$ km^2), west of the Shiyang river, had slipped by the same amount, M_0 and M_w would be $\approx 4.3 \times 10^{20}$ N m and $\approx 7\frac{3}{4}$, respectively. These numbers, which bring forth the discrepancy left between even the minimum magnitude estimated (Gongxu *et al.* 1989) and the moment inferred from spectral densities of mantle waves (Chen & Molnar 1977), should merely be viewed as illustrating the source parameters most consistent with our assessment of the regional tectonics. But an average slip value smaller than 1.5 m, as well as a magnitude significantly greater than 8 should probably be considered unlikely. At the other extreme, assuming a shortening rate of ≈4 mm yr^{-1} and the recurrence time of a 1927-type event to be on the order of 1600 yrs (Gongxu *et al.* 1989) would require larger average slip (≈6 m) on a surface about one-quarter (35×60 km^2) of the maximum surface above, in rough coincidence with the southernmost epicentral location and the contour of isoseismal X (Figs 1 and 16). Clearly, the limited information at hand does not permit derivation of more than such non-unique, first-order inferences.

SUMMARY, DISCUSSION AND IMPLICATIONS

Deep fault architecture, slip partitioning and regional kinematics. Motion of NE Tibet relative to SE Gobi

Recent deformation near the eastern extremity of the Qilian Shan involves several fault zones with different strain styles. Our study helps understand how such strains are both partitioned and linked with one another, and combine into a coherent regional picture than can be related to crustal movements in adjacent regions, within the framework of the India–Asia collision. The two main components of deformation are ESE-striking, left-lateral faulting, and NNE-directed shortening. Qualitatively, this has long been known (e.g. Tapponnier & Molnar 1977), and is in keeping with the situation found in the western Qilian Shan (e.g. Peltzer *et al.* 1988; Meyer 1991), or east of the Yellow River (e.g. Burchfiel *et al.* 1989; Zhang *et al.* 1990). But it is now possible to better assess the relative importance of either process.

At a large scale and regardless of the sense of horizontal slip, the tectonics of the area where the Haiyuan and Gulang Faults merge and veer 15–20° as they enter the Lenglong Ling mountains resembles that of the 'big bend' region east and north of Los Angeles, in California, where the San Andreas and San Jacinto Faults converge as they bend along the San Gabriel Mountains and central Transverse Ranges (e.g. Hill & Dibblee 1953; Allen 1981; Weldon, Meisling & Alexander 1993). It is the change of azimuth of the strike-slip faults that seems to be the chief cause of more prominent overthrusting and mountain building within either of those restraining bends (Figs 1 and 20), (e.g. Anderson 1971; Allen 1981; Jones *et al.* 1990).

At a more detailed level, each of the three main faults of the eastern Qilian Shan bears distinctive characters. The western Haiyuan Fault is the largest and fastest slipping. While predominantly left lateral, it shows consistent normal downthrow, either to the south or north, east of about 102.5°E (Figs 1, 2, 10, 11). Such secondary throw seems to be less in the Lenglong Ling range, west of the junction with the Gulang Fault and south of the Shiyang–Dongqingding thrust, where fully developed. East of 102.5°E, the main active strand of the fault tends to step systematically

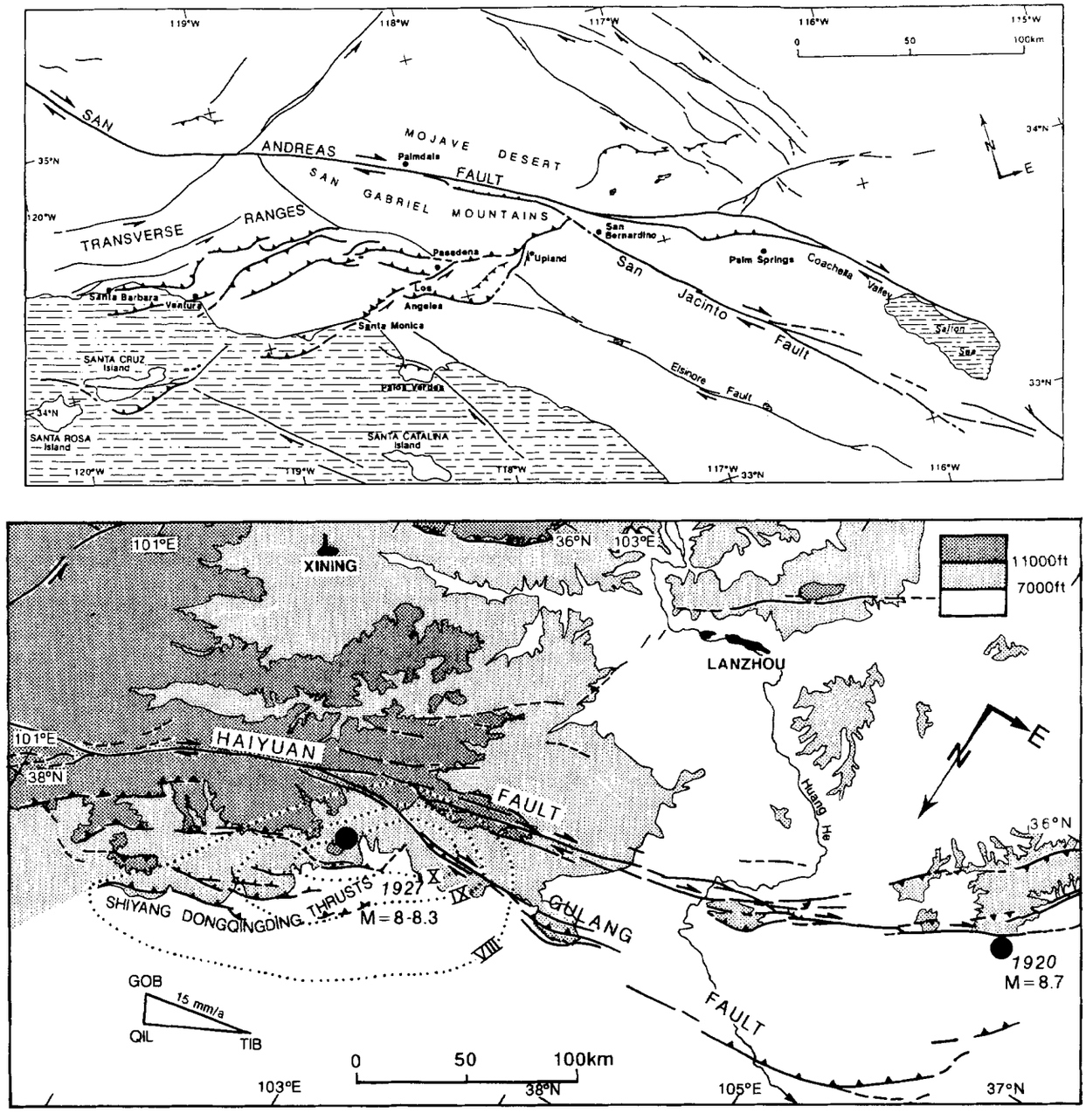

Figure 20. Comparison of east Qilian restraining bend of Haiyuan Fault system with 'big bend' of San Andreas Fault system. Top: map of principal active faults of southern California. Bold lines single out San Andreas Fault, San Jacinto Fault, and West Transverse Ranges thrusts. Bottom: map of principal active faults of NE Gansu, as seen looking up from under earth's surface, to free comparison from difference in lateral-slip sense. Resemblance and differences are discussed in text. Note similar scales in map view, and occurrence of $M \approx 8$ earthquake on restraining-bend thrusts in Gansu. Inset vector diagram depicts relationship between thrust- and strike-slip rates assuming partitioning of deep, oblique slip into strike-perpendicular and parallel components (see Figs 21, 22, and discussion in text). TIB, QIL and GOB refer to Tibet, east Qilian and Gobi blocks respectively.

northwards, resulting in the formation of asymmetric pull-apart basins of various sizes, with often prominent north-west boundary faults—the largest of which at Tianzhu—comparable to those segmenting the fault east of the Yellow River (e.g. Saltlake and Laohuyaoxian basins, Deng *et al.* 1986; Burchfiel *et al.* 1991; State Seismological Bureau 1990). The presently secondary strands of the western Haiyuan Fault show some degree of activity, however (Figs 2, 7 and 11). By contrast with those pull-apart steps, the highest, isolated mountains along the fault east of Laohu Shan (Hasi Shan, 3021 m and Nanhua Shan, 2969 m) seem to reflect contemporaneous shortening and thrusting within two clockwise restraining bends of the fault zone (Fig. 1).

The present-day slip rate on the Gulang Fault is less than half that on the western Haiyuan Fault. The secondary

component of motion on the Gulang Fault appears to be $\approx N$-directed thrusting, which has contributed to the formation of two distinct push-up mountains (Fig. 1), east of the north Gulang escarpment. That the Gulang Fault merges eastwards with the Tiangjing thrust further supports the inference that it acts as a lateral thrust ramp. Along either the Haiyuan or Gulang strike-slip faults, guidance by the early Palaeozoic fabric and/or by deep, large-scale boudinage such as that typifying the exhumed Red River–Ailao Shan shear one in Yunnan (Leloup *et al.* 1993) may account for the parallel surface strands separating lense-shaped crustal slivers (along Maomao Shan, near and east of Hasi Shan, and south of Haxi syncline, Figs 1, 2, 11, 16 and 17).

The en échelon, right-stepping Shiyang–Dongqingding thrusts provide a good example of fairly thick-skinned shortening across ancient basement, a widespread contemporary deformation process in the former peneplains of central Asia (Tapponnier *et al.* 1990; Meyer 1991; Avouac *et al.* 1993). The origin of those thrusts, and of the resulting Lenglong Ling crustal wedge or flake (Fig. 16) may be accounted for by the following scenario. Greater regional shortening west of 103°E probably led to the NNE propagation of a 10–20°S-dipping décollement splaying from the Haiyuan Fault at a depth of ≈25 km. Ramping, probably in sequence, of two equally spaced, steeply south-dipping thrusts from that décollement to the surface subsequently led to warping of the upper crust into two large fault-propagation anticlines (Fig. 16c). Contemporaneous folding of Holocene deposits ≈10 km north of the topographic front implies further north-directed propagation of the décollement into the foreland, in keeping with the inference that the thrust system evolved mostly as a leading imbricate thrust fan. Our observations are insufficient to decide whether the three principal thrust segments between 102 and 103°E are bounded to the east by lateral tip lines or ramps. But the north Gulang escarpment, if active, might represent the emergence of a right-lateral thrust ramp, and another such ramp, with even more modest expression in the cumulative relief might account for the N160E-striking, 1927 scarps reported west of the Huangyang river, if real (Fig. 16b). Finally, in spite of the predominant NNE shortening regime west of 103°E, subordinate, ESE-striking normal faults apparently contribute to accommodate hanging-wall warping in anticlinal flanks (Figs 16, 18 and 19). Whether of range-back or compatibility type (Figs 16c and 19), we surmise that such normal faults, which often reactivate inherited discontinuities of the crust, assist localized mountain building by restricting it to narrower ridges (e.g. Tapponnier 1993).

We infer both the 'controversial' complexity of the surface breaks of the 1927 earthquake, due in part to prominent, hitherto poorly understood, hanging-wall extension, and its modest thrust surface signature to be typical characteristics of great thrust events rupturing relatively deep ramps and shallow-dipping décollements under and near high mountains, in Asia and elsewhere. Our study of active faulting in the source area of the $M \approx 8$, 1906 Manas earthquake in the Dzungarian Tien Shan (Avouac *et al.* 1993) points towards the same conclusion. While involving thicker layers of crust, the strain style of large thrust earthquakes would thus generally resemble that of smaller events (e.g. Stein & King 1984). We suspect such style and characteristics to account for the 'mystery' that still shrouds the great Himalayan earthquakes of 1897, 1905, 1934, and 1950, or the 1902 and 1911 earthquakes in the Tien Shan, for which suitable surface-rupture maps are not available. Though complexly segmented, the ≈150 km long break of the 1932, $M \approx 7.6$, Changma earthquake probably owes its clearer expression to oblique slip on generally steeper fault planes (Peltzer *et al.* 1988; Meyer 1991).

The fact that the diverse faults of the eastern Qilian Shan all show evidence of coeval long-term slip, the detailed geometry of their traces, which bifurcate or step in map view, and the changes in strain styles, reflected in the cumulative relief, that coincide with such steps or bifurcations, imply that these faults connect at depth. The connections shown on the maps and section of Figs 1 and 16 are represented schematically in three dimensions on Figs 21(a) and (b). The architecture of the entire fault system resembles, in cross-section, that of a tree, with deep trunk and shallow branches. While quite complex at shallow crustal levels, it becomes simpler in the lower crust, with shear restricted to a narrower zone, a localization that probably continues in the upper mantle underneath. The fairly deep, active décollement provides an essential link between the most distant, emergent branches (see also Avouac *et al.* 1993).

At a grander scale to the west, the presence of an even deeper décollement in the mid-lower crust appears to account best for the contemporaneous growth of the parallel ranges of the central Qilian Shan (Tapponnier *et al.* 1990; Meyer 1991). To the east, it is probable that the Tiangjing, Mibo, and Yangtong Shan thrusts, which seem to reflect thin-skinned shortening (Zhang *et al.* 1990), mark the emergence of a relatively shallow décollement branching off the Haiyuan Fault one as shown in Fig. 21. We hypothesize deep connection between faults, or at least between localized, narrow shear zones in the Qilian Shan to be plausible because the crust, which is fairly old, and hence cold, thickens. Recent, relatively rapid thickening of cold crust ought to deepen further an already deep brittle-ductile transition, allowing for faulting to extend farther down, hence for greater earthquakes than is usual. Within a system like that depicted in Fig. 21, fault junctions are not stable. Even with steady-state boundary conditions at the regional scale, such a system will thus behave as a very dynamic feature, breeding short-lived jogs and splays, block rotation, and eventually slip inversion on steep ramps or high-angle strands (e.g. Peltzer *et al.* 1988). Such unstability probably suffices to account for the existence of the transient push-up mountains, pull-apart basins (with typical life times on the order of a few 10^5 yrs, given the centrimetric slip rate; e.g. Burchfiel *et al.* 1991), and shortening perpendicular normal faults observed.

A corollary of the geometry outlined in Fig. 21 and of the underlying inference that the whole 'fault tree' behaves mechanically as one system is that deep, oblique slip on the 'trunk fault' ought to be partitioned into dominantly strike-perpendicular and strike-parallel slip among the shallower branches (Armijo *et al.* 1986). The first-order rates obtained on the three principal faults may be used to test quantitatively the reality of such partitioning and to constrain the regional kinematics (Fig. 22). Combining the 11 ± 4 mm yr^{-1} slip, in the N112.5 ± 2.5E direction, on the

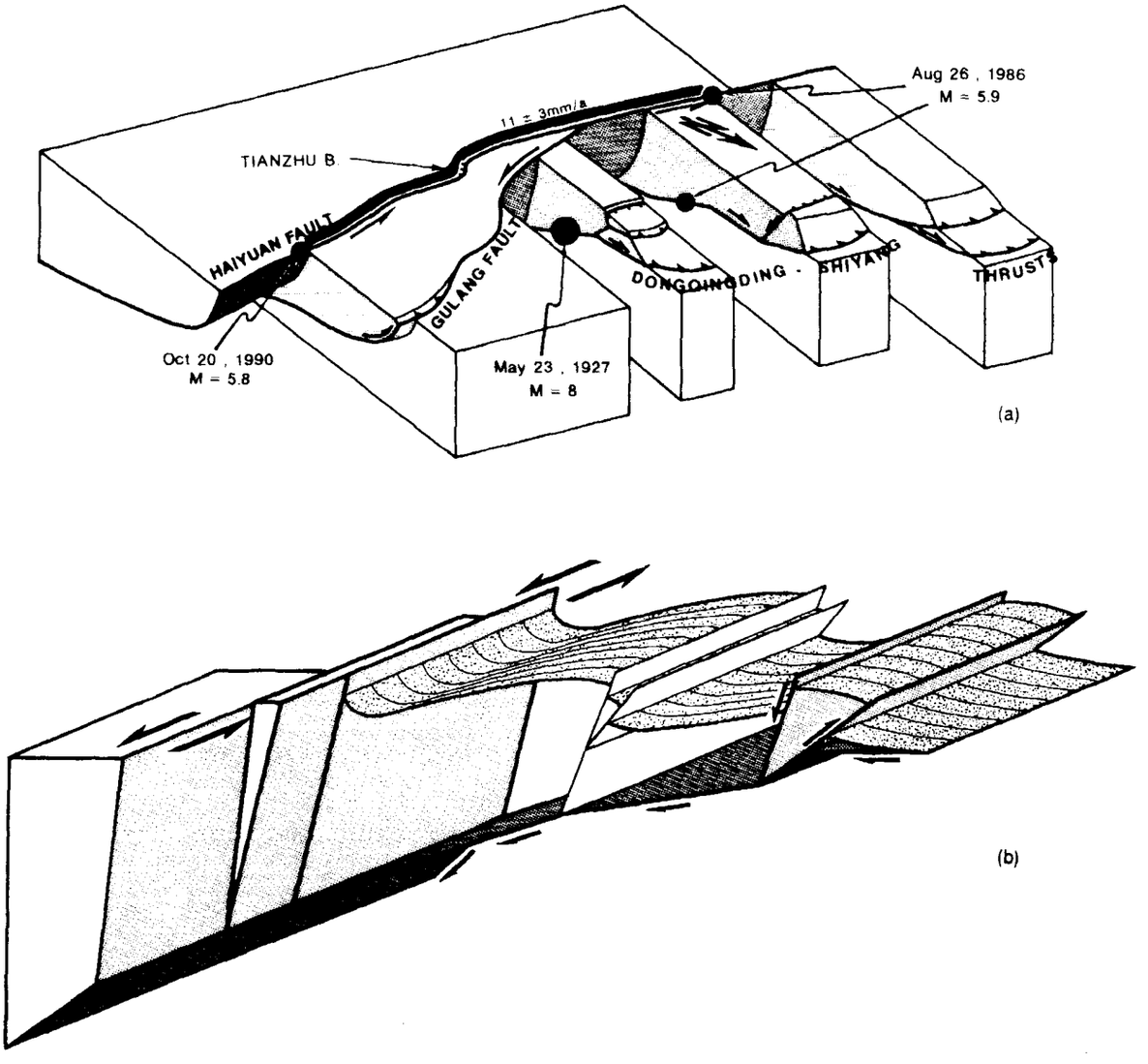

Figure 21. (a) Schematic block diagram (not to scale) showing possible links between NNE-vergent Shiyang–Dongqingding thrusts, and left-lateral Haiyuan and Gulang strike-slip faults. Solid line is probable length of Tianzhu seismic gap, capable of generating $M \geq 8$ earthquake, on Haiyuan Fault. Solid circles are hypocentres of 1927, 1986 and 1990 earthquakes (see text). (b) Simplified 3-D geometry of Haiyuan Fault, Gulang Fault, Shiyang–Dongqingding thrusts and associated fault planes assuming them to be linked, through shallow-dipping décollement, to deep oblique shear zone. Fault surfaces are shaded. Attitude of exhumed, folded and faulted décollement (stippled), is from Fig. 16(c).

Haiyuan Fault with the 4.3 ± 2.1 mm yr^{-1} slip, in the N92 ± 7E direction, on the Gulang Fault yields a total of 15.1 ± 6.0 mm yr^{-1} of left-lateral motion, in the N107 ± 4E direction (Fig. 22, top), between the north-easternmost part of Tibet (region of Lanzhou and Xining) and the southern part of the Gobi-Ala Shan platform (Tengger desert). Projecting the latter vector on the more southerly average strike (N119 ± 5E) of the Haiyuan Fault in the Lenglong Ling, between 101.2 and 102°E, west of the Gulang–Haiyuan junction, yields 14.8 ± 5.8 mm yr^{-1} of strike-parallel, left-lateral slip on that high mountain segment of the fault and 3.3 ± 1.7 mm yr^{-1} of strike-perpendicular (N29 ± 5E) shortening (Fig. 22, bottom). The first number is consistent with the rate (15 ± 5 mm yr^{-1}) implied by the offsets of the glacial valley edges visible on the SPOT image of Fig. 2(b). The second vector is comparable to the shortening rate (4 ± 2 mm yr^{-1}, N25 ± 10E) inferred from the structure and Pleistocene uplift (Fig. 22, bottom). The error ellipses are too large to allow a discussion of the misfit (≈0.7 mm yr^{-1}, ≈N07E) between the two shortening rates but, if real, it might reflect a minor component of roughly strike-perpendicular shortening along the Gulang Fault, in keeping with the interpretation that this fault is a lateral thrust ramp. We conclude that, to the first order, slip partitioning accounts well for the regional strain observed and that the postglacial and current rate of overall left-lateral motion between north-eastern Tibet and the south-western Gobi is probably about 15 ± 6 mm yr^{-1} in the N105 ± 6E direction (Fig. 22).

The results of our study of Cenozoic movements in the eastern Qilian Shan differ from those of similar studies in regions farther east. The horizontal slip rates reported by others on the Haiyuan Fault east of Jingtai (Fig. 1) are generally smaller than the one we obtain at Sange Dun

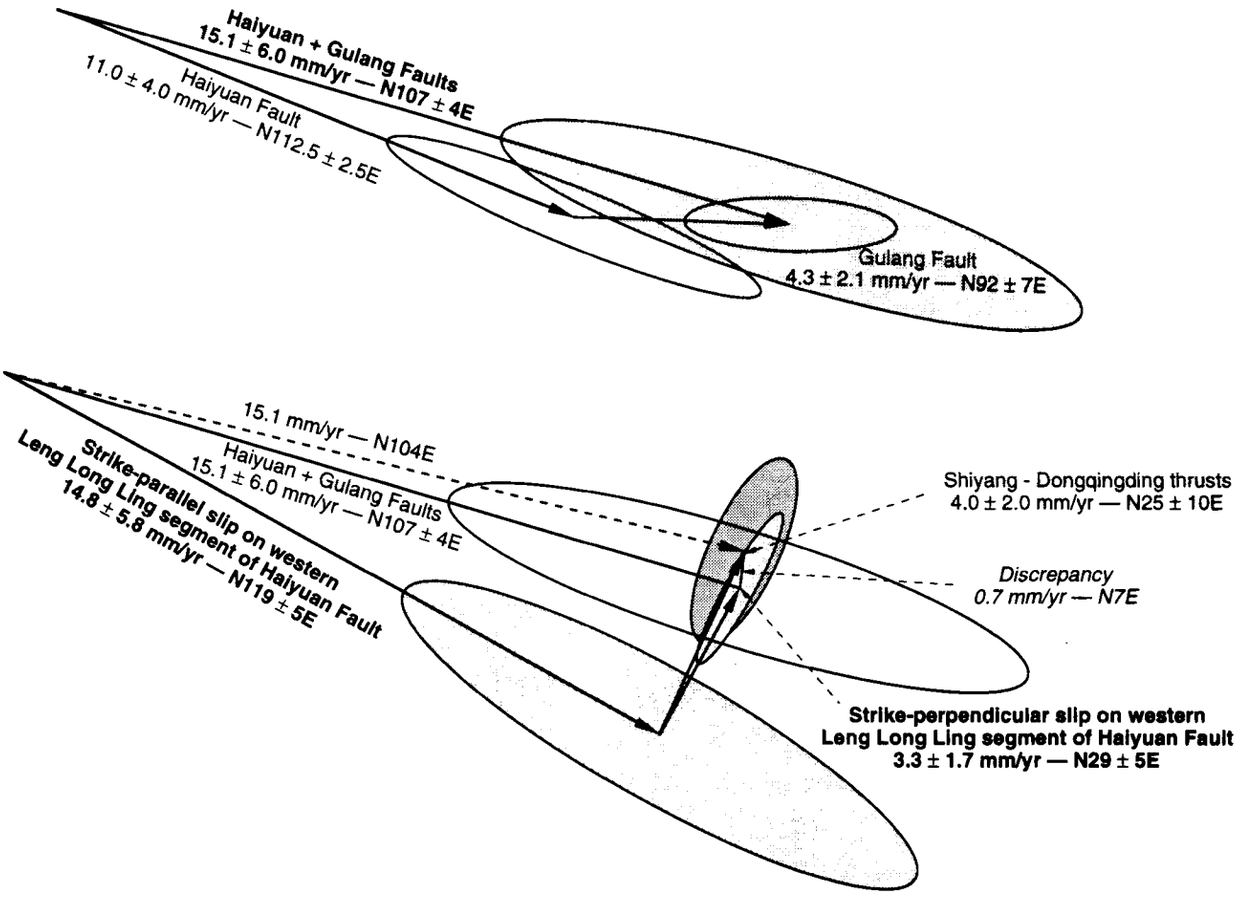

Figure 22. Vector sums summarizing slip-rate partitioning between major faults of eastern Qilian Shan. Combined left slip on Haiyuan and Gulang faults may contribute total of $\approx 15 \pm 6\,\mathrm{mm\,yr^{-1}}$ of N107 ± 4°E directed motion between NE Tibet and SE Gobi (top diagram). Partitioning of total slip into strike-perpendicular and parallel components, due to 10–15° clockwise bend of faults along Lenglong Ling, may account for most of NNE-directed, $4\,\mathrm{mm\,yr^{-1}}$ shortening on Shiyang–Dongqingding thrusts (bottom diagram). Error ellipses are shaded when derived from measurement uncertainties only. See discussion in text.

($11 \pm 4\,\mathrm{mm\,yr^{-1}}$). Liu & Zhou (1986), for instance, infer from offset Holocene ridges and creeks an average long-term slip rate of $\approx 5\,\mathrm{mm\,yr^{-1}}$, less than half the Sange Dun value. Their basis for estimating the ages of such offsets, however, is unclear. From more precise fieldwork on the Xihua-Nanhua Shan segment of the fault west of Haiyuan (Fig. 1), Zhang *et al.* (1988b) derive a left-slip rate of $8 \pm 2\,\mathrm{mm\,yr^{-1}}$ (Fig. 15a). Given the uncertainties, the Sange Dun value might be viewed as more consistent with this latter rate, but it still exceeds this rate by about 35 per cent. This discrepancy may be accounted for in various ways. First, as clearly stated by Zhang *et al.* (1988b), the work near Haiyuan, which is based on offsets of streams that incise C_{14}-dated terraces, only provides lower bounds on the slip rate and, while $\approx 7\,\mathrm{mm\,yr^{-1}}$ is the bound deemed most plausible from measurements at two preferred sites (Shaomayin and Yehupo), two other bounds may be taken to imply rates in excess of $10\,\mathrm{mm\,yr^{-1}}$ (Fig. 15a).

Secondly, the Xihua-Nanhua segment of the Haiyuan Fault strikes ≈N125E on average, ≈15° more southerly than at Sange Dun, and lies about 250 km to the east (Fig. 1). Hence, both the geographical separation and the change of strike might account for a fraction of the difference in rates. Thirdly and probably more important, fault slip south of the Xihua-Nanhua segment, on strands that reportedly did not rupture in the $M \approx 8.7$, 1920 Haiyuan earthquake, could add a few millimetres to the long-term rate documented at Shaomayin and Yehupo. Though less clear where they cross loess-blanketed landforms, the traces of such fault strands, which are discernable on Landsat images (e.g. Tapponnier & Molnar 1977, Fig. 5) and quite sharp on panchromatic SPOT scenes KJ 259–276, 260–277, 261–277, stretch along two different zones (Fig. 1). Some, mostly outside the area mapped by Burchfiel *et al.* (1991) or Deng *et al.* (1986) in the field, bound both Nanhua and Xihua Shan to the south-west. Others hug the SW flanks of Quwu and Yueliang Shan. In view of their orientation relative to N105 ± 6E, most of these presently subordinate fault strands ought to move obliquely, with components of both SW-directed thrust (Burchfield *et al.* 1991; State Seismological Bureau 1990) and left-lateral slip, possibly contributing to the rise of the four mountains, which form distinct highs, as push-up folds along the Haiyuan system. Last, and even though the high mountain site on the single-stranded fault at Sange Dun is remarkable, as are the Wallace and Cajon creeks sites on the San Andreas Fault (Sieh & Jahns 1984; Weldon & Sieh 1985), one ought to recall the strengths and weaknesses of the studies at stake here, and ponder the

different results in perspective. Our approach relies on a novel, comprehensive scrutiny of the entire Qilian–Haiyuan Fault system and on analysis of the self-consistency of offsets over great distances, a goal unattainable without the help of SPOT images, but on debatable inferences concerning the relationship between regional morphology and globally dated climate changes. In contrast, Zhang *et al.*'s approach (1988b), while limited by locally focused, if detailed, geological mapping, rests firmly on C_{14} dates. Hence, at this stage, it is probably wiser to emphasize the first-order consistency of the numbers derived at two distant places with such different approaches than to speculate on the difference between them.

The conclusions we reach regarding the date of onset of Cenozoic deformation, the kinematic regime between that date and the present, and the amounts of finite Cenozoic movement in the eastern Qilian Shan, on the other hand, are much more difficult to reconcile with those derived from fieldwork in Ningxia Hui Autonomous Region, east of the Yellow River. There, Burchfiel *et al.* (1989, see also Deng *et al.* 1986; State Seismological Bureau 1990; Burchfiel *et al.* 1991; Zhang *et al.* 1991) infer that Cenozoic regional deformation started only in the Late Pliocene, and that a ≈90° clockwise swing of the regional shortening direction (from ≈NE to ≈SE) in the Early Pleistocene triggered a radical shift in tectonic style, from shortening along NW trending thrusts and folds, to left slip on the Haiyuan Fault. That fault is thus interpreted to have originated only 1.6–1.8 Ma B.P., and to cut the thrusts and folds that it strictly postdates.

Not only do we find that the evidence discussed by the above authors does not require the interpretation they propose but there is little sign, if any, for such drastic change and late onset of deformation west of the Yellow River. Instead, in the eastern Qilian Shan, contemporaneous thrusting and strike-slip faulting take place in adjacent areas and we find no suggestion in the geological record that such a situation has not been going on unabated for at least several million years, with slip-partitioning accounting for current rates as well as for most of the finite movements. The simple interpretation that the Shiyang–Dongqingding thrusts result from compatibility shortening in a large restraining bend of the Haiyuan Fault (Figs 20–22) implies that both structures moved in tune during much of their recent history. We also find it difficult to account for the finite displacements on either the thrusts or the strike-slip faults if motion on them lasted less than 4–6 Ma. Assuming a constant, maximum shortening rate of 6 mm yr^{-1}, for instance, more than 4 Ma would have been necessary to absorb a minimum finite shortening of 25 km across the mountains north of the Haiyuan Fault. Similarly, with a constant left-slip rate of 11 mm yr^{-1}, more than 3.7 Ma or 7.3 Ma, depending on the minimum offset value chosen (40 or 80 km), would be required to form the great bend of the Yellow River across that fault (Fig. 15b). If the latter rate had only been 8 mm yr^{-1} (Zhang *et al.* 1988b), those time-spans would increase to ≈5 and ≈10 Ma, respectively. Our results are thus best interpreted to imply that shortening in the eastern Qilian Shan and left slip on the Haiyuan Fault started sometime in the late Miocene, consistent with the regional stratigraphy, rather than in the late Pliocene. Assuming partitioning of slip at constant rates on the Haiyuan Fault and eastern Qilian Shan thrusts (≈4 and 11 mm yr^{-1}, Figs 21 and 22) since 7–8 Ma B.P. would yield cumulative sinistral offset and shortening of 77–88 km, and 28–32 km, respectively. Adding cumulative slip on the Gulang Fault during that same period to that on the Haiyuan Fault would bring the total east–south-eastwards displacement of NE Tibet relative to the SE Gobi to at least 100–120 km.

That number contrasts with the small finite left-lateral slip inferred east of the Yellow River. By matching occurrences of rocks of different ages on either side of a 60 km stretch of the 600–700 km long fault, Burchfiel *et al.* (1989, 1991), Zhang *et al.* (1990, 1991), and Deng *et al.* (1986) have concluded that the total displacement on the Haiyuan Fault could not exceed 16 km (10.5–15.5 km), quite a small value for a fault of that length. While we do not question the quality of their detailed mapping, we note that the offsets they document concern only one segment of the presently active strand of the Haiyuan Fault zone. Besides, because visible outcrops north of that segment are small, close to it and extensively surrounded by a blanket of late Pleistocene (Q_3) loess, the offsets of rocks or contacts older than late Pleistocene might be underestimated. The length of fault they studied is in fact too short to rule out the existence of offsets greater than 60 km, particularly in view of the observation that Precambrian and Palaeozoic rocks similar to those used to constrain the larger offsets extend at least to Hasi Shan, about 100 km NE of Nanhua Shan, outside the Ningxia Hui Autonomous Region (Gansu Geological Bureau 1975). Thus, until a different, albeit convincing, explanation of the outstanding left-lateral deviation of the greatest river of north China across the Haiyuan Fault zone is found, and until mapping of offsets along that zone is completed at the appropriate scale, we consider it more likely that NE Tibet moved 100–150 rather than ≈16 km relative to the SE Gobi, and choose to interpret the 'total' offset in Ningxia as possibly indicative of the initiation of slip on the active Xihua–Nanhua fault strand (Fig. 15b).

Exactly how such a relatively large displacement might have been transferred to blocks farther east and south remains a target for future studies, but it could not have been entirely absorbed by crustal thickening in the modest, ≤2900 m high, Madong, Liupan and Xiaoguan mountains, where less than 18 km of shortening is reported (Zhang *et al.* 1991). Hence, while some of that displacement probably rifted and rotated the Ordos block away from the Gobi-Ala Shan platform, the greater part of it ought to have contributed to push the SE China craton towards the ESE or SE, tearing it away from the rest of north-eastern Asia (Tapponnier *et al.* 1982; Peltzer *et al.* 1985; Armijo *et al.* 1986, 1989; Peltzer & Tapponnier 1988; Zhang, Vergely & Mercier 1994).

Seismic hazard in NE Gansu and comparable regions

While several aspects of the mechanism of the great, 1927 Gulang earthquake remain obscure, one robust conclusion of our study is that this earthquake ruptured the Shiyang–Dongqingding thrusts, not the Gulang or Haiyuan Faults. Moreover, neither the Gulang nor the Haiyuan Fault bears field evidence of seismic dislocation in the last few centuries at this longitude. This is particularly clear for the

Haiyuan Fault, whose trace we inspected in detail at several localities. Whether near Sange Dun, Tianzhu or Song Shan, the smoothed-out scarps or pressure ridges that mark that trace are suggestive of infrequent, large earthquakes. That the walled city of Song Shan, located only 2 km south of the fault and built during the Ming Dynasty, remained intact until 1990 AD implies that no such earthquake has occurred since at least 1644 AD, a period of 350 years.

Additional inferences on the seismic behaviour of the western Haiyuan Fault may be derived from the Catalogue of Chinese Earthquakes (Gongxu *et al.* 1989). Since the great 1920 and 1927 earthquakes resulted in intensities of VII, VI, VI and VI, VIII, V, in Lanzhou, Wuwei, and Xining, respectively, comparable intensities would probably characterize a large event on the western Haiyuan Fault. Relatively few seismic events assigned peak intensities $\geq$VI are recorded in the catalogue within the region encompassing those three ancient cities. Before assessing the value of catalogue entries, whether in terms of location or estimated intensities, it must be recalled that very little is known of the seismicity of Tibet and Qinghai, immediately south-west of Gansu province, prior to the advent of instrumental data ($\approx$1900 AD), implying that this province always formed a frontier between nomad and sedentary ways of life. Thus, the catalogue is probably quite incomplete, and its entries must depend strongly on critical stages that have marked the history of the Chinese civilisation and empire, of its westwards conquests, and of population growth in settlements along and west of the upper reaches of the Yellow River, within lands of ancestral nomadic culture. Foremost among those stages are the establishment of the Qin dynasty (231 BC), the onset of sustained commercial exchange along the silk road ($\approx$50 BC), the successful and rapid expansion of Buddhism ($\approx$400 AD, Northern Wei dynasty), then Islam ($\approx$700 AD, Tang dynasty), and concurrent establishment of permanent centres of culture with durable architecture—none of the Mingoi (Buddhist cave monasteries) in Gansu and Ningxia, for instance, predates 400 BC, and much of the presently visible remains of the great wall in NE Gansu date from about 600 AD (Sui dynasty). In what has how become Gansu province, as in most other parts of China, there is in fact no earthquake record before the foundation of the Qin dynasty in 231 BC, 2225 years ago (Gongxu *et al.* 1989).

The cities of Lanzhou (formerly Jingcheng), Wuwei (formerly Liangzhou) and Xining are mentioned for the first time in the catalogue in 138 AD and 406 AD, 143 AD, and 318 AD, respectively, with the two oldest of these four events (peak intensities IX), as well as four more ancient ones, hitting more strongly towns located south-east of the Yellow River (Lintao, Gangu, Longxi, Wudu). Hence, we regard it likely that many events in NE Gansu, including large or very large earthquakes in the mountains roughly midway between those three cities, were not recorded prior to about 1600–1700 years ago. Since then, periods of war or important dynastic changes could have resulted in significant loss of information, and we doubt that location or intensity assessment in that part of China, even for such large events, becomes acceptable prior to the Mongol conquest (1206 AD) and its subsequent consolidation into the Yuan (1271 AD) and Ming dynasties (1368 AD). It must be noted, for example, that the first peak intensity of XI ($M \approx 8$), reported in the catalogue is that of the 1303 Linfen earthquake, in the much more central and populated province of Shanxi, to the east.

Hence, we infer that a large earthquake on the western Haiyuan Fault would probably have been located and identified as such in the last $\approx$800 years, might have been felt in certain cities but assigned incorrect location and size in the preceding $\approx$800–900 years, and would probably have been missed altogether prior to about 300 AD. With this in mind, shocks assigned intensities of VI to VII felt repeatedly in Wuwei in the fourth, sixth and eleventh centuries AD (362, 366, 374; 506, 575; 1092) (Gongxu *et al.* 1989; State Seismological Bureau 1991), closest to either the Shiyang–Dongqingding thrusts, or the Gulang and western Haiyuan Faults, might have been great events rupturing either strike-slip fault or, since apparently none of these shocks was felt in Lanzhou, 'smaller' ones on the nearer thrusts. The major historical event felt in and around Lanzhou in 1125 AD ($I \approx$ IX, $M \approx 7.2$?, Fig. 1), whose location is uncertain (Gongxu *et al.* 1989), might have activated the Haiyuan Fault, but the fact that it was not felt in Wuwei may be taken to imply that it activated a smaller fault south of Lanzhou (Fig. 1). Similarly, the two shocks felt in 1440 at and south of Yongden (VIII, VII), but neither in Lanzhou nor Wuwei, more likely activated a fault within 30–40 km of that city, probably to the south-west. The $I \approx$ VIII, ($M = 6.5$?) 1888 February 1 earthquake near Jingtai, on the other hand, which is felt nowhere else, may be safely inferred to be a moderate-size event on one strand of the Haiyuan Fault. New field evidence (Liu Baichi, personnal communication, 1992), in fact suggests that this event ruptured a 20–30 km long stretch of the main fault strand in the Lao Hu Shan, $\approx$20 km east of Song Shan, with 1.5–2 m of maximum left slip. While this discussion mostly emphasizes how little we know of the pre-instrumental seismicity of NE Gansu, it does suggest that, short of gross omissions in the catalogue, no large earthquake occurred along most of the lengths of the Gulang and western Haiyuan Faults during the last 800 years at least, in keeping with the qualitative impression gained in the field. Barring the occurrence of fault creep, for which there is no evidence at this time, both faults thus ought to be singled out as likely sites for such earthquakes in the future.

The western Haiyuan Fault, in particular, whose left-slip rate is fairly fast, looms as the foremost seismic-hazard source to the region. Such hazard is all the more serious that great earthquakes, rupturing several discrete segments, with millenal return intervals, are not rare on comparable fault zones in north-eastern China. Peltzer *et al.* (1988), for instance, estimated a recurrence interval between 900 and 1900 years for events comparable to the $M = 7.6$, 1932 earthquake, which ruptured at least five distinct segments of the Changma Fault zone, in the north-western Qilian Shan (Meyer 1991). Zhang *et al.* (1987) derived a recurrence interval of 800 to 1600 years for events similar to the $M = 8.7$, 1920 earthquake, which ruptured eight segments, separated by several kilometres wide pull-aparts, of the eastern Haiyuan Fault (Deng *et al.* 1986). It would thus be no surprise if the western stretch of that fault behaved in a similar way.

At a more detailed level, a rate of $\approx$11 mm yr^{-1} would imply more than 9 m of cumulative left slip along the

western Haiyuan Fault in over 800 years. The main geometric features that may be inferred to segment the fault are the Gulang–Haiyuan junction, the Tianzhu pull-apart basin, and the Song Shan junction and pull-apart basin. Independent rupture of the three western segments, whose lengths are respectively ≈90, ≈50 and ≈60 km, to depths of ≈20 km, each with ≈6 m of average slip, would generate three earthquakes with $M_w \geq 7.5$. If the entire length of the fault (≈220 km) west of the site of the 1888 event ruptured to ≈20 km, with ≈10 m of slip in a single earthquake, then a $M_w \geq 8$ event ($M_0 \approx 1.4 \times 10^{21}$ N m), comparable to the 1920, Haiyuan earthquake would ensue. Although alternative scenarios are possible, we find the latter more plausible in view of the usually accepted scaling law between average slip and rupture length for intraplate earthquakes (e.g. Scholz, Aviles & Wesnousky 1986), and of the examples of the 1920, 1927 and 1932 earthquakes.

That the Qilian–Haiyuan Fault system, seen as a whole (Fig. 21), generated the 1888, 1920 and 1927 earthquakes, the last two only seven years apart, after a long period of quiescence, implies that it re-entered an active phase of its cycle about 100 yrs ago. That two events with $M > 5.5$, the strongest since 1928, have taken place since 1985 near either extremity of the apparently quiescent, 220 km long, western stretch of fault—which we call the Tianzhu seismic gap—(Figs 1 and 21a), raises even greater concern. The first one (1986 August 26; $M \approx 5.9$), which struck the region north of Menyuan, is located either ≈20 km north of the trace of the Haiyuan Fault (centroid-moment-tensor inversion, Dziewonski *et al.* 1987), or a few kilometres south of it (broad-band body-wave phases, Ekström 1987) (Figs 1 and 21a). Its focal mechanism is compatible with ≈NE-directed thrusting on ≈SE-striking planes (Fig. 1) (Dziewonski *et al.* 1987; Ekström 1987; see also, Molnar & Lyon-Caen 1989; Molnar 1990). The second one (1990 October 20; $M \approx 5.8$) occurred in the Lao Hu Shan, ≈20 km east of Song Shan (Figs 1 and 21a), where it caused significant damage; segments of the Ming walls, for instance, collapsed. Its focal mechanism is consistent with pure left-lateral slip on a vertical, ≈N100E-striking plane (Dziewonski *et al.* 1991), corresponding either to the main strand of the Haiyuan Fault or to that north of it (Fig. 1). Both the 1986 and the 1990 events, therefore, apparently ruptured faults belonging to the Qilian–Haiyuan system as defined on Fig. 21. We conclude that the likelihood of impending large or great earthquakes on the western Haiyuan Fault, between Song Shan and Menyuan, only ≈100 km north of the most densely populated region of west-central China, is such that extensive instrumental monitoring of that part of the fault should be implemented at once.

Finally, to those of us who study great earthquakes and active faults in China, the urge for a comparison with southern California comes to mind once more. The geometrical resemblance brought out by Fig. 20 may be taken to imply simple kinematic and mechanical similarities. For instance, given the combined slip rate (≈42 mm yr^{-1}) on the San Andreas and San Jacinto Faults, south of the San Bernardino Mountains (Weldon & Sieh 1985; Weldon & Humphreys 1986; Weldon *et al.* 1993), and the angle that they make with the Mojave segment of the San Andreas Fault, between Cajon and Tejon Passes (≈18°), a vector diagram similar to that in Fig. 22 would imply as much as 13 mm yr^{-1} of strike-perpendicular (SSW) shortening along that segment, much of which on the thrusts south of the San Gabriel Mountains. This would be consistent with the recent revision, based on GPS measurements, of shortening rates south of the fault (11 ± 3 mm yr^{-1}; e.g. Donnellan, Hager & King 1995; Yeats 1993).

The similarities should not take precedence over the differences, however, which are significant. While the Haiyuan and Gulang Faults straddle the north-eastern edge of the Tibet plateau, the San Andreas and San Jacinto Faults extend south-eastwards into the extensional, Gulf of California, plate boundary. Boundary-movement rates in California (Minster & Jordan 1984; DeMets *et al.* 1990) are more than three times greater than in Gansu. More deformation occurs adjacent to the San Andreas Fault zone (e.g. Feigl *et al.* 1993). Horizontal slip at rates of 7–8 mm yr^{-1} takes place north-east of the San Andreas Fault, along the Garlock Fault (e.g. McGill & Sieh 1993) and the east Mojave shear zone, recently activated by the 1992 June 28, $M_w = 7.3$, Landers earthquake (e.g. Sieh *et al.* 1993). South-west of the San Andreas Fault, more dextral motion of crustal slivers along the Elsinore, Palos Verdes and other offshore faults contributes to make the central and western transverse Range thrusts more complex and to load them differently (e.g. Jones *et al.* 1990; Hauksson & Jones 1991) with increasing amount of shortening westwards (e.g. Yeats 1988). Many of those thrusts remain oblique to the Mojave segment of the San Andreas, which accounts for the sinistral component of slip on them (Fig. 20, top) and further kinematic complication arises from the clockwise block rotations thus induced (Jackson & Molnar 1990). The crust in eastern Gansu is thicker than in southern California, and has a different structure. Hence, although the relief in both regions is comparable, the elevations are not. Last, the thickness of recent, poorly consolidated sediments appears to be much greater in southern California, which probably implies more widespread occurrence of flat décollements at various depths (e.g. Yeats 1983, 1988; Davis, Nanson & Yerkes 1989).

But the resemblance illustrated in Fig. 20, and its implications regarding 3-D geometry and kinematics (Figs 21 and 22), adds weight to simple inferences. For instance, even at the hundred kilometre scale, in California or China, earthquake coupling and fault interaction (e.g. Stein, King & Lin 1992) should probably be considered to coinvolve, in three dimensions, all active faults, whether thrust, normal or strike slip. Also, as argued elsewhere (e.g. Hauksson & Jones 1991; Avouac *et al.* 1993), nucleation of the greatest thrust earthquake in the Los Angeles region deep under the highest and steepest relief, with propagation to a number of apparently discrete, shallower ramp segments and tear faults, as illustrated by the examples of the Changma (e.g. Peltzer *et al.* 1988; Meyer 1991), Manas (Avouac *et al.* 1993), and Gulang earthquakes (Fig. 20, bottom), ought not to be discarded as a remote possibility.

ACKNOWLEDGMENTS

This study is part of a long-term cooperation program between the Institut National des Sciences de l'Univers and

Centre National de la Recherche Scientifique (Paris, France), and the State Seismological Bureau of China (Beijing and Lanzhou). The leadership and efforts of G. Aubert, J. C. Rossignol, Fang Zhang Shun, Gao Wenshue, Chen Zhangli, Gu Ping, Xu Houde, Qian Jiadong and Zhang Feng made this co-operation possible. We are grateful to Xiang Hongfa, Xiang Guangzhong, Cai Shuhua and Yin Kelun who, with the assistance of Chen Hongfei and Zhao Xiaochen, provided great help, and substance for lively scientific exchange in the field. We acknowledge thoughtful discussions of the tectonics of central China with R. Armijo, R. Lacassin and Wang Yipeng. Our motivation to compare active faulting processes in NE Tibet and southern California was stimulated by talks with R. Weldon, L. Jones and K. Sieh. We thank P. Molnar, R. Yeats, J. Mercier and R. Weldon for careful reviews that improved the paper. We are thankful for the financial support provided jointly by programs Dynamique et Bilan de la Terre, Imagerie et Structure de la Terre (Tectoscope) of INSU, by the French Ministry of Foreign Affairs, and the State Seismological Bureau of China. Guy Aveline is responsible for the quality of the figures. This is IPGP contribution Nb 1230.

REFERENCES

Allen, C.R., 1981. The modern San Andreas fault, in *The geotectonic development of California*, ed. Ernst, W.G., Prentice-Hall.

Anderson, D.L., 1971. The San Andreas fault, *Sci. Am.*, **5,** 52–68.

Armijo, R., Tapponnier, P. & Han, T., 1989. Late Cenozoic right-lateral strike-slip faulting in southern Tibet, *J. geophys. Res.*, **94,** 2787–2838.

Armijo, R., Tapponnier, P., Mercier, J.L. & Han, T., 1986. Quaternary extension in southern Tibet: field observations and tectonic implications, *J. geophys. Res.*, **91,** 13 803–13 872.

Avouac, J. Ph., Meyer, B. & Tapponnier, P., 1992. On the growth of normal faults and the existence of flats and ramps along the El Asnam active fold and thrust system, *Tectonics*, **11,** 1–11.

Avouac, J.-Ph., Tapponnier, P., Bai, M., You, H. & Wang, G., 1993. Active faulting and folding in the northern Tien Shan and rotation of Tarim relative to Dzungaria and Kazakhstan, *J. geophys. Res.*, **98,** 742–745.

Bally, A.W., Mingchou, I., Clayton, R., Heugster, H., Kidwell, S., Meckel, L., Ryder, R., Watts, A.B. & Wilson, A., 1986. Notes on sedimentary basins in China, reports of the American Sedimentary Basins Delegation to the People's Republic of China, *U.S. Geol. Surv. Open File Rep.*, **86-237.**

Bard, E., Hamelin, B., Fairbanks, R.G. & Zindler, A., 1990. Calibration of the ^{14}C timescale over the past 30,000 years using mass spectrometric U-Th ages from Barbados corals, *Nature*, **345,** 405–410.

Bellier, O., Mercier, J.-L., Vergely, P., Long, C. & Ning, C., 1988. Evolution sédimentaire et tectonique du graben cénozoïque de la Wei He (province du Shaanxi, Chine du Nord), *Bull. Soc. Géol. France*, **6,** 979–994.

Bloom, A., 1978. *Geomorphology—A systematic analysis of late Cenozoic landforms*, Prentice Hall, Englewood Cliffs, NJ.

Blusson, A., Tapponnier, P. & Meyer, B., 1989. SPOT images reveal a 450 km long extension of the Haiyuan strike-slip fault (Gansu, China), *EOS Trans. Am. geophys. Un.*, **90,** 1350.

Boyer, S.E. & Elliott, D., 1982. Thrust systems, *Am. Assoc. Petrol. Geol. Bull.*, **66,** 1196–1230.

Bucknam, R.C. & Anderson, R.E., 1979. Estimation of fault-scarp ages from a scarp-height slope-angle relationship, *Geology*, **7,** 11–14.

Bull, W.B., 1991. *Geomorphic Responses to Climatic Change*, Oxford University Press, Oxford.

Burchfiel, B.C., Deng, Q., Molnar, P., Royden, L.H., Wang, Y., Zhang, P. & Zhang, W., 1989. Intracrustal detachment within zones of continental deformation, *Geology*, **17,** 478–752.

Burchfiel, B.C., Zhang, P., Wang, Y., Zhang, W., Song, F., Deng, Q., Molnar, P. & Royden, L.H., 1991. Geology of the Haiyuan fault zone, Ningxia-Hui Autonomous region, China, and its relation to the evolution of the northeastern margin of the Tibetan Plateau, *Tectonics*, **10,** 1091–1110.

Bureau of Geology and Mineral Resources of Qinghai Province, 1991. *Geological map of Qinghai province of the People's Republic of China*, scale 1:1,000,000, Geological Publishing House, Beijing.

Carroll, A.R., Liang, Y., Xiao, X., Hendrix, M.S., Chu, J. & McKnight, C.L., 1990. Junggar basin, northwest China: Trapped Late paleozoic ocean, *Tectonophysics*, **181,** 1–14.

Chen, W.P. & Molnar, P., 1977. Seismic moments of major earthquakes and the average rate of slip in central Asia, *J. geophys. Res.*, **82,** 2945–2969.

Chorley, R.J., Schumm, S.A. & Sugden, D.E., 1984. *Geomorphology*, Methuen, London.

Defense Mapping Agency, 1972. Operational Navigation Chart, scale 1/1,000,000, sheets G8 (4th edition) and G9 (5th edition), Saint Louis, Missouri.

Davis, T.L., Namson, J. & Yerkes, R.F., 1989. A cross section of the Los Angeles area: Seismically active fold and thrust belt, the 1987 Whittier Narrows earthquake and earthquake hazard, *J. geophys. Res.*, **94,** 9644–9664.

Deng, Q., Song, F., Zhu, S., Li, M., Wang, T., Zhang, W., Burchfiel, B.C., Molnar, P. & Zhang, P., 1984. Active faulting and tectonics of the Ningxia-Hui autonomous region, China, *J. geophys. Res.*, **89,** 4427–4445.

Deng, Q., Chen, S., Zhu, S., Wang, Y., Zhang, W., Jiao, D., Burchfiel, B.C., Molnar, P., Royden, L.H. & Zhang, P., 1986. Variation in the geometry and amount of slip on the Haiyuan fault zone, China, and the surface rupture of the 1920 Haiyuan earthquake, in *Earthquake Source Mechanics, Geophys. Monogr. Ser. vol.* 37, pp. 169–182, eds Das, S., Boatwright, J. & Scholz, C., Am. geophys. Un., Washington, DC.

DeMets, C., Gordon, R.G., Argus, D.F. & Stein, S., 1990. Current plate motions, *Geophys. J. Int.*, **101,** 425–478.

Ding, G., 1985. *The Fuyun earthquake fault zone in Xinjiang, China*, Seismological Press, Beijing.

Donellan, A., Hager, B.H. & King, R.W., 1993. Discrepancy between geological and geodetic deformation rates in the Ventura basin, *Nature*, **366,** 333–336.

Dziewonski, A.M., Ekström, G., Franzen, J.E. & Woodhouse, J.H., 1987. Centroid moment tensor solutions for July–September 1986, *Phys. Earth planet. Inter.*, **46,** 305–315.

Dziewonski, A.M., Ekström, G., Woodhouse, J.H. & Zwart, G., 1991. Centroid moment tensor solutions for October–December 1990, *Phys. Earth planet. Inter.*, **68,** 201–214.

Ekström, G., 1987. A broad-band method of earthquake analysis, *PhD thesis*, Harvard University, Cambridge, MA.

Enkin, R., Yang, Z., Chen, Y. & Courtillot, V., 1992. Paleomagnetic constraints on the geodynamic history of the major blocks of China from the Permian to the present, *J. geophys. Res.*, **97,** 13 953–13 989.

Fairbanks, R.G., 1989. A 17,000-year glacio-eustatic sea level record: influence of glacial melting rates on the Younger Dryas event and deep-ocean circulation, *Nature*, **342,** 637–642.

Feigl, K.L. *et al.* 1993. Space geodetic measurement of crustal deformation in central and southern California, 1984–1992, *J. geophys. Res.*, **98,** 21 677–21 712.

Gansu Geological Bureau, 1975. *Geological map of Gansu Province*, scale 1:1,000,000, Geological Press, Beijing.

Gasse, F., Arnold, M., Fontes, J.C., Fort, M., Gibert, E., Huc, A., Li, Y., Liu, Q., Mélières, F., Van Compo, E., Wang, F. & Zheng, Q., 1991. A 13,000 yr climatic record in western Tibet, *Nautre*, **353,** 742–745.

Gaudemer, Y., Tapponnier, P. & Turcotte, D.L., 1989. River offsets across active strike-slip faults, *Ann. Tecton.*, **3,** 55–76.

Graham, S.A., Xiao, X., Carroll, A.R., Demaison, G., McKnight, C.L., Liang, Y., Chu, J. & Hendrix, M., 1990. Characteristics of selected petroleum-source rocks, Xinjiang Upper Autonomous Region, northwest China, *Am. Assoc. Petrol. Geol. Bull.*, **74,** 493–512.

Gongxu, G., Tinghuang, L. & Zheniliang, S., *Catalogue of Chinese earthquakes* (1831 BC–1969 AD), Science Press, Beijing, China.

Hanks, T.C., Bucknam, R.C., LaJoie, K.R. & Wallace, R.E., 1984. Modification of wave-cut and faulting-controlled landforms, *J. geophys. Res.*, **89,** 5771–5790.

Hauksson, E. & Jones, L.M., 1991. The 1988 and 1990 Upland earthquakes: left-lateral faulting adjacent to the central Transverse Ranges, *J. geophys. Res.*, **96,** 8143–8165.

Hendrix, M.S., Graham, S.A., Carroll, A.R., Sobel, E.R., McKnight, C.L., Schulein, B.J. & Wang, Z., 1992. Sedimentary record and climatic implications of recurrent deformation in the Tien Shan: Evidence from Mesozoic strata of north Tarim, south Junggar, and Turpan basins, northwest China, *Geol. Soc. Am. Bull.*, **104,** 53–79.

Hill, M.L. & Dibblee, T.W., 1953. San Andreas, Garlock and Big Pine faults, California—A study of the character, history, and tectonic significance of their displacement, *Geol. Soc. Am. Bull.*, **64,** 443–458.

Jackson, J. & Molnar, P., 1990. Active faulting and block rotations in the western Transverse Ranges, California, *J. geophys. Res.*, **95,** 22 073–22 087.

Jia, Y., 1982. Preliminary discussion of geotectonical background and genesis of Gulang strong earthquakes in 1927 (in Chinese), *Northwest. Seism. J.*, **4,** 78–82.

Jones, L.M., Sieh, K.E., Hauksson, E. & Hutton, L.K., 1990. The 3 December 1988 Pasadena, California earthquake: evidence for strike-slip motion on the Raymond fault, *Bull. seism. Soc. Am.*, **80,** 474–482.

Kanamori, H., 1977, The energy release in great earthquakes, *J. geophys. Res.*, **82,** 2981–2987.

King, G.C.P. & Vita-Finzi, C., 1981. Active folding in the algerian earthquake of October 10, 1980, *Nature*, **292,** 22–26.

Lee, W.H.K., Wu, F.T. & Jacobsen, C., 1976. A catalog of historical earthquakes in China compiled from recent Chinese publications, *Bull. seism. Soc. Am.*, **66,** 2003–2016.

Leloup, P.H., Harrison, T.M., Ryerson, F.J., Wenji, C., Qi, L.P., Tapponnier, P. & Lacassin, R., 1993. Structural, petrological and thermal evolution of a Tertiary ductile strike-slip shear zone, Diancang Shan, Yunnan, *J. geophys. Res.*, **98,** 6715–6743.

Liu, B. & Zhou, J., 1986. The research on the active Haiyuan fault in China, *Northwestern Seism. J.*, **8,** 79–88.

Mattauer, M., 1986. Les subductions intracontinentales des chaînes tertiaires d'Asie; leurs relations avec les décrochements, *Bull. Soc. Géol. France*, **8,** 143–157.

McGill, S. & Sieh, K.E., 1993. Holocene slip rate of the central Garlock fault in southeastern Searles Valley, California, *J. geophys. Res.*, **98,** 14 217–14 231.

Minster, J.B. & Jordan, T.H., 1984. Vector constraints on Quaternary deformation of the western United States east and west of the San Andreas fault, in *Tectonics and sedimentation along the California margin*, **38,** 1–16, eds Crouch, J.K., & Bachman, S.B., Pacific Section, Society of Economic Paleontologists and Mineralogists, Los Angeles.

Meyer, B., 1991. Méecanismes des grands tremblements de terre et due raccourcissement crustal oblique au bord nord-est du Tibet, *PhD thesis*, Université Paris VI, Paris, France.

Meyer, B., Avouac, J.P., Tapponnier, P. & Meghraoui, M., 1990. Mesures topographiques sur le segment SW de la zone faillee d'E Asnam et interprétation mécanique des relations entre failles inverses et normales, *Bull. Soc. Géol. France*, **8,** 447–456.

Molnar, P., 1990. *S*-wave residuals from earthquakes in the Tibetan region and lateral variations in the upper mantle, *Earth planet. Sci. Lett.*, **101,** 68–77.

Molnar, P. & Deng, Q., 1984. Faulting associated with large earthquakes and the average rate of deformation in central and eastern Asia, *J. geophys. Res.*, **89,** 257–396.

Molnar, P. & Lyon-Caen, H., 1989. Fault plane solutions of earthquakes and active tectonics of the Tibetan Plateau and its margins, *Geophys. J. Int.*, **99,** 123–153.

Nabelek, J.L., 1984. Determination of earthquake source parameters from inversion of body waves, *PhD thesis*, MIT, Cambridge, MA.

Peltzer, G. & Tapponnier, P., 1988. Formation and evolution of strike-slip faults, rifts, and basins during the India–Asia collision: an experimental approach, *J. geophys. Res.*, **93,** 15 095–15 117.

Peltzer, G., Tapponnier, P. & Armijo, R., 1989. Magnitude of Late Quaternary left-lateral displacements along the northern edge of Tibet, *Science*, **246,** 1283–1289.

Peltzer, G., Tapponnier, P., Zhang, Z. & Xu, Z., 1985. Neogene and Quaternary faulting in and along the Qinling Shan, *Nature*, **317,** 500–505.

Peltzer, G., Tapponnier, P., Gaudemer, Y., Meyer, B., Guo, S., Yin, K., Chen, Z. & Dai, H., 1988. Offsets of late Quaternary morphology, rate of slip and recurrence of large earthquakes on the Chang Ma fault (Gansu, China), *J. geophys. Res.*, **93,** 7793–7812.

Peng, X. & Zhang, G., 1989. Tectonic features of the Junggar basin and their relationship with oil and gas distribution, in *Chinese Sedimentary Basins, Sedimentary Basins of the World 1*, pp. 17–31, ed. Hsü, K., Elsevier, Amsterdam.

Philip, H. & Meghraoui, M., 1983. Structural analysis and interpretation of the surface deformation of the El Asnam earthquake of October 10, 1980, *Tectonics*, **2,** 17–49.

Repetti, W.C., 1928. The epicenter of the Kansu earthquake of May 23, 1927, *Bull. seism. Soc. Am.*, **18,** 1–14.

Rothé, J.P., 1955. La tremblement de terre d'Orléansville et la sismicité de l'Algérie, *La Nature*, **3237,** 1–9.

Scholz, C.H., Aviles, C.A. & Wesnousky, S.G., 1986. Scaling differences between large interplate and intraplate earthquakes, *Bull. seism. Soc. Am.*, **76,** 65–70.

Sieh, K.E. & Jahns, R.H., 1984. Holocene activity of the San Andreas fault at Wallace Creek, California, *Geol. Soc. Am. Bull.*, **95,** 883–896.

Sieh, K.E. *et al.* 1993. Near-field investigations of the Landers earthquake sequence, April to July 1992, *Science*, **260,** 171–176.

State Seismological Bureau, 1990. *The Haiyuan active fault zone*, ed. Deng Qidong, Seismological Publishing House, Beijing.

State Seismological Bureau, 1991. *Summary catalog of Chinese earthquakes of different historical periods*, eds Chen, J. *et al.*, Seismological Publishing House, Beijing. (on magnetic diskettes)

State Seismological Bureau, 1993. *The Qilian Mountain-Hexi Corridor active fault system*, ed. Guo Shunmin, Seismological Publishing House, Beijing.

Stein, R.S. & King, G.C.P., 1984. Seismic potential revealed by surface folding: 1983 Coalinga, California, earthquake, *Science*, **224,** 869–872.

Stein, R.S., King, G.C.P. & Lin, J., 1992. Change in failure stress on the San Andreas and surrounding faults caused by the 1992 $M = 7.4$ Landers earthquake, *Science*, **258,** 1328–1332.

Tapponnier, P., 1993. Mèchanisms of 'extensional or denudation' faulting in regions of crustal shortening: an updated review, in

Late orogenic extension in mountain belts, Abstracts, p. 192, eds Séranne, M. & Malavieille, J., Document BRGM No. 219, Editions du BRGM, Orléans.

Tapponnier, P. & Molnar, P., 1977. Active faulting and tectonics in China, *J. geophys. Res.*, **82,** 2905–2930.

Tapponnier, P., Peltzer, G., Le Dain, A.Y., Armijo, R. & Cobbold, P., 1982. Propagating extrusion tectonics in Asia: new insights from simple experiments with plasticine, *Geology*, **10,** 611–616.

Tapponnier, P., Meyer, B., Avouac, J.Ph., Peltzer, G., Gaudemer, Y., Guo, S., Xiang, H., Yin, K., Chen, Z., Cai, S. & Dai, H., 1990. Active thrusting and folding in the Qilian Shan, and decoupling between upper crust and mantle in northeastern Tibet, *Earth planet. Sci. Lett.*, **97,** 382–403.

Wallace, R.E., 1978. Geometry and rates of change of fault-generated range fronts, north-central Nevada, *J. Res. U.S. Geol. Surv.*, **6,** 637–650.

Weldon, R.J. & Humphreys, E., 1986. A kinematic model of southern California, *Tectonics*, **5,** 33–48.

Weldon, R.J. & Sieh, K.E., 1985. Holocene rate of slip and tentative recurrence interval for large earthquakes on the San Andreas fault in Cajon Pass, southern California, *Geol. Soc. Am. Bull.*, **96,** 793–812.

Weldon, R.J., Meisling, K.E. & Alexander, J., 1993. A speculative history of the San Andreas fault in southern California, A reconstruction based on a new cross-fault correlation, in *The San Andreas Fault system: Displacement, palinspastic reconstruction and geologic evolution*, eds Powell, R.E., Weldon, R.J. & Matti, J.C., *Geol. Soc. Mem.*, **178,** 161–198.

Xu, W., He, Y. & Yan, Y., 1989. Tectonic characteristics and hydrocarbons of the Hexi corridor, in *Chinese Sedimentary Basins, Sedimentary Basins of the World I*, ed. Hsü, K., 53–62, Elsevier, Amsterdam.

Yeats, R.S., 1983. Large-scale Quaternary detachments in Ventura Basin, southern California, *J. geophys. Res.*, **88,** 569–583.

Yeats, R.S., 1993. Late Quaternary slip rates on the Oak Ridge fault, Transverse Ranges, California: Implications for seismic risk, *J. geophys. Res.*, **93,** 12 137–12 149.

Yeats, R.S., 1993. Converging more slowly, *Nature*, **366,** 299–301.

Yielding, G., Jackson, J.A., King, G.C.P., Sinvhai, H., Vita-Finzi, C. & Wood, R.M., 1981. Relation between surface deformation, fault geometry, seismicity and rupture characteristics during the El Asnam (Algeria) earthquake of 10 October 1980, *Earth planet. Sci. Lett.*, **56,** 287–304.

Zhang, B., Liao, Y., Guo, S., Wallace, R.E., Bucknam, R.C. & Hanks, T.C., 1986. Fault scarp related to the 1739 earthquake and seismicity of the Yinchuan graben, Ningxia Huizu Zizhiqu, China, *Bull. seism. Soc. Am.*, **76,** 1253–1296.

Zhang, W., Jiao, D., Zhang, P., Molnar, P., Burchfiel, B.C., Deng, Q., Wang, Y. & Song, F., 1987. Displacement along the Haiyuan fault associated with the great 1920 Haiyuan, China, earthquake, *Bull. seism. Soc. Am.*, **77,** 117–131.

Zhang, P., Molnar, P., Zhang, M., Deng, Q., Wang, Y., Burchfiel, B.C., Song, F., Royden, L.H. & Jiao, D., 1988a. Bounds on the recurrence interval of major earthquakes along the Haiyuan fault in north-central China, *Seism. Res. Lett.*, **59,** 81–89.

Zhang, P., Molnar, P., Burchfiel, B.C., Royden, L.H., Wang, Y., Deng, Q. & Song, F., 1988b. Bounds on the Holocene slip-rate on the Haiyuan fault, north-central China, *Quater. Res.*, **30,** 151–164.

Zhang, P., Burchfiel, B.C., Molnar, P., Zhang, W., Jiao, D., Deng, Q., Wang, Y., Royden, L.H. & Royden, L.H. & Song, F., 1990. Late Cenozoic tectonic evolution of the Ningxia-Hui autonomous region, China, *Geol. Soc. Am. Bull.*, **102,** 1484–1498.

Zhang, P., Burchfiel, B.C., Molnar, P., Zhang, W., Jiao, D., Deng, Q., Wang, Y., Royden, L.H. & Song, F., 1991. Amount and style of late Cenozoic deformation in the Liupan Shan area, Ningxia autonomous region, China, *Tectonics*, **10,** 1110–1129.

Zhang, Y., Vergely, Q.P. & Mercier, J.L., 1994. Active faulting in and along the Qinling ranges (China) from SPOT imagery analysis and extrusion tectonics of southern China, *Tectonophysics, submitted.*